The Pennsylvania State University

The Graduate School

Department of Chemistry

ION CONDUCTION MECHANISMS IN POLYMER ELECTROLYTES FOR LITHIUM BATTERIES AND FUEL CELLS, AND CRYSTAL ENGINEERING OF CYCLOPHOSPHAZENES

A Dissertation in

Chemistry

by

David Kim Yong Lee

Submitted in Partial Fulfillment
of the Requirements
for the Degree of

Doctor of Philosophy

August 2010

The dissertation of David Kim Yong Lee was reviewed and approved* by the following:

Harry R. Allcock
Evan Pugh Professor of Chemistry
Dissertation Advisor
Chair of Committee

Alan J. Benesi
Director of NMR Facility
Lecturer of Chemistry

John V. Badding
Professor of Chemistry

Michael A. Hickner
Assistant Professor of Materials Science and Engineering

Barbara J. Garrison
Shapiro Professor in Chemistry
Head of the Department of Chemistry

*Signatures are on file in the Graduate School

ABSTRACT

The work described in this thesis is divided into two parts. The first part focuses on the synthesis and characterization of polyphosphazenes for polymer electrolytes in lithium batteries and fuel cells. The overall goal is to gain an understanding of the ion conduction mechanisms in these materials to aid future designs of ion conducting polymers. The second part of this thesis describes the design and synthesis of cyclophosphazenes with asymmetric spirocyclic side groups. The reaction mechanism for the selective formation of the cis-isomer is proposed and the inclusion behavior of crystals formed by these molecules was studied. The theme that ties the two parts of this thesis is the chemistry of phosphazenes.

Chapter 1 outlines the fundamental concepts for polymer electrolytes used in lithium batteries and fuel cells. The properties of the polymers that are used as electrolytes and the current understanding of the ion conducting mechanism in these materials are described. Furthermore, the chemistry and applications of phosphazenes is also outlined.

Chapter 2 is a study on the ion conduction mechanism in a polyphosphazene electrolyte. Lithium trifluoromethanesulfonate (LiTf), lithium bis(trifluoromethanesulfonyl)imidate (LiTFSI), magnesium trifluoromethanesulfonate ($MgTf_2$) and magnesium bis(trifluoromethane sulfonyl)imidate ($MgTFSI_2$) were dissolved in poly[bis(2-(2-methoxyethoxy)ethoxy)phosphazene] (MEEP) to compare the effect on solvent-free polymer ionic conductivity of monovalent versus divalent cations, and two anions with different degrees of dissociation. The polymer electrolytes with the bis(trifluoromethanesulfonyl)imidate anion had higher ionic conductivities even though the glass transition temperatures, which reflected polymer molecular motion, were higher than those of their counterparts with the trifluoromethanesulfonate anion. Furthermore, polymer electrolytes with magnesium salts achieved their maximum conductivity at lower salt concentrations than the counterparts with lithium salts. The temperature

dependence of the ionic conductivity of the solid solutions was fitted to the Vogel-Tamman-Fulcher (VTF) equation. The pseudo-activation energy term, B, of the VTF equation showed a strong dependence on the anion present. The result suggests that the dominant mobile species is the anion, while the cation remains relatively bound to the polymer. The manuscript has been submitted to the journal *Solid State Ionics.*

Chapter 3 describes a synthetic method to produce a proton conductive polymer membrane with a polynorbornane backbone and inorganic-organic cyclic phosphazene pendent groups that bear sulfonic acid units. This hybrid polymer combines the inherent hydrophobicity and flexibility of the organic polymer with the tuning advantages of the cyclic phosphazene to produce a membrane with high proton conductivity and low methanol crossover at room temperature. The ion exchange capacity (IEC), the water swelling behavior of the polymer, and the effect of gamma radiation crosslinking were studied, together with the proton conductivity and methanol permeability of these materials. A typical membrane had an IEC of 0.329 mmol g^{-1} and had water swelling of 50 wt%. The maximum proton conductivity of 1.13 x 10^{-4} S cm^{-1} at room temperature is less than values reported for some commercially available materials such as Nafion. However the average methanol permeability was around 10^{-9} cm s^{-1}, which is one hundred times smaller than the value for Nafion. Thus, the new polymers are candidates for low-temperature direct methanol fuel cell membranes. The author was responsible for the synthesis of the materials used in this study and this work was done in collaboration with Shih-To Fei, Richard M. Wood, David A. Stone and Hwei-Liang Chang. The manuscript is published in the *J. Membrane Science* (year **2008**, volume 320, pages 206-214).

Chapter 4 deals with the characterization of water absorbed in proton conducting membranes. The proton conducing membranes were hydrated with $^{2}H_2O$ and ^{2}H T_1 NMR relaxation was used to probe the molecular dynamics of the water. The state of water in the proton conducting membrane was correlated to the chemical and morphological properties of the

polymer. An understanding of the state of water in proton conducting membranes is as important as the morphological characterization of the proton conducting membrane because water is the medium for proton transport. Furthermore, this vital information will aid in the design of future proton conducting membranes, especially ones that can operate at low humidity and at temperatures above 100 ˚C. This work was done in collaboration with Professor Alan Benesi and Professor Michael Hickner. The intended target for submission is *Journal of Physical Chemistry B.*

Chapter 5 describes layer-by-layer (LbL) films of poly[bis(methoxyethoxyethoxy)phosphazene] (MEEP) and poly (acrylic acid) (PAA) that are assembled by utilizing the hydrogen bonding between these two polymers. These films show controlled thickness growth, high ionic conductivity, and excellent hydrolytic stability. The ionic conductivity of these films is studied by changing the assembly pH of initial polymer solutions and thereby controlling the hydrogen bonding characteristics. Despite similar film composition, MEEP/PAA LbL films assembled at higher pH values have enhanced water uptake and transport properties, which play a key role in increasing ion transport within the films. At fully humidified conditions, the ionic conductivity of MEEP/PAA is 7×10^{-4} S cm^{-1}, over one order of magnitude higher than previously studied hydrogen bonded LbL systems. Finally, free standing films are isolated from low-energy surface substrates, which allows for bulk characterization of these thin films. This work was done in collaboration with Avni A. Argun, J. Nathan Ashcraft, Marie K. Herring, and Professor Paula T. Hammond from the Massachusetts Institute of Technology. The manuscript has been accepted in *Chemistry of Materials*. (year 2010, volume 22, pages 226–232)

Chapter 6 describes the synthesis and characterization of two novel cyclic phosphazenes with asymmetric spiro rings. The phosphazene molecules were synthesized via reactions of hexachlorocyclotriphosphazene with chiral amino alcohol residues. The reactions showed preferential formation of the *cis* isomer possibly due to the delocalization of the lone pair

electrons of the spirocylic nitrogen, which reduces its ability to solvate protons. Crystals of these phosphazenes were analyzed by x-ray crystallography which confirmed the formation of cis isomers and showed their ability to include guest molecules within the crystal lattices. The selective inclusion of epoxides by one of the phosphazenes was an effective method for the separation of thermally sensitive guest molecules. This work was carried out in collaboration with Anne Jackson and Toshiki Fushimi, and has been published in *Dalton Transactions*. (DOI**:** 10.1039/b925734a)

Appendix A describes the exploratory synthesis of a novel sulfonated polyphosphazene. The sulfonic acid group of this new polyphosphazene is tethered to the polyphosphazene backbone by a flexible side chain. The synthetic strategy of the polymer is compared to sulfonated polyphosphazenes synthesized previously. The logic behind this work is to examine the effect of distancing the sulfonic acid group from the polymer to the proton conductivity of the polymer.

TABLE OF CONTENTS

LIST OF FIGURES x

LIST OF TABLES xiv

ACKNOWLEDGEMENTS xv

Chapter 1 Introduction 1

1.1 Polymer Electrolytes 1
1.1.1 Polymer Electrolytes for Batteries 3
1.1.2 Polymer Structures for Secondary Lithium Battery Electrolytes 8
1.1.3 Ionic Transport Mechanism in Lithium Battery Electrolytes 10
1.1.4 Polymer Electrolytes for Fuel Cells 12
1.1.5 Chemical Structure and Morphology of Proton Conducting Membranes 15
1.1.6 Current State of Polymer Electrolytes 18
1.2 Phosphazenes 19
1.2.1 Background and History of Polyphosphazenes 19
1.2.1 Polymerization Methods 21
1.2.1 Properties of Polyphosphazenes 24
1.2.4 Polyphosphazene Electrolytes 27

Chapter 2 The Effects of Cations and Anions on the Ionic Conductivity of Poly[bis(2-(2-methoxyethoxy)ethoxy)phosphazene] Doped with Lithium and Magnesium Salts of Trifluoromethanesulfonate and Bis(trifluoromethanesulfonyl)imidate 32

2.1 Introduction 32
2.2 Experimental 35
2.2.1 Materials 35
2.2.2 Equipment 36
2.2.3 Syntheses 36
2.3 Results and Discussion 37
2.3.1 Glass Transition Behavior 37
2.3.2 Ionic Conductivity Behavior 40
2.4 Conclusions 46

Chapter 3 Inorganic-Organic Hybrid Polymers with Pendent Sulfonated Cyclic Phosphazene Side Groups as Potential Proton Conductive Materials for Direct Methanol Fuel Cells 48

3.1 Introduction 48
3.2 Experimental 53
3.2.1 Materials: 53
3.2.2 Instrumentation 53
3.2.3 Syntheses 54
3.2.4 Characterization 57

3.3 Results and Discussion....59
3.3.1 Polymer Synthesis....59
3.3.2 Sulfonation and IEC Values....60
3.3.2 Crosslinking and Physical Property Changes....61
3.3.3 Water Swelling Behaviour....62
3.3.4 Methanol Swelling Behavior....63
3.3.5 Proton conductivity....64
3.3.6 Methanol Permeability....65
3.3.7 Relationship of IEC, Swelling, Conductivity and Permeability....68
3.4 Conclusions....70

Chapter 4 Characterization of Water in Proton Conducting Membranes by Deuterium NMR T_1 Relaxation....74

4.1 Introduction....74
4.2 Experimental....77
4.2.1 Membrane Material....77
4.2.2 Cleaning Procedure....77
4.2.3 *In-Situ* NMR Tube Hydration....78
4.2.4 NMR T_1 Relaxation Experimental....79
4.2.5 Water Uptake and Proton Conductivity....80
4.3 Results and Discussion....80
4.3.1 Overview of Membranes....80
4.3.2 Water Uptake Behavior....83
4.3.3 Presence of Bound Water....84
4.3.4 ^{2}H T_1 Relaxation Behavior of Different Membranes....87
4.4 Conclusions....91

Chapter 5 Ion Conduction and Water Transport in Polyphosphazene Based Multilayers....93

5.1 Introduction....93
5.2 Experimental Section....95
5.2.1 Chemicals....95
5.2.2 LbL Assembly Methods....96
5.2.3 Ionic Conductivity....96
5.2.4 Bulk Characterization....97
5.2.5 Water Uptake Behavior....97
5.3 Results and Discussion....98
5.3.1 Multilayer Assembly and Ionic Conductivity....98
5.3.2 FTIR Analysis....102
5.3.4 Bulk Characterization of Free-standing Films....103
5.3.5 Water Transport....106
5.4 Summary and Perspective....109

Chapter 6 Synthesis and Inclusion Behavior of Cyclotriphosphazene Molecules with Asymmetric Spiro Rings....112

6.1 Introduction....112
6.2 Experimental Methods....114

6.2.1 Reagents and Solvents....114
6.2.2 Equipment....114
6.2.3 Syntheses....115
6.2.4 Recrystallization Methods....117
6.2.5 X-Ray Analysis....118
6.3 Results and Discussion....119
6.3.1 Synthesis and Mechanism of *Cis* Isomer Formation....119
6.3.2 Crystallization and Inclusion Behavior....124
6.4 Conclusions....130

Appendix Exploratory Synthesis of New Polyphosphazenes with Tethered Sulfonic Acid Groups....132

LIST OF FIGURES

Figure 1-1 A Ragone plot comparing different energy conversion devices 3

Figure 1-2 Schematic representation of a Lithium Battery and a Fuel Cell.....3

Figure 1-3 Different categories of battery polymer electrolytes.....4

Figure 1-4 Common small molecule additives for gel polymer electrolytes. Clockwise from top left: ethylene carbonate, propylene carbonate, N-methyl pyrrolidone, tetramethylene sulfone, γ-butyrolactone. 6

Figure 1-5 Polymers with cation solvating capability 8

Figure 1-6 One stable geometry for Li^+-pentaglyme obtained using ab initio electronic structure calculations. Hydrogen atoms were omitted for clarity. 8

Figure 1-7 Comb branched polymer electrolyte structures (a) polymethacrytale, (b) polyitaconate, (c) poly(ethylene oxide), (d) polyphosphazene, and (e) polysiloxane.....10

Figure 1-8 Cation migration mechanisms in a polymer electrolyte[17] 11

Figure 1-9 A polyphosphazene electrolyte exhibiting VTF behavior. Numbers in the legend represents the repeat unit to salt ratio [MEEP:Salt] 12

Figure 1-10 Various proton conducting polymer structures 14

Figure 1-11 Proton conduction mechanisms: a) Grotthuss chain and b) vehicle mechanism 16

Figure 1-12 Morphology comparison between Nafion and sPEEKK.....18

Figure 1-13 Various structures of phosphazenes 19

Figure 1-14 General polymerization and reactions of phosphazenes 20

Figure 1-15 Cationic ring-opening polymerization of hexachlorocyclotriphosphazene.....22

Figure 1-16 Cationic condensation polymerization of trichloro(trimethylsilyl) phosphoranimine.....22

Figure 1-17 Alternate polyphosphazene geometries.....23

Figure 1-18 Degradation of amino acid substituted polyphosphazenes.....26

Figure 1-19 Ion conducting polyphosphazene electrolytes a) MEEP, b) polyphosphazene with varying ethyleneoxy chain length, and c) single-ion polyphosphazene.....27

Figure 1-20 Proton conducting polyphosphazene architectures 28

Figure 2-1 Poly[bis(2-(2-methoxyethoxy)ethoxy)phosphazene] (MEEP).....33

Figure 2-2 Salts used in this study. 34

Figure 2-3 Glass Transition behavior of MEEP with increasing salt concentration. 38

Figure 2-4 Isothermal ionic conductivity of LiTf:MEEP 40

Figure 2-5 Isothermal ionic conductivity of LiTFSI:MEEP 41

Figure 2-6 Isothermal ionic conductivity of $MgTf_2$:MEEP 41

Figure 2-7 Isothermal ionic conductivity of $MgTFSI_2$:MEEP.....41

Figure 2-8 VTF equation B value for MEEP polymer electrolytes 44

Figure 3-1 Synthetic scheme for the monomer.....51

Figure 3-2 Synthetic scheme for the sulfonated polymer: Polymerization, hydrogenation and sulfonation reactions 52

Figure 3-3 Schematic diagram for methanol permeability measurements.....58

Figure 3-4 IEC values of the polymer versus the amount of SO_3 used for sulfonation. 60

Figure 3-5 Water swelling vs the IEC value of the uncrosslinked and crosslinked polymer ..63

Figure 3-6 Methanol crossover of membranes relative to the IEC values of the materials 65

Figure 3-7 Dependence of methanol crossover on ionic conductivity of the membranes 67

Figure 3-8 Relationship between ion conductivity and water uptake of 20Mrad crosslinked membranes 67

Figure 3-9 Relationship of methanol crossover to water and methanol uptake of 20Mrad crosslinked membranes 68

Figure 4-1 Experimental setup for *in-situ* humidification.....78

Figure 4-2 Structures of Proton Conducting Polymers 80

Figure 4-3 (a) Water uptake and (b) hydration number of proton conducting membranes with respect to humidity.....83

Figure 4-4 ^2H T_1 relaxation times of ^2H_2O in (a) Nafion, (b) Aquivion, and (c) S-Radel 1.95 at different magnetic fields at 25 ˚C.....86

Figure 4-5 ^2H T_1 relaxation times at 45.05 MHz for different proton conducting membranes with hydration number.....88

Figure 4-6 Conductivity versus hydration number of the different proton conducting membranes 90

Figure 5-1 Chemical structures of poly[bis(methoxyethoxyethoxy)phosphazene] (MEEP) and poly (acrylic acid) (PAA). 94

Figure 5-2 The assembly pH dependence of ionic conductivity at 100% RH (circles) and bilayer thickness (triangles). 101

Figure 5-3 The relative humidity dependence of ionic conductivity of MEEP/PAA films assembled at pH = 2.5 and pH = 3.0. Also shown is the conductivity enhancement of a dry film upon addition of a small molecule plasticizer (propylene carbonate). 102

Figure 5-4 FTIR spectra of the carboxylic acid region of MEEP/PAA multilayers assembled at pH 1.8 and 3.3 on IR-transparent ZnSe substrates. The relative intensity of peak at 1710 cm^{-1} appears to decrease as assembly pH increases. 103

Figure 5-5 DSC thermogram for a free-standing MEEP/PAA film assembled at pH = 2.5, along with neat PAA and MEEP (inset). All MEEP/PAA LbL films displayed one T_g indicative of a homogenous blend. MEEP/PAA films assembled at different pH values showed little change in T_g. 105

Figure 5-6 (a) Water vapor uptake and desorption as a function of time for MEEP/PAA LbL films assembled at pH=2.5 and pH=3.3 at 30°C. A step change in the sample chamber relative humidity from 0 to 100% occurs at t=300 s, while a step change from 100 to 0% occurs at t=3900 s. (b) Water vapor sorption isotherm at 30°C for a MEEP/PAA film assembled at pH=2.5. 107

Figure 6-1 Cyclic phosphazenes with symmetric spiro rings and novel cyclic phosphazenes with asymmetric spiro rings. 113

Figure 6-2 Stepwise introduction of amino alcohol residues. 119

Figure 6-3 Probability of non-selective isomer formation. 120

Figure 6-4 Substituent solvating effect by Goldschmidt involving a six member ring stabilized transition state. 121

Figure 6-5 The spiro cyclic P-N bond length is 1.62 Å and the P-N-C bond angle is 116˚ 122

Figure 6-6 Preference for *cis*-isomer through substituent solvating effect. 123

Figure 6-7 Molecular structure of phosphazenes **2** and **3** obtained from x-ray crystallography. 124

Figure 6-8 Crystal structure of Phosphazene 2 with benzene inclusion 126

Figure 6-9 Crystal structure of Phosphazene 3 without inclusion 127

Figure 6-10 Unit cell of phosphazene 3 with propylene sulfide and detailed view of tunnel shaped clathrate. 128

LIST OF TABLES

Table 1-1 Different fuel cell systems. 13

Table 1-2 Performance comparison between proton conducting polyphosphazenes 29

Table 2-1 Highest room temperature conductivity of different salts. 42

Table 3-1 Properties of uncrosslinked sulfonated polymers 61

Table 3-2 Performance data for crosslinked sulfonated polymers 62

Table 4-1 Property comparisons of different proton conducting membranes 82

Table 5-1 Diffusion coefficients, solubilities, and permeabilites of water in MEEP/PAA films assembled at pH=2.5 and pH=3.3, along with neat MEEP, PAA and LbL assembled PEO/PAA films (T = 30°C) 109

Table 6-1 Summary of crystal structures 125

Table 6-2 Selectivity of epoxide inclusion 129

ACKNOWLEDGEMENTS

I would like to thank my advisor, Professor Harry Allcock, for taking me under his wing and giving me the opportunity to work on such interesting research projects. I have learned greatly from you, both scientific and non-scientific, and I will be eternally grateful for the guidance and patience that you have shown me. I also thank Noreen Allcock for running the group and for keeping us in check. I shall always remember the wonderful conversations we had.

I also want to thank my collaborators whom I had the honor to work with, especially Professor Alan Benesi, Professor Michael Hickner, Dr. Hemant Yennawar, and Anne Jackson. I could not have come so far without your help.

No man is an island. To all my colleagues and friends, thanks for being there for me. I want to thank Dr. Toshiki Fushimi especially, one of the most interesting people that I have met, for teaching me that life is a battle against monotony.

Last but not least, I want to thank my parents, Kong Beng Lee and Lee Yin Fung, my siblings, William and Grace Lee, and my lovely fiancée, Lynda Goh, for their perpetual love and support. I dedicate this thesis to you, for without you I am nothing.

Chapter 1 Introduction

1.1 Polymer Electrolytes

An electrolyte is any substance that contains free ions. Usually, an electrolyte consists of salt or salts that are dissolved in a medium. However, molten salts can also be considered electrolytes. Electrolytes are an integral component in many electrochemical devices such as oxidation cells, batteries, electrochromic devices etc. The role of the electrolyte is to provide a medium for transporting ions from one electrode to another, while simultaneously functioning as an electrical insulator so that electrons travel through the outer circuit of the device. Conventional electrolytes consist of liquids, which may be caustic or sometimes flammable, such as a potassium hydroxide solution in an alkaline battery, sulfuric acid in a lead-acid battery, or the organic solvents in lithium batteries. Therefore, devices that contain liquid electrolytes must be robustly contained to prevent leakage. Furthermore, the use of liquid electrolytes is limited to use at low pressures and moderate or low temperature systems. Various solid electrolytes have been developed as alternatives to liquid electrolytes. Of the different solid electrolytes, polymer electrolytes are the most viable for widespread use. The advantages of polymer electrolytes include the ease of fabrication into various forms, especially thin films, and the low cost of manufacturing compared to other solid electrolytes. Furthermore, the weight and bulk of devices using polymer electrolytes can also be reduced because, unlike liquid electrolytes, robust containment is not required. The potential advantages of polymer electrolytes have motivated the intensive research in this area for the past few decades.

Polymer electrolytes can be used in virtually any device which conventionally depends on liquid electrolytes. The most straightforward application of polymer electrolytes is in batteries in which cations are transported from the anode to the cathode through the polymer electrolyte medium. Armand is credited as the person who recognized the potential for a polymer electrolyte to be used in batteries,[1] although Wright was the first to study the transport of ions in a polymeric material.[2] Polymer electrolytes are also applicable in cases wherein the transport of anions is required, as in electrochromic devices and dye-sensitized solar cells. The fuel cell is another application where polymer electrolytes show promise. In this case, the function of the polymer electrolyte is different from the previously mentioned devices because the conduction of protons occurs in water channels that are formed within the polymer matrix. In the other examples, the polymer itself is the medium in which ion conduction occurs.

This thesis is focused on the synthesis of polymer electrolytes and the characterization of the ion conduction mechanism in these materials for lithium battery and fuel cell applications. These are both energy conversion devices which transform chemical energy into electrical energy. The main difference between a battery and a fuel cell is that the electrical energy of a battery is limited by the amount of chemical energy that can be stored within the device, whereas a fuel cell can produce electrical energy continuously as long as fuel is supplied to it. The significance of these devices has been realized in recent years because of their ability to provide clean and quiet sources of electrical energy. Furthermore, these devices are also the cornerstone for lessening our dependence on fossil fuels for transportation. However, the utility of these two devices is still limited in vehicular applications due to their lower performance compared to the internal combustion engine. Intensive research is currently being carried out, both in the academic and industrial fields, to improve the performance and utility of these two devices.

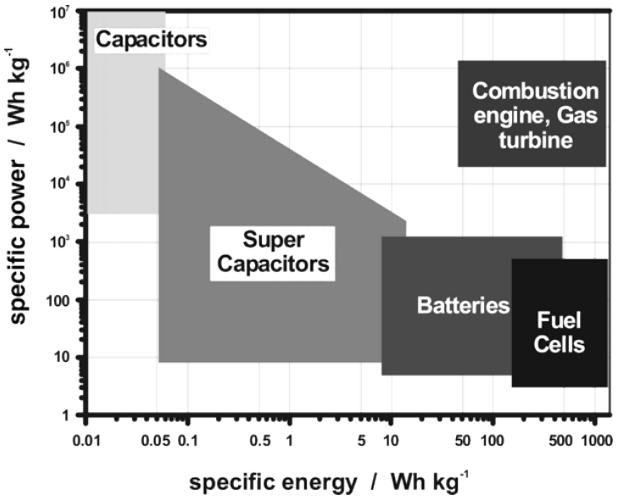

Figure 1-1 A Ragone plot comparing different energy conversion devices[3]

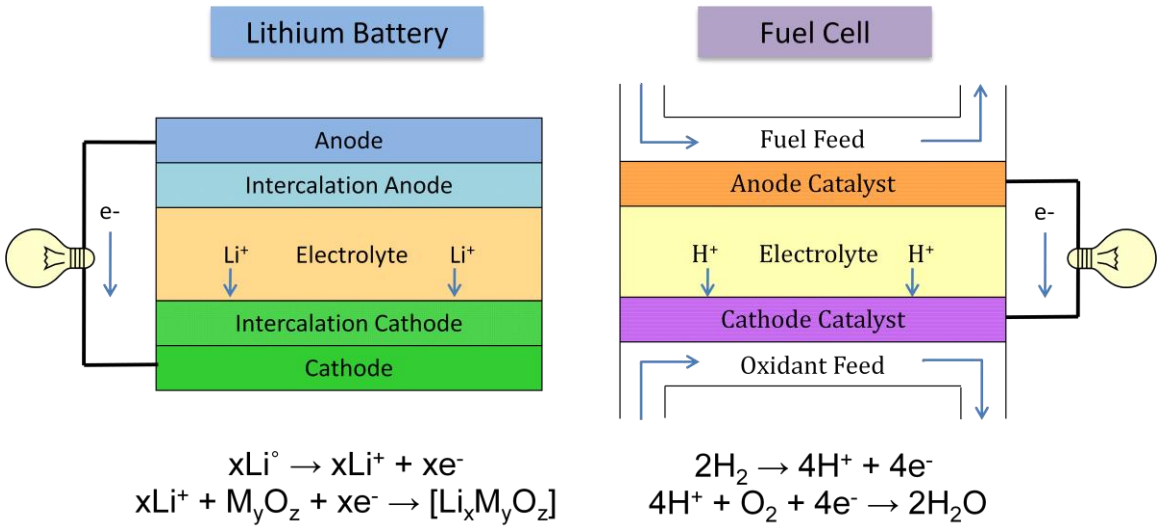

Figure 1-2 Schematic representation of a Lithium Battery and a Fuel Cell

1.1.1 Polymer Electrolytes for Batteries

The electrolyte is a vital component of a battery assembly. It provides a medium of transport for cations to migrate from the anode to the cathode. In addition to the aforementioned

advantages of using polymer electrolytes in regard to safety and reduced weight, the use of polymer electrolytes also suppresses the formation of dendrites which are detrimental to the lifetime of lithium batteries.[4] Furthermore, the rubbery properties of polymers imparts flexibility and mechanical resilience to polymer electrolytes, which is a major advantage over brittle inorganic solid electrolytes such as ion conducting solid oxides and glasses. The pliability of polymer electrolytes also allows excellent interfacial adhesion to the electrodes, and the fabrication of batteries with complex shapes.

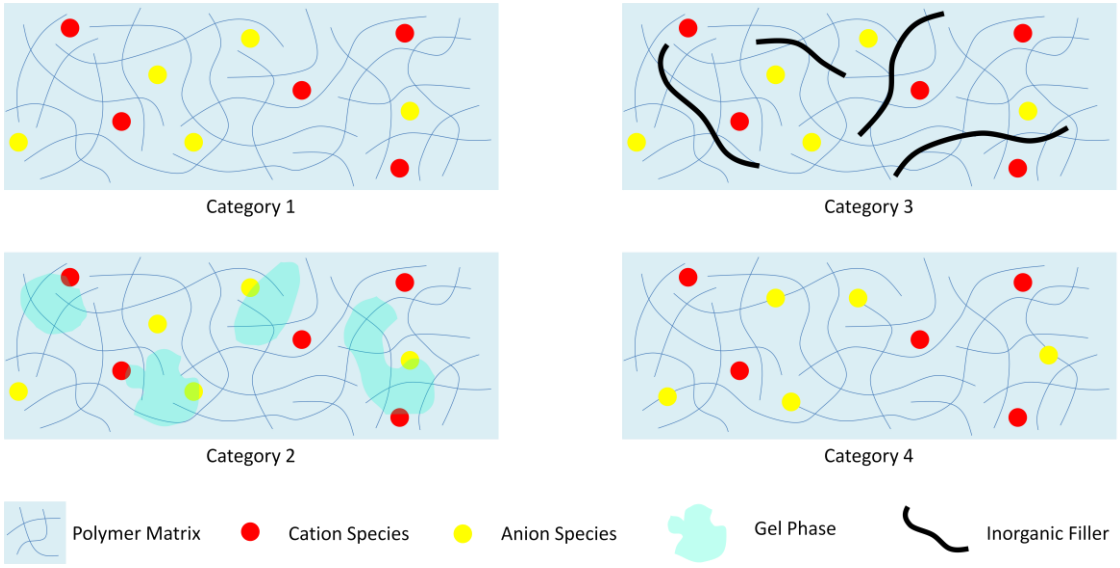

Figure 1-3 Different categories of battery polymer electrolytes

Battery polymer electrolytes can be divided roughly into four different categories.[5] Category 1 systems are solvent free, salt-polymer complexes. This is the quintessential system, developed first by Wright[2,6] who showed that poly(ethylene oxide) (PEO) was able to dissolve certain metal salts and that the solid solution exhibited ion conductivity similar to that of a liquid electrolyte. The main disadvantage of PEO:salt systems is their low conductivity, roughly 10^{-5} S/cm at room temperature. For the polymer electrolyte to be useful in a practical application, the ionic conductivity must be in the range of at least 10^{-3} S/cm. The low ionic conductivity of PEO

is attributed to its crystallinity because ion conduction only occurs in the amorphous phase. When the operating temperature is increased above the melting temperature of PEO (~65 ˚C), ionic conductivity values of 10^{-3} S/cm are attainable.[7]

Category 2 systems are gel electrolytes, which are polymers that contain small molecule additives. Commonly used additives include cyclic carbonates, esters and sulfones which are chosen for their ion solvating ability, low volatility, and relative electrochemical stability.[8] The addition of small molecule additives typically lowers the mechanical strength of a polymer electrolyte and hence the term "gel" is used. The role of the additive depends on the relative amount that is present in the polymer system. When the additive content is low, it functions as a plasticizer to reduce polymer crystallinity and lower the glass transition temperature (T_g). This increases the mobility of the polymer chains, which in turn promotes ion conduction. A suitable choice of plasticizer can increase the ionic conductivity to 10^{-2} S/cm. As the proportion of the small molecules is increased, the polymer ceases to function as the medium for ion conduction and that role is taken over by the small molecules. In this case, the polymer merely acts as a supporting matrix to provide dimensional stability to the liquid component. Some argue that this is not a true polymer electrolyte system. However, these systems are attractive due to their high ionic conductivity, which resembles liquid systems, while they are still able to incorporate some of the advantages of a true polymer electrolyte such as better mechanical stability and lowered dendrite formation. This has led to the commercialization of such solvent-swelled systems by companies such as Sony[9] (undisclosed components) and Bellcore[10] which uses an inert polymer, poly(vinylidene fluoride-co-hexafluoropropylene), and cyclic carbonates.

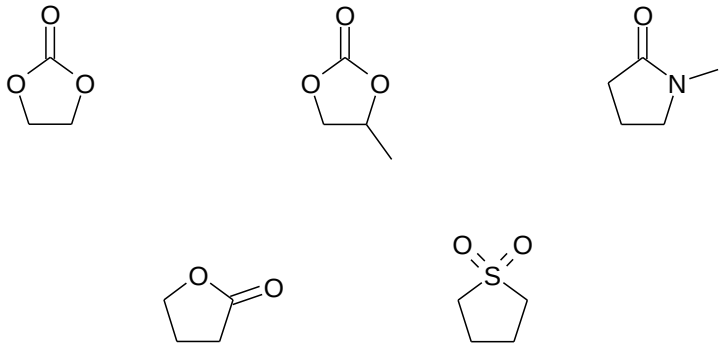

Figure 1-4 Common small molecule additives for gel polymer electrolytes. Clockwise from top left: ethylene carbonate, propylene carbonate, N-methyl pyrrolidone, tetramethylene sulfone, γ-butyrolactone.

In Category 3 systems, another type of additive in the form of inorganic fillers is added to the polymer electrolyte to form composites. Typical inorganic fillers used are micro or nanoparticles of Al_2O_3, SiO_2, TiO_2, and MgO.[11] Layered silicates such as montomorillonite are also used.[12] The addition of inorganic fillers brings many improvements to the polymer electrolyte. First, the mechanical properties of the polymer electrolyte are reinforced by the inorganic filler. An increase in T_g occurs, which typically results in the decreased ionic conductivity. Paradoxically, a two- to five-fold increase in ionic conductivity is often detected in systems with Al_2O_3. The increase in conductivity is attributed to two reasons. First, the addition of inorganic particles suppresses the formation of crystalline phases, thus increasing the volume fraction of the amorphous phase.[13] Secondly, cation conduction can occur on the grain boundaries of the inorganic particles and this provides a faster alternative ion conduction mechanism, similar to that of ceramic electrolytes.[14] The advantages of composite polymer electrolytes may bring the possibility of a completely solvent-free system closer to reality.

Finally, Category 4 systems are single-ion polyelectrolytes. In other words, these polymers have immobilized anions linked to the polymer chain so that the lithium cation is the only mobile species within the polymer matrix.[15] There are many advantages to immobilizing the

anion. First, in a Category 1 system, the anion may be the dominant mobile species.[16] The mobility of the anion is higher than the cation because the anion is not coordinated to the polymer. Hence, reported bulk ion conductivity values are often misleading when the transference numbers of the different ionic species are not taken into consideration. The high mobility of the anion in Category 1 systems causes concentration polarization across the cell which reduces the total ionic conductivity. Furthermore, passivitation of the electrode also occurs when unstable anions react with the surface of the electrode. Unfortunately, the immobilization of anions on a polymer often leads to lower conductivities (10^{-6} S/cm) due to associated ion species. These associated ion species participate in the ion conduction mechanism in Category 1 systems in a way that is not fully understood. By immobilizing the anion, the contribution of these associated ion species to ion conduction is not only limited, but the associated ion species also crosslink the polymer. Therefore, plasticization in Catergory 4 systems is often required to obtain reasonable conductivity.

The requirements for a successful polymer electrolyte in practical applications are listed below.[5]

- High ionic conductivity of at least 10^{-3} S/cm. (If possible, a cation transference number of 1.)
- High electronic resistivity.
- Good mechanical and dimensional strength.
- Good interfacial contact with the electrodes.
- Chemical and thermal stability.
- Ease of processing.
- Non-hazardous.

In practice, it is hard to achieve all the desired properties from the improvements within a single class of materials. However, by combining the strategies from different categories, it is possible

to maximize the advantages of a particular system while suppressing the disadvantages of another system. Therefore, an in-depth understanding of the ion conduction mechanism is advantageous for the design of a future polymer electrolyte system that will fulfill all the requirements.

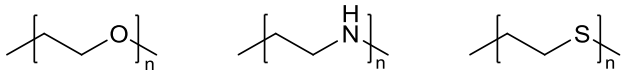

Figure 1-5 Polymers with cation solvating capability

1.1.2 Polymer Structures for Secondary Lithium Battery Electrolytes

The most basic requirement of a polymer electrolyte is the ability to solvate ions. For a lithium battery electrolyte, the lithium cation can be solvated by electron lone pairs at oxygen, nitrogen or sulfur in polyethers, polyesters, polyamines or polythiols.[17] The solvation enthalpy of a salt in a polymeric solvent depends on the cation-polymer interaction which can be described according to hard/soft acid base principle (HSAB).[18] For a hard cation such as lithium, the strongest interaction is with hard oxygen atoms. Furthermore, the poly(ethylene oxide) repeat unit (CH_2CH_2O) provides the best spacing for the solvation of lithium. Therefore, most polymer electrolyte structures are based on poly(ethylene oxide) and derivatives thereof.

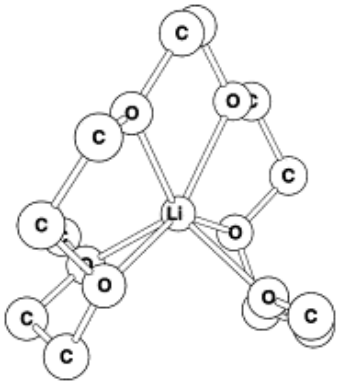

Figure 1-6 One stable geometry for Li^+-pentaglyme obtained using ab initio electronic structure calculations. Hydrogen atoms were omitted for clarity.[19]

PEO may appear to be the perfect polymer electrolyte from the advantages mentioned above; however the high crystallinity of PEO, which can be as high as 65%, hinders its ability for ion conduction. One of the strategies to produce an amorphous polymer without the addition of plasticizers is the synthesis of comb branched polymers. Typical designs have short ethyleneoxy chains grafted onto various polymer backbones. The comb architecture enhances ion conductivity in two ways. First, the short side chain increases the free volume of the polymer chain which suppresses crystallinity and lowers T_g. Secondly, the ion conduction occurs through the side chains, and thus it is decoupled from the backbone polymer chain. Because the polymer backbone is not vital to the ion conduction mechanism, various organic polymer backbones such as polymethacrylate,[20] polyitaconate,[21] and PEO[22,23] have been investigated. Comb polymers with flexible inorganic backbones, such as polyphosphazenes[24] and polysiloxanes,[25] have also been investigated. Conductivities of 10^{-4} S/cm at 25 ˚C and 10^{-3} S/cm at 80 ˚C were observed in a polyphosphazene:LiTFSI system, which is tantalizingly close to the touchstone ionic conductivity at room temperature for a solvent free system.[26] One of the disadvantages is the poor dimensional stability of the polyphosphazene which causes it to flow even at room temperature. Strategies to enhance the dimensional stability of the polymer are discussed in a later section.

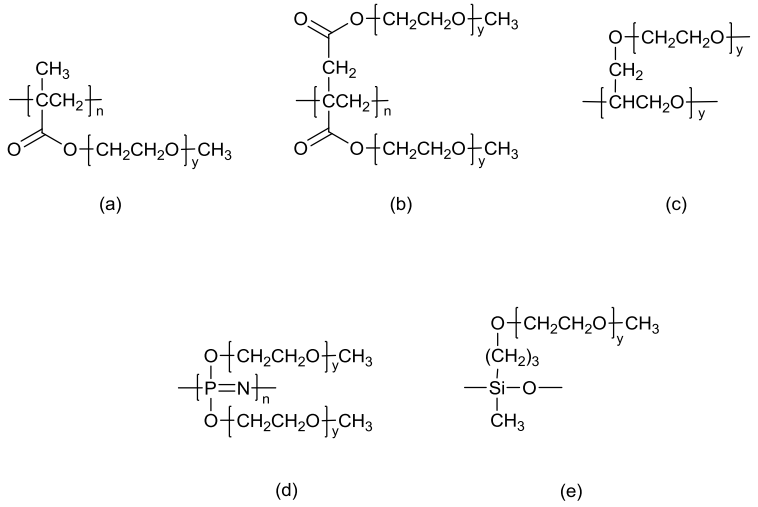

Figure 1-7 Comb branched polymer electrolyte structures (a) polymethacrytale, (b) polyitaconate, (c) poly(ethylene oxide), (d) polyphosphazene, and (e) polysiloxane

1.1.3 Ionic Transport Mechanism in Lithium Battery Electrolytes

Crystalline PEO chains have a helical conformation. In the late 1970s, researchers postulated that the lithium cation is able to migrate by a tunneling mechanism inside the polymer helix. This has now proved to be untrue because the helical conformation of PEO is not able to solvate the cation. Furthermore, observations of a dramatic increase in ion conductivity above the T_m of PEO (65 ˚C) is strong evidence that the amorphous phase is responsible for ion conduction. However, even in a totally amorphous polymer, the ionic conductivity is still slow compared to a liquid system because the motion of ions is coupled to the segmental motion of the polymer. Crankshaft torsional motions around the C-C and C-O bonds allow segmental motion of the polymer and thus ion migration through the polymeric medium. This view is still an oversimplification of the real mechanism because incompletely dissociated species have been found to assist in ion conduction by providing hopping sites.[27] After four decades, many researchers are still studying the ion conduction mechanism by spectroscopic and computational methods.

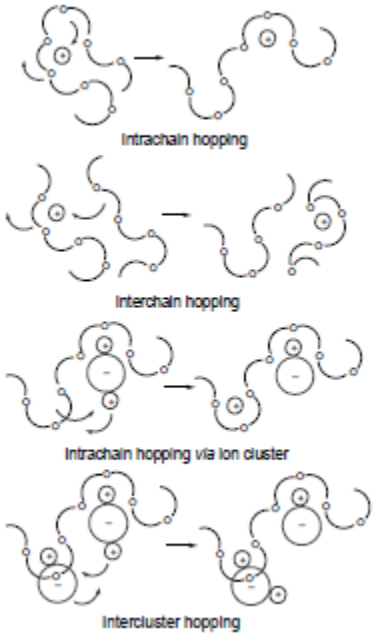

Figure 1-8 Cation migration mechanisms in a polymer electrolyte[17]

The temperature dependence of ionic conductivity in a polymer system can be modeled by the Vogel-Tamman-Fulcher (VTF) equation.[28] The equation was initially devised to describe reactions in viscous liquids and is similar to the Arrhenius equation.

$$k = Aexp\left[\frac{E_a}{RT}\right] \qquad \text{Arrhenius Equation}$$

$$\sigma = \sigma_0 exp\left[\frac{-B}{T-T_0}\right] \qquad \text{VTF Equation}$$

In the VTF equation, σ_0 is a pre-exponential factor related to the number of charge carriers. The B term is related to the E_A term in the Arrhenius equation and has the dimensions of Kelvin units, but cannot be regarded as a simple activation energy. T_0 is the ideal glass transition temperature at which ion mobility goes to zero. Above T_0, thermal motion of the polymer chains initiates the transport of ions. T_0 is sometimes set as T_g but is usually found to be 30 – 50 K below T_g.

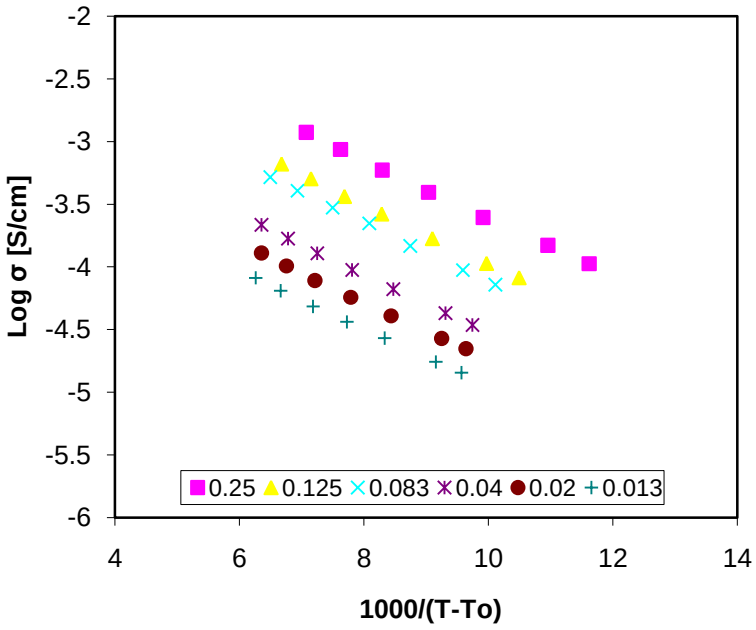

Figure 1-9 A polyphosphazene electrolyte exhibiting VTF behavior. Numbers in the legend represents the repeat unit to salt ratio [MEEP:Salt].[26]

1.1.4 Polymer Electrolytes for Fuel Cells

Fuel cells are electrochemical devices that convert chemical energy into electrical energy. Different fuel cell systems are differentiated mainly by the type of electrolyte used and these are summarized in the table below.[3] Different systems have their advantages and disadvantages. However, the proton exchange membrane fuel cell (PEMFC) and the direct methanol fuel cell (DMFC) are the most suitable for consumer-type applications due to the low operating temperatures and high power density.

Table 1-1 Different fuel cell systems.

Design	**Electrolyte**	**Operating Temperature (˚C)**	**Comments**
Proton Exchange Membrane	Polymer Membrane	60 - 90	Expensive catalyst, CO poisoning, water management
Direct Methanol	Polymer Membrane	60 - 90	MeOH crossover, high catalyst loading, water management
Alkaline	Aqueous KOH Solution	20 - 80	Used in Apollo space program, limited life, caustic electrolyte
Phosphoric Acid	Molten Phosphoric Acid	200	Caustic electrolyte, low conductivity
Molten Carbonate	Molten Sodium Bicarbonate	500	Fast electrode kinetics, limited life, high operating temperature
Solid Oxide	Proton Conducting Ceramic Oxide	900	High operating temperature, severe material constraints, fast kinetics

The reactions in the proton exchange membrane fuel cell and the direct methanol fuel cell are as follows:

	PEMFC	**DMFC**
Anode:	$H_2 \rightarrow 2H^+ + 2e^-$	$CH_3OH + H_2O \rightarrow 6H^+ + 6e^- + CO_2$
Cathode:	$½O_2 + 2H^+ + 2e^- \rightarrow H_2O$	$^3/_2\ O_2 + 6H^+ + 6e^- \rightarrow 3H_2O$
Overall:	$½O_2 + 2H^+ \rightarrow H_2O$	$CH_3OH + {}^3/_2\ O_2 \rightarrow 2H_2O + CO_2$

Fuel in the form of hydrogen or methanol is separated into protons and electrons or protons, electrons and CO_2 by a catalyst in the anode of the fuel cell. The function of the polymer electrolyte in the fuel cell is to transport protons generated at the anode to the cathode where they react with oxygen to form water. The atmosphere is usually the source of oxygen. Unlike battery polymer electrolytes, in most cases proton conduction is not coupled to the polymer internal motion. Rather, the fuel cell membrane is swollen with water, causing the polymer to phase-

separate into hydrophilic and hydrophobic domains. Therefore, the main medium for proton conduction is the water molecules that swell the polymer.

Required properties for polymer electrolytes for fuel cells are:[29]

- High protonic conductivity (10^{-1} S/cm)
- High electronic resistivity
- Low permeability to fuel and oxidant
- Low water transport through diffusion and electro-osmosis
- Oxidative and hydrolytic stability
- Good mechanical properties in both dry and hydrated states
- Capability for fabrication into membrane electrode assemblies

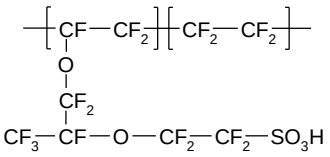

Nafion

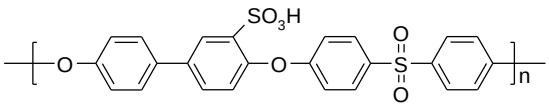

S-Radel

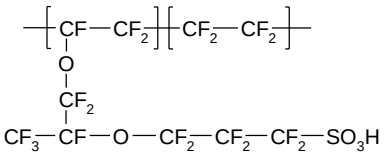

Aciplex

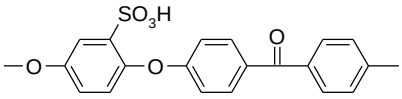

S-PEEK

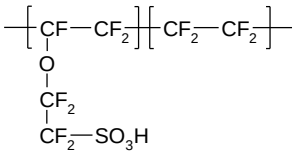

Aquivion

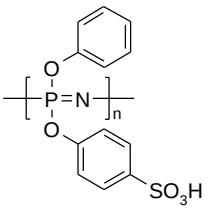

S-DPP

Figure 1-10 Various proton conducting polymer structures

1.1.5 Chemical Structure and Morphology of Proton Conducting Membranes

Most polymer designs used as proton exchange membranes share a few common traits. Typical polymer backbones are either a perfluorinated alkyl polymer or a poly(arlyene ether). These two polymer backbones are preferred due to their excellent hydrolytic and oxidative stability, which is required to withstand the harsh conditions in a fuel cell. Furthermore, these polymers are hydrophobic and thus they will phase-separate when swelled with water. Although perfluorinated polymers typically show higher proton conductivities than poly(arlyene ethers), there is an impetus to develop poly(arylene ether) polymers due to their lower cost, higher resistance to methanol crossover and lower environmental impact.

Most proton conducting polymers also contain acidic groups which are linked to the polymer to provide protons for conduction. The arylsulfonic acid or perfluorosulfonic acid groups are attached directly to the polymer backbone or tethered by a spacer respectively. Sulfonic acid groups are preferred because they can be introduced to the polymer by directly incorporating the sulfonic acid moiety in the monomer or through post-polymerization sulfonation by reacting the polymer with a sulfonating agent. Although phosphonic acid groups are possible acidic sites, they are less preferred due to their lower acidity and more challenging synthesis. Perfluorosulfonic acids have higher acidity than arylsulfonic acids because of the electron-withdrawing fluorine atoms which are able to draw electron density from the sulfonate ion, thus stabilizing the negative charge.

The main disadvantage of the above mentioned polymer systems is the need for water to conduct protons. Therefore, the operating temperature of these proton conducting polymers is limited to below 80 ˚C unless the fuel cell system is pressurized. Researchers are seeking novel polymers that can conduct protons in the absence of water or in low humidity.[30] These novel polymers bear either imidazole or triazole heterocyclic rings because of their ability to undergo a

Grotthuss chain mechanism of proton conduction. However, the proton conductivity of these systems is much lower because the kinetics of proton transfer of the larger heterocycles is much slower than in water. It is also dependent of the T_g on the polymer as evidenced by the VTF behavior of the proton conductivity. Hence, imidazole-functionalized polysiloxanes have been investigated, but the highest proton conductivity obtained was still only 10^{-3} S/cm at 160 ˚C.[31]

In water, proton conduction proceeds via two mechanisms. The main mechanism is through proton hopping between water molecules, also known as the Grotthuss chain mechanism. The other mechanism, which is only significant at low levels of hydration, is the vehicle mechanism in which the protons are carried by Zundel ($H_5O_2^+$) or Eigen ($H_9O_4^+$) ion.[32] Due to the complexities of water-water and water-polymer interactions, an understanding of the proton conduction mechanism in proton exchange membranes is still being developed. Extensive reviews on the subject have been written by Kreuer[33] and Paddison[34]

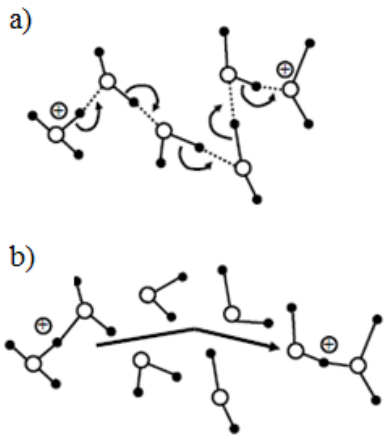

Figure 1-11 Proton conduction mechanisms: a) Grotthuss chain and b) vehicle mechanism[33]

The morphology of proton exchange membranes is perhaps the most important factor in determining the performance of the membrane. The absorption of water is not uniform throughout the membrane as the polymer phase separates into hydrophobic and hydrophilic phases. The hydrophobic phase consists of either amorphous or microcrystalline polymer chains and provides mechanical stability to the membrane. The hydrophilic phase consists of nanometer sized water domains in which proton conduction occurs. The size, shape and connectivity of these pores is the subject of intensive research because it affects the proton conductivity and methanol permeability of the membrane. Factors that affect morphology include chemical composition of the polymer, molecular weight, and degree of crosslinking to name a few. The morphology can also be affected by processing and thermal history. In general, perfluorinated polymers such as Nafion, which has a lower T_g and higher hydrophobicity, generate larger and more interconnected pores. Conversely, poly(arlyene ethers) have smaller, less connected pores because the polymer backbone is stiffer and less hydrophobic.[35] The larger pores give higher proton conductivity but also result in higher methanol permeability. It is evident that the control of morphology, and consequently water management in the fuel cell membrane is vital to its performance.

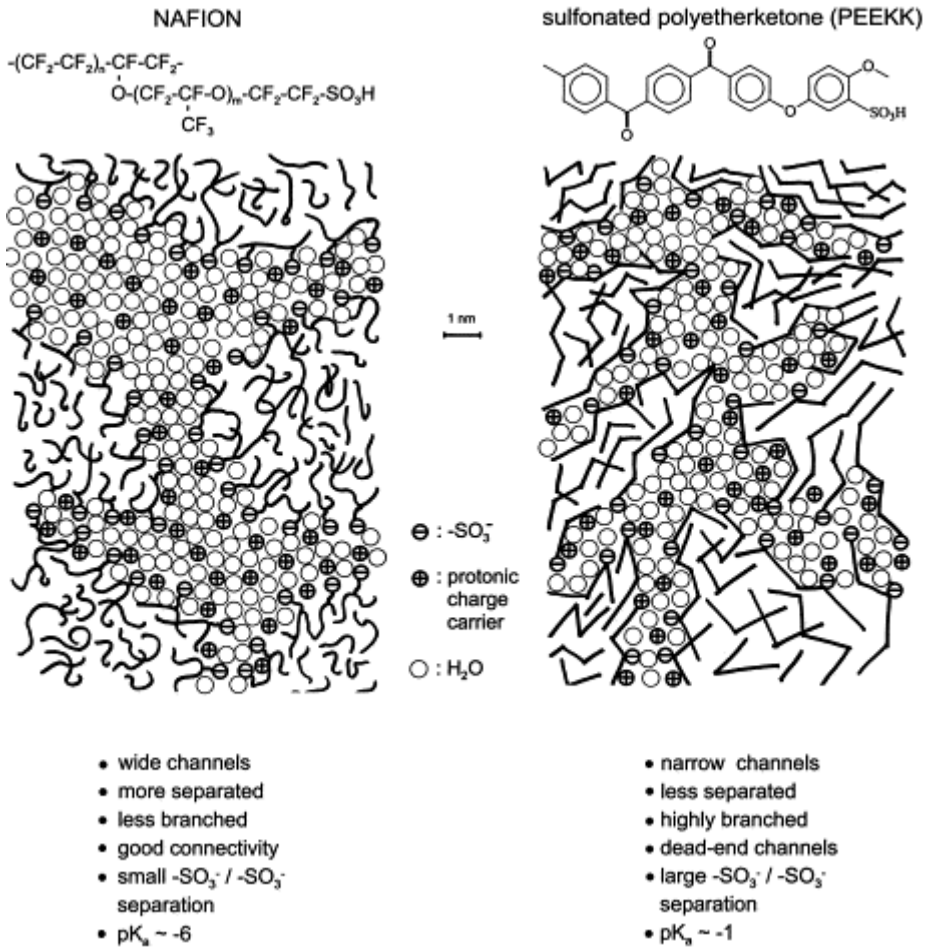

Figure 1-12 Morphology comparison between Nafion and sPEEKK[36]

1.1.6 Current State of Polymer Electrolytes

The research and development of polymer electrolytes is crucial for the advancement of both lithium battery and fuel cell technologies. Polymer electrolytes offer many advantages compared to other electrolytes in their respective fields but there are still serious technical hurdles to be overcome before polymer electrolytes can undergo more widespread use. It is vital to gain an intimate understanding of the conduction mechanism in order to design the next generation of polymer electrolytes. Furthermore, the addition of non-polymeric components such as inorganic fillers and small molecules might be necessary for polymer electrolytes to fulfill the requirements.

Therefore, a close collaboration between scientists from synthetic, fabrication and analytical backgrounds will be vital for the success of polymer electrolytes.

1.2 Phosphazenes

1.2.1 Background and History of Polyphosphazenes

Phosphazenes are a class of compounds in which a phosphorus atom is joined to a nitrogen atom by formal a double bond and to three other atoms by single bonds. Phosphazenes are formed in a wide variety of configurations from small molecules, to cyclic species in which the ring consists of alternating phosphorus and nitrogen atoms, to linear oligomers and high polymers with −P=N− repeating units. Research in the Allcock group has focused on the synthesis and characterization of rings, short chains, and linear high polymers.

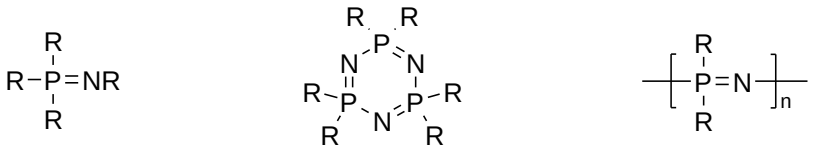

Figure 1-13 Various structures of phosphazenes

The starting material for most phosphazene reactions are chlorophosphazenes. The first reported synthesis of chlorophosphazenes was in 1834's when Rose reacted PCl_5 with NH_3 to yield a white crystalline solid.[37] Six decades later, Stokes proposed that this solid was hexachlorocyclotriphosphazene $(NPCl_2)_3$ which has a cyclic structure. He also identified higher cyclic homologues with up to seven repeating units of $(NPCl_2)$.[38] Furthermore, he detailed a description on how to thermally polymerize these chlorophosphazenes to produce an insoluble,

elastic "inorganic rubber", which was found to be hydrolytically unstable. A new synthetic method that produced higher yields of hexachlorocyclotriphosphazene was devised by Schlenk in 1924 which involved reacting PCl_5 with NH_4Cl, instead of NH_3.[39] However, it was not until the 1960s when Allcock, Kugel, and Valan published groundbreaking work which demonstrated that soluble polyphosphazenes can be synthesized by controlling the conditions of the thermal polymerization of hexachlorocyclotriphosphazene to yield soluble poly(dichlorophosphazene).[40] They also found that the chlorine atoms can be replaced easily by a broad array of nucleophiles such as alkoxides and amines. This facile macromolecular replacement of chlorine atoms allows a high level of tailorability of the polyphosphazene side group structures and affords a broad range of polyphosphazenes with different properties. Currently, more than 500 polyphosphazenes have been made and are studied in many countries for various applications, such as optical materials, biomedical materials, and polymer electrolytes.[41,42,43]

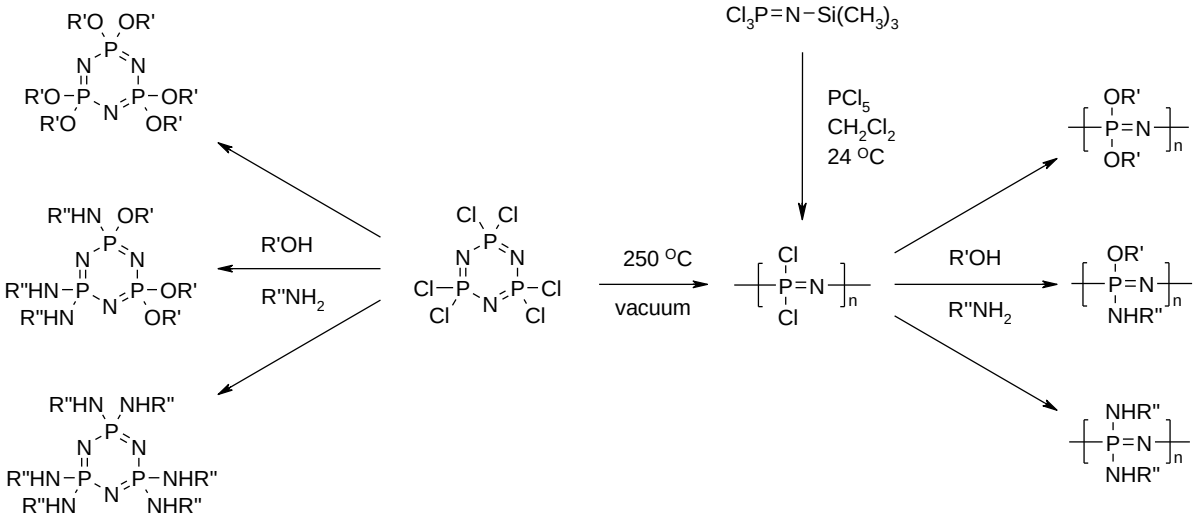

Figure 1-14 General polymerization and reactions of phosphazenes

1.2.1 Polymerization Methods

Even though the thermal ring-opening polymerization of hexachlorocyclotriphosphazene was developed almost half a century ago, it is still the most widely used method for obtaining poly(dichlorophosphazene). The key to obtaining a soluble product lies with the starting material. Hexachlorocyclotriphosphazene must be purified extensively, first by recrystallization in hexanes, and then by sublimation, before it can be used in the polymerization. The reason for the formation of the 'insoluble inorganic rubber' that was obtained by Stokes was the presence of impurities, such as water and residual PCl_5, which cause side reactions in the poly(dichlorophosphazene) and crosslink the polymer. The purified hexachlorocyclotriphosphazene is then sealed under vacuum in a Pyrex tube and placed in an oven, which is set at 250 ˚C, for 8 – 12 hours.[41] After the polymerization is complete, the Pyrex tube is broken under inert atmosphere and the residual unpolymerized hexachlorocyclotriphosphazene is removed by sublimation. Typical yields by the thermal ring opening polymerization are 70 – 75%.

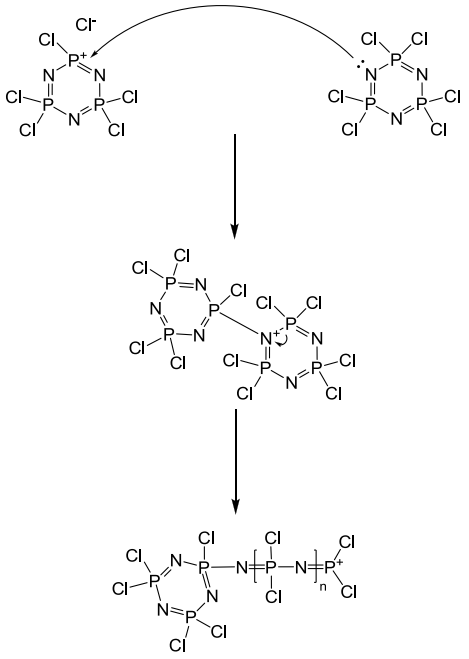

Figure 1-15 Cationic ring-opening polymerization of hexachlorocyclotriphosphazene

The mechanism of the thermal ring-opening polymerization is believed to occur via a cationic ring-opening route.[44] Initially, one of the P-Cl bonds in hexachlorocyclotriphosphazene is thermally ionized to produced a phosphazenium ion. This cation then attacked by the lone pair electrons from the nitrogen atom of another hexachlorocyclotriphosphazene molecule, which results in ring cleavage. The cationic charge then resides on the terminal phosphorus and the process repeats itself to create chain propagation.

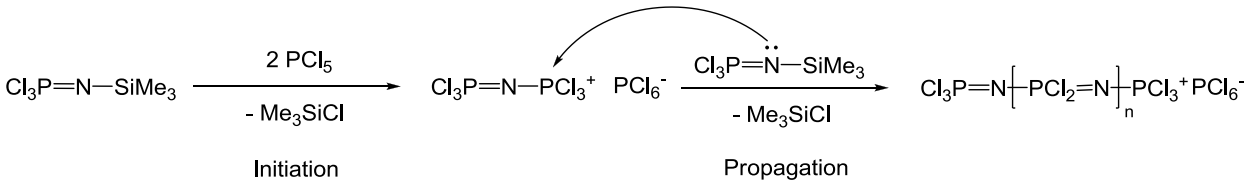

Figure 1-16 Cationic condensation polymerization of trichloro(trimethylsilyl)phosphoranimine

There are inherent disadvantages to the thermal ring opening polymerization method, such as poor molecular weight control, high polydispersity indices and the need for an elevated

polymerization temperature. Hence, the need exists for an alternative polymerization method that will lead to more controllable molecular weights and lower polymerization temperatures. Recently, an ambient temperature solution synthesis of poly(dichlorophosphazene) was developed by Allcock and Manners.[45] The polymerization process involves the treatment of trichloro(trimethylsilyl)phosphoranimine ($Cl_3P{=}NSiMe_3$) with trace amounts of a cationic initiator, phosphorus pentachloride (PCl_5). The reaction starts with the formation of the PCl_4^+ PCl_6^- ion pair. The PCl_4^+ cation displaces the trimethylsilyl chloride group. From then on, the propagating cationic species continues to react with the remainder of the monomer molecules until the monomer is depleted. By varying the ratio of monomer to initiator, polyphosphazenes with controlled molecular weights and low polydisperisty indicies can be obtained. Another significant advantage of this polymerization method is that an initiating site can be placed on different molecular structures to form polyphosphazenes with various geometries such as block, comb or star architectures.

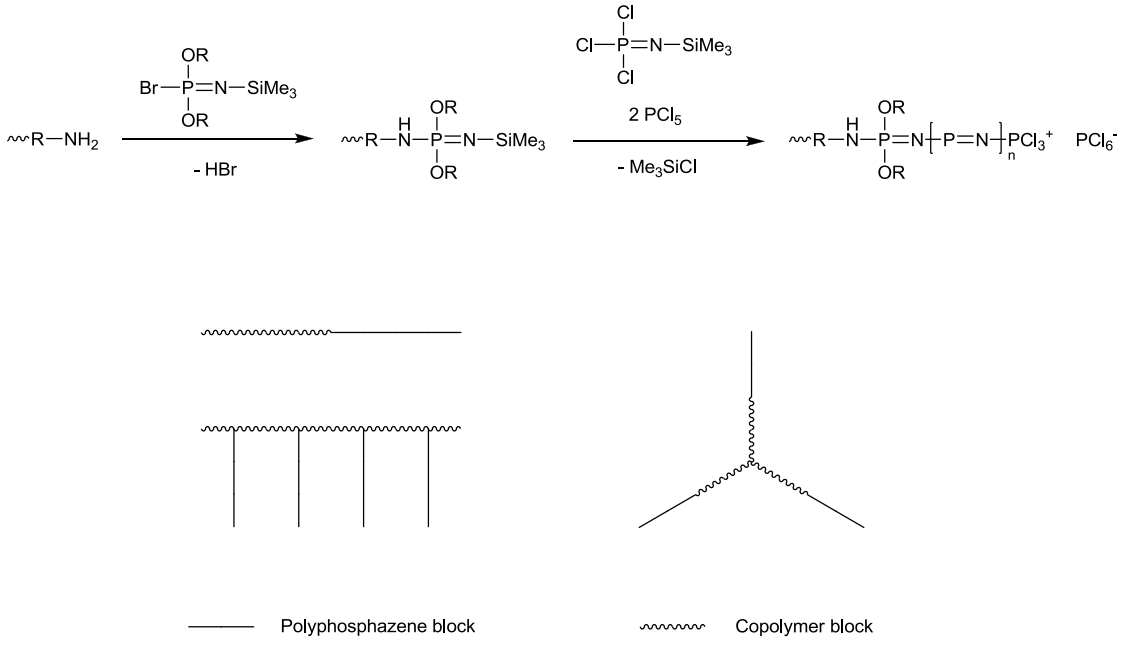

Figure 1-17 Alternate polyphosphazene geometries

1.2.1 Properties of Polyphosphazenes

The unique inorganic backbone of polyphosphazenes offers certain advantages over conventional organic polymers. First, the P-N phosphazene bond has a very high torsional mobility which leads to polymers with very low glass transition temperatures (T_g), often as low as -100 ˚C. The low T_g is in the same range as another inorganic backbone polymer, polysiloxanes. It is unusual for a polymer backbone with alternating single-double bonds to have such a high level of flexibility, but the bonding behavior of the phosphazene backbone is unusual because of the participation of the *d*-orbitals from the phosphorus atoms, and thus cannot be explained simply by a valence bond model. Various theories have been put forward to explain the bonding structure in polyphosphazene but the topic is still being debated.[41] The low T_g of polyphosphazenes make them advantageous as low temperature elastomers.

Secondly, the fire-resistance of polyphosphazenes is another property that is particularly useful. When poly(aryloxyphosphazenes) are added to polyurethanes at a weight ratio of 20%, the materials show self-extinguishing behavior.[46] Two mechanisms contribute to the fire-resistance of polyphosphazenes. The first is the formation of a ceramic-type char during the combustion of polyphosphazenes which forms an insulating layer that prevents the propagation of the fire to the rest of the material. The other mechanism is believed to be the radical scavenging ability of polyphosphazene decomposistion products which terminate the radical chain reactions that occur at the flame front.[47] The fire retarding ability of phosphazenes makes them an attractive alternative to toxic bromine or chlorine containing fire retardants, which are currently being phased out.

Third, the polyphosphazene backbone has a wide window of optical transparency which ranges from the near infrared region to the mid-UV region of the electromagnetic spectrum.[48] The high transparency of the polyphosphazene backbone underlies the development of

polyphosphazenes as optical materials.[41] Recently, Fushimi and Allcock have synthesized a new class of polyphosphazene materials which have a high refractive index (n = 1.65 @ 598 nm) and low optical dispersion (ν = 39).[49] The high refractive index of this material is comparable to inorganic glasses a property that is attributed to the high electron density in the phosphazene backbone. The advantage that this material has over inorganic glasses is the low molding temperature which allows the formation of lenses at temperatures of only 165 ˚C. The transparency of the phosphazene backbone is also exploited to make liquid crystalline polymers[50] and non-linear optical materials.[51]

Perhaps the most important influence on the properties of polyphosphazenes is the type of side groups that are attached to the backbone. Side groups can be linked to the polyphosphazene backbone through a P-C, P-O or P-N linkage. P-C linkages are hydrolytically stable, but difficult to incorporate into polyphosphazenes. The P-O linkage yields polyphosphazenes that are also hydrolytically stable. One of first polyphosphazenes synthesized contained fluoroalkoxy side groups. Conveniently, they are also some of the most useful polyphosphazenes. The fluorinated alkoxy side groups impart chemical stability and hydrophobicity to the polyphosphazene.[52] Coupled with the inherently low T_g from the phosphazene backbone, poly(fluoroalkoxyphosphazenes) are commercialized as solvent resistant, low temperature elastomers under the trade name Eypel-F® and PN-F®. When non-fluorinated ethyleneoxy groups are attached to the polyphosphazene, a very hydrophilic material is created. Furthermore, the cation solvating ability of ethyleneoxy groups allows dissolution of various metal salts in the polyphosphazene. Bulky aryloxy side groups are chosen to produce polyphosphazenes with higher T_gs. The aryloxy substituents prevent free rotation around the phosphazene skeletal bonds and force the polymer to assume a cis-trans conformation.

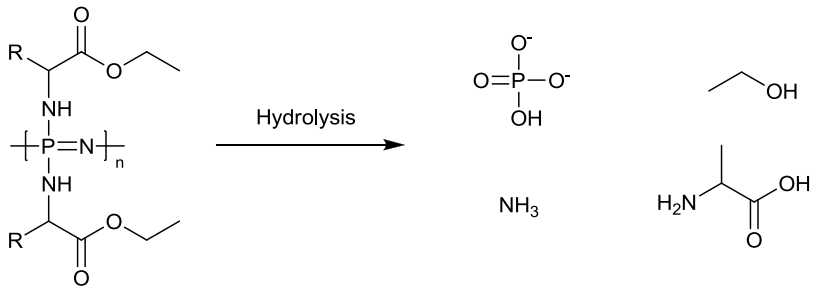

Figure 1-18 Degradation of amino acid substituted polyphosphazenes

Conversely, a P-N side group linkage can be hydrolytically unstable. This feature can be utilized to make erodible polymers for biomedical materials for hard tissue repair and drug delivery.[53] When polyphosphazenes bear amino acid esters side groups, such as alanine, valine or phenylalanine, the hydrolytic degradation products are phosphates, ammonia, and the amino acid which are bioacceptible.[54] For uses as biomaterials, polyphosphazenes are usually blended with poly(lactic-co-glycolic acid) (PLGA), which is a commonly used as biodegradable materials but degrades into acidic products that causes cell necrosis. An advantage of the polyphosphazene-PLGA blends is that the degradation products from the polyphosphazenes buffer the acidic degradation products formed by PLGA. An additional quality of degradable polyphosphazenes is that the rate of degradation can be tuned by variations to the side group structures. Polyphosphazenes with sterically hindered or hydrophobic amino acid groups, such as phenylalanine ester, have a slower degradation rate than polyphosphazenes with alanine ester as a side group. Hence, the rate of degradation can be controlled by the type and the ratio of the side groups attached to the polymer.

1.2.4 Polyphosphazene Electrolytes

One of the most actively researched areas in the Allcock research group in recent years is the use of polyphosphazenes as electrolytes. The first investigation of a polyphosphazene electrolyte was in 1984.[55,56,57] The polyphosphazene of interest was poly[bis(2-(2-methoxyethoxy)ethoxy)phosphazene] or MEEP. MEEP showed ionic conductivities three to four orders of magnitude higher than PEO when combined with lithium salts. There are several reasons for the high ionic conductivity of MEEP. First, salts are able to dissociate in the MEEP matrix because the etheric oxygens, and perhaps the backbone nitrogen atom also, are able to solvate the cation and hence promote dissociation. The high degree of dissociated species leads to more mobile charge carriers. Secondly, the inherent flexibility of the polyphosphazene backbone and the side chains impart a low glass transition temperature (Tg = −84 ˚C) to the polymer. Because ionic conduction is coupled to macromolecular flexibility, it is vital to have a low T_g polymer to aid in ion transport. Finally, MEEP is completely amorphous. It has been established that ionic conduction only occurs in amorphous regions of PEO. Therefore, MEEP exhibits some of the highest conductivities for an unplasticized polymer electrolyte system. The combination of these factors make MEEP a very attractive material for use in polymer electrolytes for lithium batteries.

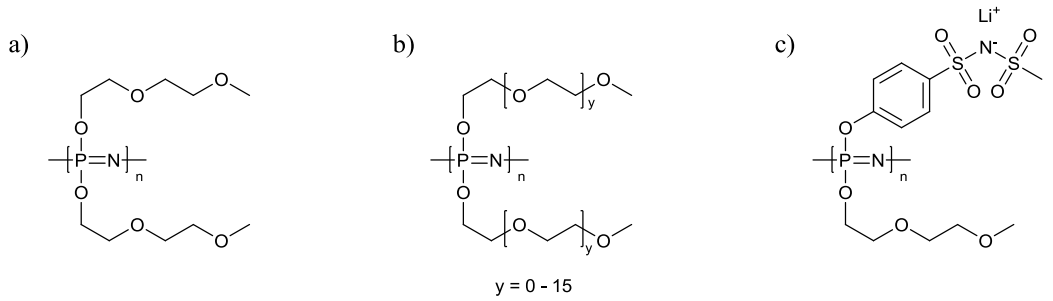

Figure 1-19 Ion conducting polyphosphazene electrolytes a) MEEP, b) polyphosphazene with varying ethyleneoxy chain length, and c) single-ion polyphosphazene

The main disadvantage of MEEP is the low dimensional stability. However, MEEP can be crosslinked by γ-irradiation,[58] uv-induced crosslinking[59] and by the sol-gel techniques.[60] This does not increase the T_g significantly because only a limited number of ethyleneoxy side chains are crosslinked and the polyphosphazene backbone is unaffected. Because the T_g is not affected, the ionic conductivity is also unaffected. Polyphosphazenes with longer ethyleneoxy chain lengths were also investigated.[61] It was found that the ionic conductivity increases with chain length until eight ethyleneoxy units (CH_2CH_2O) are in the side chains. Beyond eight units, the ethyleneoxy side chains begin to crystallize and conductivity is adversely affected. Polyphosphazene single ion polyelectrolytes were also synthesized.[62] Attachment of sulfonimide groups to the polyphosphazene backbone increased the T_g significantly. In addition to immobility of the anions, the ionic conductivity of this polymer was an order of magnitude lower compared to a MEEP system with the same salt concentrations. However, an ion conductivity of 10^{-3} S/cm at room temperature was achieved when the polymer was swelled with *N*-methyl-2-pyrolidinone.

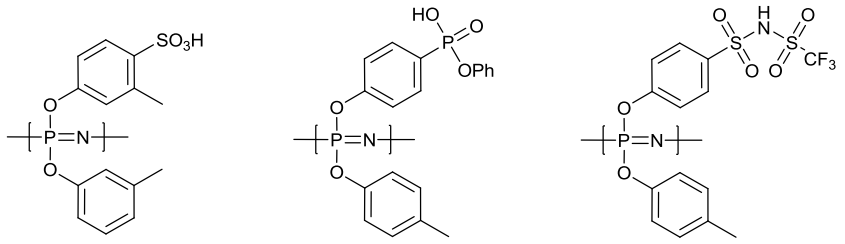

Figure 1-20 Proton conducting polyphosphazene architectures

Polyphosphazenes have also been investigated for fuel cell applications. Initial investigations of proton conducting polyphosphazenes were carried out by Pintauro who sulfonated poly[bis(methylphenoxy)phosphazene] and poly[bis(ethylphenoxy)phosphazene] with SO_3.[63] Other polyphosphazenes with different acidic groups were synthesized by the Allcock group. A phosphonic acid containing polyphosphazene was obtained by reacting a p-bromophenoxy substituted polyphosphazene with butyllithium followed by treatment with a

dialkyl chlorophosphate.[64] A sulfonimide containing polyphosphazene was also obtained by co-substitution of the polyphosphazene with methylphenoxy and sulfonimide groups.[65] The function of the alkylphenoxy groups is to allow UV crosslinking of the polymer to enhance its mechanical properties.

Table 1-2 Performance comparison between proton conducting polyphosphazenes[66]

Polymer	IEC (meq/g)	Crosslinking (Mrad)	Conductivity[a] (10^{-2} S/cm)	Water Uptake (% wt)	Methanol Diffusion[b] (10^{-6} cm^2/s)
Sulfonated	1.07	20	1.1	38	1.02
Phosphonated	1.35	20	4.4	13	0.77
Sulfonimide	0.99	20	7.1	73	-
Nafion 117	0.91	-	10.0	30	6.22

a 100% relative humidity, 25 ˚C

b 12 M MeOH, 80 ˚C, 2.8 bar.

The proton conductivity of polyphosphazenes is typically in the range of 10^{-2} S/cm when fully hydrated at room temperature. An advantage of polyphosphazenes is their lower methanol crossover compared to Nafion. In order to improve the performance of proton conducting polyphosphazenes, characterization of the morphology of these membranes is required. Due to the poor mechanical properties, the preparation of a pure polyphosphazene proton conducting system is probably unrealistic. However, production of an acceptable polyphosphazene system is attainable through enhancements such as crosslinking, blending with other polymers, or forming composites with inorganic fillers.

---

[1] M. B. Armand, J. M. Chabagno, M. J. Ducolt, in: *Abstracts of Papers, Second International Meeting on Solid Electrolytes*, St. Andrews, Scotland, **1978,** 65
[2] D. E. Fenton; J. M. Parker; P. V. Wright *Polymer*, **1973**, *14*, 589
[3] M. Winter, R. J. Brodd *Chem. Rev.*, **2004**, *104*, 4245–4270
[4] M. Armand, *Faraday Discuss. Chem. Soc*., **1989**, *88*, 65
[5] B. Scrosati; C. A. Vincent *MRS Bulletin*, **2000**, 28-30
[6] P.V. Wright *British Polymer Journal*, **1975**, *7*, 319-327

[7] M. Armand, W. Gorecki, R. Anreani *Proc. 2nd Int. Symp. On Polymer Electrolytes*, Ed. B. Scrosati, Elsevier, New York, **1990**, 91
[8] J.Y. Song, Y.Y. Wang, C.C. Wan *Journal of Power Sources* **1999**, *77*, 183–197
[9] K. Kezuka, T. Hatazawa, K. Nakajima *Journal of Power Sources*, **2001**, *97-98*, 755-757
[10] J. -M. Tarascon, A. S. Gozdz, C. Schmutz, F. Shokoohi, P. C. Warren *Solid State Ionics*, **1996**, *86-88*, 49-54
[11] B. Kumar, L. G. Scanlon *J. Power Sources* **1994**, *52*, 261
[12] R. A. Vaia, B. B. Sauer, O. K. Tse, E. P. Gianellis *J Polym Sci Part B.*, **1997**, *351*, 59-67
[13] B. Kumar, L. Scanlon, R. Marsh, R. Mason, R. Higgins, R. Baldwin *Electrochimica Acta*, **2001**, *46*, *1515-1521*
[14] W. Krawiec, L. G. Scanlon Jr., J. P. Fellner, R. A. Vaia, S. Vasudevan, E. P. Giannelis *Journal of Power Sources*, **1995**, *54*, 310-315
[15] Donald R. Sadoway, Biying Huang, Patrick E. Trapa, Philip P. Soo, Pallab Bannerjee, Anne M. Mayes *Journal of Power Sources*, **2001**, *97-98*, 621-623; Masayoshi Watanabe, Hiroyuki Tokuda, Shunsuke Muto *Electrochimica Acta*, **2001**, *46*, 1487-1491; W. Xu, M.D. Williams, C.A. Angell *Chem. Mater*., **2002**, *14*, 401
[16] P. G. Bruce, M. T. Hargeave, C. A. Vincent *Solid State Ionics*, **1992**, *53-56*, 1087; W. Gorecki, M Jeannin, E. Beloriszky. E. Roux, M. Armand *J Phys.: Condens. Matter*., **1995**, *7*, 6823
[17] F. M. Gray *Polymer Electrolytes* Royal Chemical Society, Cambridge **1997**, 10
[18] R. G. Pearson *Chemical Hardness* Wiley-VCH Verlag GmbH, Weinheim, **1997**
[19] P. Johansson, J. Tegenfeldt and J. Lindgren. *Polymer*, **1999**, ***40***, 4399
[20] D. W. Xia, J. Smid *J. Polym. Sci. Polym. Lett. Ed*. **1984**, *22*, 617-621
[21] J.M.G Cowie; A.C.S. Martin *Polymer*, **1987**, *28*, 627 -632
[22] D. G. H. Ballard, P. Cheshire, T. S. Mann, J. E. Przeworski *Macromolecules*, **1990**, *23*, 1256–1264
[23] L. Marchese, M. Andrei, A. Roggero, S. Passerini, P. Prosperi and B. Scrosati *Electrochim. Acta*, **1992**, *37*, 1559-1564
[24] P. M. Blonsky, D. F. Shriver, P. E. Austin, H. R. Allcock *J. Am. Chem. Soc*. **1984**, *106*, 6854-6855.
[25] I. M. Khan, Y. Yuan, D. Fish, E. Wu, J. Smid *Macromolecules*, **1988**, *21*, 2684–2689
[26] D. Lee, H. R. Allcock *Submitted to Solid State Ionics*
[27] R. Frech, S. York, H. R. Allcock, C. Kellam, *Macromolecules*, **2004**, *37* 8699-8702
[28] H. Vogel *Phys. Z.* **1921**, *22*, 645; G. Tammann; W Hesse *Z. Anorg. Allg. Chem.*, **1926**, *156*, 245; G.S. Fulcher *J. Am. Chem. Soc.* **1925**, *8*, 339
[29] M. A. Hickner, H. Ghassemi, Y. S. Kim, B. R. Einsla, J. E. McGrath *Chem. Rev.*, **2004**, *104*, 4587–4612
[30] R. Subbaraman, H. Ghassemi, T. A. Zawodzinski *J. Am. Chem. Soc.*, **2007**, *129*, 2238-2239; M. F. H. Schuster, W. H. Meyer, M. Schuster, K. D. Kreuer *Chem. Mater.* **2004,** *16*, 329-337; Z. Zhou, S. Li, Y. Zhang, M. Liu, W. Li *J. Am. Chem. Soc.*, **2005**, *127*, 10824-10825
[31] G. Scharfenberger, W. H. Meyer, G. Wegner, M. Schuster, K.-D. Kreuer, J. Maier *Fuel Cells*, **2006**, *6*, 237-250
[32] T. A. Zawodzinski Jr., M. Neeman, L. O. Sillerud, S. Gottesfeld *J. Phys. Chem.*, **1991**, *95*, 6040–6044
[33] K.-D. Kreuer, S. J. Paddison, E. Spohr, M. Schuster *Chem. Rev.*, **2004**, *104*, 4637–4678
[34] S. J. Paddison *Annu. Rev. Mater. Res.*, **2003**, *33*, 289-319
[35] M.A. Hickner, B. S. Pivovar *Fuel Cells*, **2005**, *5*, 213-229
[36] K.-D. Kreuer *Journal of Membrane Science*, **2001**, *185*, 29-39
[37] H Rose *Ann Chem* **1834**, *11*, 131; J. Liebig *Ann Chem* **1894**, *11*, 139
[38] H. N. Stokes *Am. Chem. J.* **1896**, *18*, 629; H. N. Stokes *Am. Chem. J.* **1897**, *19*, 782; H. N. Stokes *Am. Chem. J.* **1898**, *20*, 740; H. N. Stokes *Am. Chem. J.* **1895**, *28*, 437
[39] R. Schlenk, G. Romer *Chem. Ber.* **1924**, *57B*, 1343
[40] Allcock, H.R.; Kugel, R.L. *J. Am. Chem. Soc.* **1965**, *85*, 4216; H. R. Allcock, R. L. Kugel, K. J. Valan *J. Am. Chem. Soc.* **1966**, *5*, 1709; H. R. Allcock, R. L. Kugel *J. Am. Chem. Soc.* **1966**, *5*, 1716
[41] H. R. Allcock, *Chemistry and Applications of Polyphosphazenes* Wiley-Interscience: New Jersey, **2003**
[42] *Phosphazenes: A Worldwide Insight*; Editors: R. De Jaeger, M. Gleria; Nova Science Publishers: New York, **2004**
[43] *Polyphosphazenes for Biomedical Applications*, Ed: A. K. Andrianov, Wiley: New York, **2009**

[44] H. R. Allcock, *Phosphorus-Nitrogen Compounds* Academic Press, Inc: Orlando, **1972**
[45] C. H. Honeyman, C. T. Morrissey, C. T., I. Manners, H. R. Allcock *J. Am. Chem. Soc*. **1995**, *117*, 7035; H. R. Allcock, C. A. Crane, C. T. Morrisey, J. M. Nelson, S. D. Reeves, C. H. Honeyman, I. Manners *Macromol*., **1996**, *29*, 7740
[46] Y. Kurachi, T. Okuyama, T. Oohasi *J Mater Sci*, **1989**, *24*, 2671-2764
[47] Y. Hu, W. Fan, Q. Wang, T. Kawamora, N. Koseki, Y. Akutsu, M. Tamura, *Progress in Natural Science*, **1999**, *9*, 103-108
[48] E. Powell, A. Maher, R. V. Morford, H. R. Allcock, unpublished work.
[49] Toshiki Fushimi, H. R. Allcock ***Dalton Trans.***, 2010, **DOI:** 10.1039/b926069b
[50] C. Kim, H. R. Allcock, *Macromol*, **1987**, *20*, 1726-1727; R. E. Singler, R. A. Willingham, C. Noel, C. Friedrich, L. Bosio, E. D. T. Adkins, R. W. Lenz, *Macromol*, **1991**, *24*, 520-526; H. R. Allcock, E. H. Klingenberg *Macromol*. **1990**, *23*, 3881-3887
[51] H. R. Allcock, A. A. Dembek, C. Kim, R. L. S. Devine, Y. Shi, W. H. Steier, C. W. Spangler *Macromol*, **1991**, *24*, 1000; A. A. Dembek, C. Kim, H. R. Allcock, R. L. S. Devine, W. H. Steier, C. W. Spangler *Chem Maters*, **1990**, *2*, 97
[52] H. R. Allcock, L. Steely, A. Singh, M. D. Hindenlang *J. Adhesion Sci. & Technol.* **2009**, *23*, 435-445.
[53] N. R. Krogman, P. W. Brown, H. R. Allcock Allcock, C. T. Laurencin *J. Biomed. Nanotechnol*. **2009**, *5*, 69-75.
[54] H . R. Allcock, T. J. Fuller, K. Matsumura *Inorg. Chem*. **1982**, 515-521; H. R. Allcock, S. R. Pucher, A. G. Scopelianos, *Macromolecules* **1994**, *27*, 1071-1075.
[55] Blonsky, P. M.; Shriver, D. F.; Austin, P. E.; Allcock, H. R. *J. Am. Chem. Soc*., **1984**, *106*, 6854-6855
[56] Allcock, H. R.; Austin, P. E.; Neenan, T. X.; Sisko, J. T.; Blonsky, P. E.; Shriver, D. F. *Macromol*., **1986**, *19*, 1508-1512
[57] Blonsky, P. M.; Shriver, D. F.; Austin, P. E.; Allcock, H. R. *Polym. Mater. Sci. Eng.*, **1985**, *53*, 118
[58] Bennett, J. L.; Dembek, A. A.; Allcock, H. R.; Heyen, B. J.; Shriver, D. F. *Chemistry of Materials* **1989**, *1*, 14-16
[59] Nelson, C. J.; Coggio, W. D.; Allcock, H. R. *Chemistry of Materials* **1991**, *3*, 786-787
[60] Allcock, H. R.; Chang, Y.; Welna, D. T. *Solid State Ionics* **2006**, *177*, 569-572
[61] H. R. Allcock, S. J. M. O'Connor, D. L. Olmeijer, M. E. Napierala, C. G. Cameron, *Macromolecules* **1996**, *23*, 7544-7552
[62] H. R. Allcock, D. T. Welna, A. E. Maher *Solid State Ionics*, **2006,** *177*, 741-747
[63] R. Wycisk, P. N. Pintauro, *J. Membr. Sci.* **1996**, *119*, 155; H. Tang, P. N. Pintauro, Q. Guo, S. J. O'Connor, *Appl. Polym. Sci.* **1999**, *71*, 387; Q. Guo, P. N. Pintauro, H. Tang, S. O'Connor, *J. Membr. Sci.*, **1999**, *154*, 175.
[64] H. R. Allcock, M. A. Hofmann, C. M. Ambler, R. V. Morford, *Macromolecules,* **2002**, *35*, 3484.
[65] M. A. Hofmann, C. M. Ambler, A. E. Maher, E. Chalkova, X. Y. Zhou, S. N. Lvov, H. R. Allcock *Macromolecules,* **2002**, *35*, 6490
[66] H. R. Allcock, R. M. Wood *Journal of Polymer Science Part B: Polymer Physics* 44, 2006, 2358-2368

Chapter 2 The Effects of Cations and Anions on the Ionic Conductivity of Poly[bis(2-(2-methoxyethoxy)ethoxy)phosphazene] Doped with Lithium and Magnesium Salts of Trifluoromethanesulfonate and Bis(trifluoromethanesulfonyl)imidate

2.1 Introduction

The mechanism of ion transport in solid and gel polymer systems is a subject of widening interest since lithium-type rechargeable batteries have assumed a prominent role in electronic devices and future automotive technology. This subject has been the focus of considerable debate that started with the original discovery by Wright[1] of ion transport in poly(ethylene oxide) (PEO), and the subsequent recognition by Armand[2] that polymeric ionic conductors have the potential to replace or supplement the existing technology based on organic solvent-based electrolytes. The advantages of polymer electrolytes over liquid-based systems include resistance to combustion, robustness under challenging conditions, and access to compact energy storage devices that can be fabricated into intricate shapes.[3]

The main disadvantage of polymer electrolytes is their low ionic conductivity when compared to liquid electrolytes. This is due to the slower dynamics of polymer chain motion compared to small molecule motions in the liquid state. An unplasticized PEO system has an ambient temperature conductivity of only 10^{-6} S/cm mainly due to high levels of crystallinity.

This conductivity does not meet the minimum requirement of 10^{-3} S/cm for practical energy storage applications. Poly[bis(2-(2-methoxyethoxy)ethoxy)phosphazene] (MEEP) is an alternative, totally amorphous polymer that has been studied intensively as a polymer electrolyte since its initial synthesis and evaluation in the laboratories of Allcock and Shriver in 1984.[4,5,6] Studies have shown that room temperature ionic conductivities as high as 10^{-4} S/cm are possible even without plasticizers. This is several orders of magnitude higher than the value for PEO, but is still lower than the optimum values. The higher conductivity of MEEP electrolytes is attributed to the flexible phosphorus-nitrogen backbone and the oligomeric etheric side chains, both of which are responsible for the low glass transition temperature (T_g) of -80 °C. Although the low T_g gives MEEP poor dimensional stability, crosslinking of this polymer yields a dimensionally stable material without a significant sacrifice of ionic conductivity.[7]

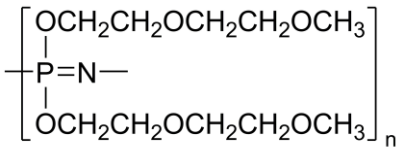

Figure 2-1 Poly[bis(2-(2-methoxyethoxy)ethoxy)phosphazene] (MEEP)

The conductivity of lithium salts in SPEs including MEEP has been studied extensively because lithium has the highest electrode potential, which leads to the prospect of high energy density batteries.[8] However, lithium metal is reactive if the cell is breached. In the search for alternatives, metals with multivalent cations have been considered. The rationale for studying the ionic conductivity of multivalent cations is that they might generate higher conductivities than monovalent cations since each cation carries more than one charge.[9] Among the possible multivalent cations, Mg^{2+} was chosen for this study due to the similar chemical hardness and size compared to Li^{+}. Therefore, in principle the cation-polymer interactions should be similar for both, although the charges are different. The conductivity of Mg^{2+} in polymer electrolytes has been studied previously with other polymer systems and its use in battery applications has been

considered.[10,11] Although magnesium does not have as high an electrode potential as lithium, the cost and safety of using magnesium could outweigh the electrode potential disadvantage. Salts of trifluoromethanesulfonate (Tf) are commonly used in polymer electrolyte studies because the negative charge on the Tf ion is delocalized over the sulfate group. Hence, the salt dissociates easily. However, bistrifluoromethanesulfonimidate (TFSI), shown in Figure 2-2, is a "new generation" anion that has more extensive charge delocalization than Tf, and it promotes a higher degree of dissociation.[12]

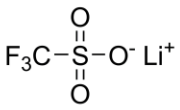

Lithium Trifluoromethanesulfonate
(LiTf)

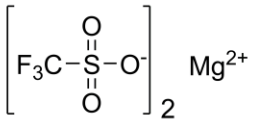

Magnesium Trifluoromethanesulfonate
($MgTf_2$)

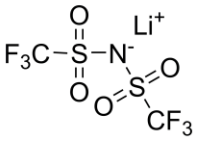

Lithium Bis(trifluoromethanesulfonyl)imidate
(LiTFSI)

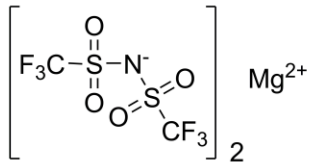

Magnesium Bis(trifluoromethanesulfonyl)imidate
($MgTFSI_2$)

Figure 2-2 Salts used in this study.

One of the main questions about the mechanism of ionic conduction in polymers such as PEO or MEEP is the specific role played by the anions and cations. Most polymer electrolyte studies report the bulk ionic conductivity. However, ionic conduction in a polymer is the result of contributions from both cations and anions because both ions carry charge and are mobile.[13] Some investigators have favored the view that the cations carry most of the charge, while others have identified the anions as the main charge carriers. Therefore, it is important to differentiate their separate contributions, especially when evaluating the performance of a polymer electrolyte for a rechargeable lithium battery.[14] Different types of measurements, different salts, or different

polymers often favor one mechanism or the other. Furthermore, the cationic and anionic conduction mechanisms are not the same. The study reported here was designed to throw further light on this situation, especially with respect to the roles played by Tf and TFSI anions and the consequences of replacing lithium cations by magnesium. Thus, we have examined the effect of two different cations and two anions on the ionic conductivity of MEEP and have identified the dominant mobile species.

2.2 Experimental

2.2.1 Materials

All materials were used as received unless stated otherwise. Sodium (ACS reagent grade), lithium trifluoromethanesulfonate (99.995%), magnesium trifluoromethanesulfonate (97%), lithium bis(trifluoromethanesulfonyl)imidate (99.95%), bis(trifluoromethane)sulfonimide (95%), magnesium acetate tetrahydrate (98%) were obtained from Aldrich and were stored in an argon atmosphere glove box. 2-(2-Methoxyethoxy)ethanol (99.0%)was obtained from Aldrich and was purified by drying over CaH_2 and distillation under reduced pressure. Hexachlorocyclotriphosphazene was obtained from Fushimi Pharmaceutical Co. Ltd. (Japan) and was purified by recrystallization twice from heptanes followed by sublimation at 30 °C at 0.01 mmHg. Tetrahydrofuran (99.99%, EMD) was dried by passage through Glass Contour alumina columns before use. De-ionized water was obtained from a Barnstead Nanopure Diamond water purification system. All synthesis reactions were carried out under an atmosphere of dry nitrogen.

2.2.2 Equipment

High-field ^{1}H (360.14 MHz) and ^{31}P (145.79 MHz) NMR spectra were obtained with use of a Bruker AMX-360 NMR spectrometer. ^{1}H NMR spectra were referenced to internal tetramethylsilane, while ^{31}P NMR spectra were proton-decoupled and referenced to external 85% phosphoric acid in D_2O. Mass spectra were collected using a Micromass Quattro-II triple quadrupole mass spectrometer. Polymer molecular weights and polydispersities were estimated using a Hewlett-Packard HP 1090 gel permeation chromatograph equipped with an HP-1047A refractive index detector, Phenomenex Phenogel 10 μm linear columns were calibrated against polystyrene standards. Sample elution was carried out at 40 °C with a 0.1 wt % solution of tetra-*n*-butylammonium nitrate in THF. Thermal transitions were identified with use of a TA Q10 differential scanning calorimeter. Calibration was accomplished with indium, water, and cyclohexane standards. All analyses were performed over a range of -100 to 100 °C at a heating rate of 10 °C/min. Ionic conductivity measurements were obtained using a Hewlett-Packard 4192A LF impedance analyzer at a potential of 0.1 V with an alternating current frequency range of 5 Hz-1 MHz. The samples were placed between platinum electrodes with a Teflon O-ring spacer, and the polymer electrolyte cell was compressed between aluminum blocks held in a Teflon fixture. Electrical leads were attached between the impedance analyzer and the polymer electrolyte cell sample holder. All ionic conductivity measurements were carried out over a temperature range of 25-80 °C under an inert atmosphere of dry argon.

2.2.3 Syntheses

Poly[bis(2-(2-methoxyethoxy)ethoxy)phosphazene] (MEEP) was synthesized using previously published procedures.[4,5]

Magnesium bis(trifluoromethanesulfonyl)imidate – Magnesium acetate tetrahydrate was allowed to react with 2 equivalents of bis(trifluoromethanesulfonyl)imide in water under ambient conditions for an hour.[15] The water was removed by rotary evaporation. The $MgTFSI_2$ was dried further in vacuum for 5 days at 40 °C. The product composition was confirmed by ^{19}F NMR and mass spectrometry.

Polymer Electrolyte Fabrication – The salts were added to MEEP dissolved in stirred THF until a homogenous, clear solution was obtained. The THF was allowed to evaporate and residual solvent was removed by drying under vacuum at 40°C for 5 days.

2.3 Results and Discussion

2.3.1 Glass Transition Behavior

The conduction of ions in a polymer electrolyte depends partly on the flexibility of the polymer chains. Flexible macromolecules allow faster ion migration than rigid polymers, and consequently give higher ionic conductivities. The flexibility of the polymer chain is related to the glass transition temperature (T_g), the point at which the polymer undergoes a phase transition from a glassy solid to a rubbery material. The relationship between the T_g of MEEP and the concentration of different salts is shown in Figure 2-3. The x-axis of the graph represents the salt concentration in the form of the mole fraction of salt with respect to the repeating units of MEEP. The y-axis of the graph gives the T_g of MEEP in degrees Celsius. The addition of salt to MEEP increased the T_g in a roughly linear fashion with respect to the concentration of the salt. The T_gs of SPEs that contained Mg salts

were higher than those with Li salts. MEEP with TFSI salts also had higher T_gs compared to Tf salts with the same cation.

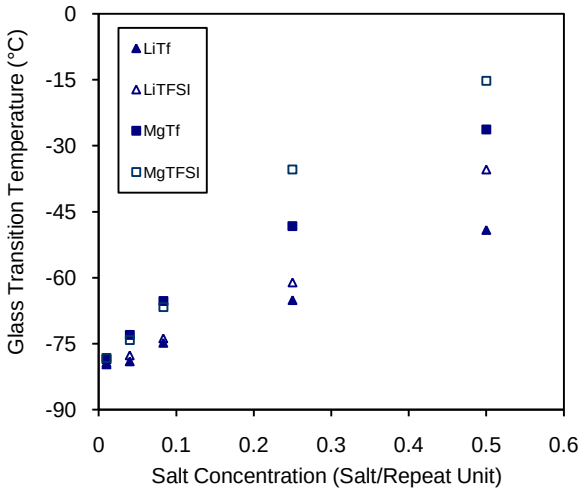

Figure 2-3 Glass Transition behavior of MEEP with increasing salt concentration.

For the formation of a solid polymer electrolyte, the polymer must function as a solvent and favor dissociation of the salts. The dissolution of salts in the polymer matrix produces cations, anions, and also anion-cation associated species. The ability of a polymer electrolyte to dissolve salts depends on the ability of the polymer to stabilize ions by solvation. In MEEP, the cations are stabilized by coordination to the oxygen atoms in the side chains and possibly to the nitrogen atoms in the backbone.[16] Interactions between the cation and the polymer can be understood according to the Hard/Soft acid base (HSAB) principle, which dictates that hard non-polarizable acids interact strongly with hard non-polarizable bases. Mg^{2+} and Li^{+} are hard cations with similar hardness values of 35.12 η and 32.55 η respectively.[17] Hence, Mg^{2+} and Li^{+} would interact with MEEP similarly, with a stronger interaction to the hard oxygen of the side chains than to the soft nitrogen atoms of the backbone. However, the divalent cation Mg^{2+} has a higher coordination ability compared to the monovalent Li^{+} cation. Therefore, MEEP with dissolved Mg^{2+} salts results in higher T_gs than with comparable concentrations of Li^{+} salts. Cation

coordination to the side chain oxygen atoms forms inter and intrachain transient crosslinks. However, studies by Stewart[18] and ourselves have shown that crosslinking via the side chains does not necessarily contribute to an increase in T_g. In our studies, covalent crosslinks between the side chains induced by γ irradiation of MEEP did not raise the T_g significantly even when 1 crosslink was formed for every 1.4 polymer repeat units.[19] The reason is because the etheric side chains are sufficiently long and flexible that crosslinks do not impede the flexibility of the backbone. This implies that any T_g increases in the presence of a dissolved salt are connected with cation coordination to the inner oxygen atoms or to the skeletal nitrogen atoms which reduce the flexibility of the backbone.

Unlike cations, anions are not expected to coordinate to the polymer electrolyte. Nevertheless, our results show that there is a difference in T_g when different anions are used. It has been proposed that TFSI has a plasticization effect on polymers such as PEO by reducing both the crystallinity and the T_g.[20] The same effect was not detected with MEEP because pure MEEP is totally amorphous. In fact, the T_gs of MEEP SPEs that contain TFSI salts were higher than those that contained Tf salts. These higher T_gs can be explained by a greater degree of dissociation of TFSI salts because of their lower lattice energies than Tf salts. Frech and coworkers used diglyme and LiTFSI as a model system to study ion dissociation in etheric polymers, and showed that LiTFSI is fully dissociated when the O:Li ratio is more than 6:1.[21] In a separate study by the same group using diglyme and LiTf, only 23% of the salt was fully dissociated even when the O:Li ratio was 40:1.[22] The remainder are associated ionic species such as ion pairs [LiTf] and triple ions species $[Li_2Tf]^+/[LiTf_2]^-$. Therefore, the higher degree of dissociation of TFSI salts generates more cations that coordinate to the polymer. This outweighs the plasticizing effect that was detected in PEO, and results in higher T_gs for MEEP with TFSI salts.

2.3.2 Ionic Conductivity Behavior

Figures 4 to 7 show the ionic conductivities of MEEP with each salt at temperatures from 25 to 80 °C. The x-axis of each graph represents the salt concentration in molar fraction, X_{salt}; and the y-axis shows the ionic conductivity in terms of *log* S/cm. The ionic conductivity of MEEP increased initially with increasing salt concentration until a maximum was reached. Further increases in salt concentration lowered the ionic conductivity. Table 2-1 shows the maximum room temperature conductivity of MEEP with each salt. Salts with the same anion showed similar maximum conductivities. Even though the MEEP systems containing the TFSI salts had higher T_gs, nevertheless the ionic conductivities were higher than for MEEP electrolytes with Tf salts.

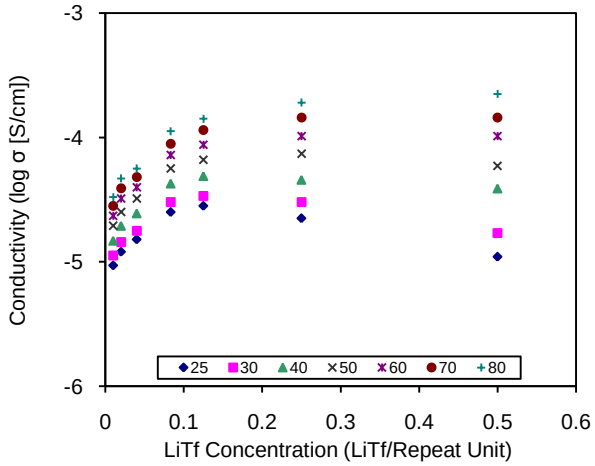

Figure 2-4 Isothermal ionic conductivity of LiTf:MEEP

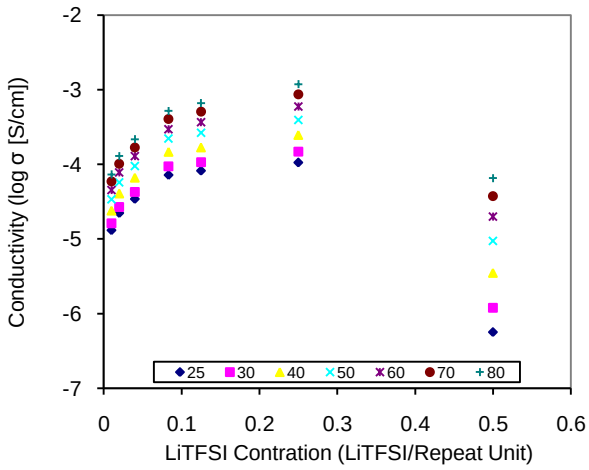

Figure 2-5 Isothermal ionic conductivity of LiTFSI:MEEP

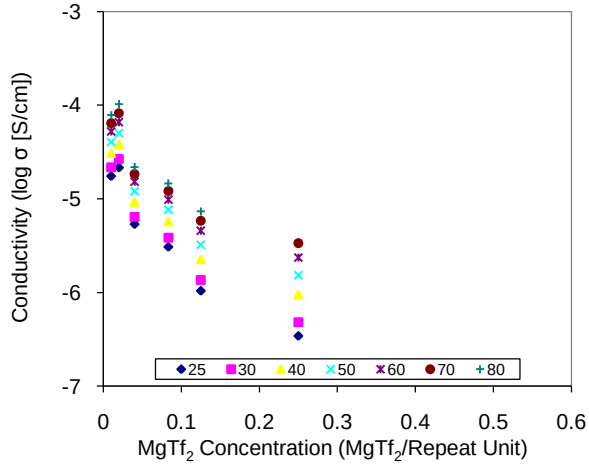

Figure 2-6 Isothermal ionic conductivity of $MgTf_2$:MEEP

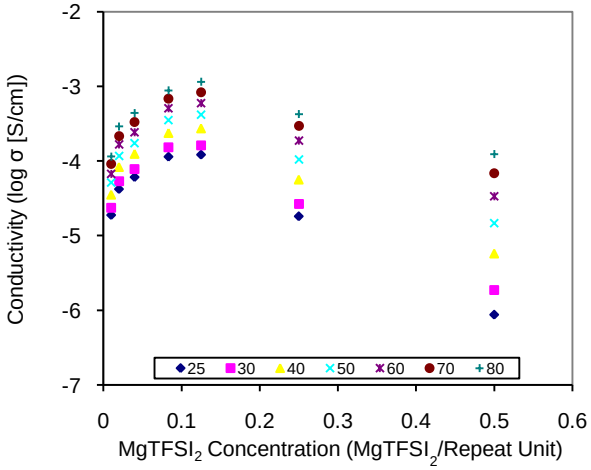

Figure 2-7 Isothermal ionic conductivity of $MgTFSI_2$:MEEP

Table 2-1 Highest room temperature conductivity of different salts.

Salt	Highest Conductivity (10^{-4} S/cm)	Salt Molar Fraction (Salt/Repeat Unit)
LiTf	0.28	0.125
LiTFSI	1.06	0.250
$MgTf_2$	0.22	0.020
$MgTFSI_2$	1.21	0.125

We favor the following interpretation for the initial increase and subsequent decrease of ion conductivity as a function of salt concentration. The ionic conduction increases initially because the number of charge carriers rises with salt concentration. However, increasing salt concentrations also increase the T_g. This lowers the ionic conductivity because a higher T_g corresponds to lower polymer chain mobility. The decrease in ionic conductivity can also be attributed to the formation of contact ion pairs and triple ion species. As the salt concentration increases, the average distance between ionic species also decreases, which leads to the formation of associated ionic species as mentioned before. Frech and coworkers carried out a study of LiTf dissolved in MEEP and showed that at MEEP:Li ratio of 8:1, only 21% of the LiTf was dissociated and the remainder consisted of aggregated species.[23] It was proposed that associated ionic species are likely to be immobile because [LiTf] is neutral and does not experience any force under an electric field whereas $[LiTf_2]^-$ or $[Li_2Tf]^+$ may have limited mobility due to its mass. It was postulated that these associated species can still contribute to ionic conduction by functioning as hopping sites for ions, albeit at a slower rate. It is believed that the low conductivity of polymer electrolytes with $MgTf_2$ salt is due to the extensive formation of associated species even at low concentrations. Hence, the ionic conductivity of MEEP containing $MgTf_2$ starts to decrease at a much lower concentration compared to the other three systems. No appreciable conductivity was detected at a MEEP:$MgTf_2$ ratio of 2:1.

As shown in Table 2-1, the maximum conductivities of polymer electrolytes with the same anion were essentially the same. Furthermore, the polymer systems that contain TFSI salts have ionic conductivities that are almost one order of magnitude higher than their counterparts with Tf salts. Although other polymers with higher T_gs often give lower conductivities, the opposite was found in the MEEP system where polymer solutions of TFSI salts had higher T_gs and also higher conductivities. This phenomenon is probably related to the higher degree of dissociation of TFSI salts, and therefore to the presence of a larger number of mobile species that are able to participate in ionic conduction. The ionic conductivity of the polymers with $MgTFSI_2$ reached its maximum at a salt molar fraction of 0.125. On the other hand, systems with LiTFSI reached a maximum conductivity at salt molar fraction of 0.25; in other words, at twice the concentration of the electrolytes that contained $MgTFSI_2$. This indicates that $MgTFSI_2$ has twice the charge carrying capability compared to the LiTFSI in MEEP. Classically, the cations were thought to be the dominant charge carriers due to the limitations imposed by the mass of the anion. The Mg^{2+} cation can carry twice the charge of Li^+. Therefore the maximum conductivity of MEEP:$MgTFSI_2$ should be achieved at half the concentration of MEEP:LiTf. However, recent studies have suggested that the dominant charge carriers are the anion species.[24] In that case, one $MgTFSI_2$ molecule can dissociate to yield 2 $TFSI^-$ anions whereas one LiTFSI molecule will yield only one. Consequently, the maximum conductivity of $MgTFSI_2$ will also be achieved at half the concentration of LiTFSI. The identity of the charge carrier is discussed below.

An equation that is used to describe the temperature dependence of ionic conductivity is the Vogel-Tamman-Fulcher (VTF) equation.[25]

$$\sigma(T) = \sigma_0 \exp\left[\frac{-B}{(T - T_0)}\right] \tag{1}$$

In this term, σ_0 is a pre-exponential factor related to the number of carriers. The B term is related to the E_A term in the Arrhenius equation and has the dimensions of Kelvin units, but cannot be

regarded as a simple activation term. T_0 is the ideal glass transition temperature at which ion mobility goes to zero. Above T_0, thermal motion contributes to the transport of ions and it is sometimes set as T_g but, as will be discussed later, T_0 is sometimes found to be 30 -50 K below T_g.

During curve fitting operations, the σ_0 and B parameters were set as variables. T_0 was initially set as T_g but the data points did not fit well. When T_0 was set at T_g – 30 K, the data points consistently fitted better. Setting T_0 to be 30 - 50 K below the T_g is a common practice during curve fitting of the VTF equation and has been reported previously for polyphosphazene solid polymer electrolytes.[26] If the T_0 value was set as T_g in the VTF equation, it might be assumed that the segmental motion of the polymer is the rate limiting step in ionic conduction. However, ion-ion and ion-polymer interactions cannot be neglected and both need to be overcome in ionic conduction.[27] Hence, the T_0 is set below T_g to account for the additional energy required for the transport of ions. The B parameters in the VTF equation of the SPEs were obtained and displayed in Figure 2-8.

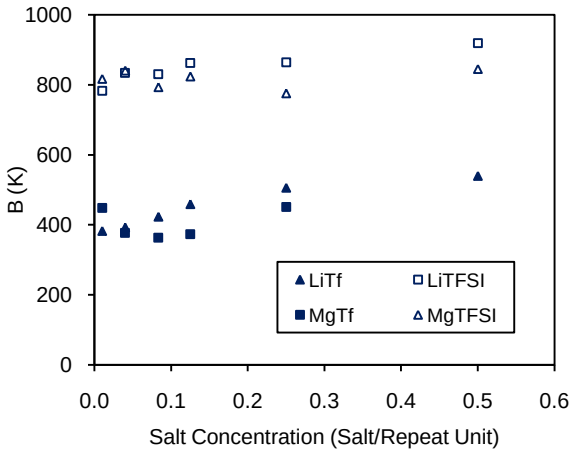

Figure 2-8 VTF equation B value for MEEP polymer electrolytes

Figure 2-8 shows that polymer electrolytes with the same anion show similar B values and that counterparts with TFSI salts have almost twice the B values of electrolytes with Tf salts. The strong dependence of the B value on the anionic species present suggests that the dominant charge carriers in MEEP are the anions. Assuming a minimal interaction between anion and the polymer, the B value can be described according to the Doolittle-Cohen free volume theory

$$B = \frac{f^*}{\alpha_f} \tag{2}$$

where B is the pseudo-activation energy in the Arrhenius (high-temperature) limit of the VFT relation and f^* is the averaged free volume required for transport of a molecule and α_f is the thermal expansion coefficient of the free volume.[28] The α_f value is the same for all samples because all the electrolytes contained the same polymer. Thus, the B value is only dependent on f^*. The higher B value of systems with TFSI is due to the larger volume of the $TFSI^-$ anion compared to the Tf^- anion. This result is supported by observations made in previous studies where the anion was immobilized on the side chain of the polyphosphazene.[29] The conductivities of polyphosphazenes with covalently immobilized sulfonamide side groups were 10^{-6} – 10^{-7} S/cm; which is 1 – 2 orders of magnitude less than polyphosphazenes with free salts. When the cations were immobilized to the side chains of polyphosphazenes, the conductivities were still within the range of polyphosphazenes with free salts.[30]

Although the B values indicate that anions are the main contributor to ion conduction in the MEEP system, the cations are not totally immobile. Different techniques such as pulsed field gradient NMR, DC polarization, and AC impedance have shown that cations contribute to ion conduction although the transference number for cationic species is < 0.5.[31] Although polymer electrolytes prepared with magnesium salts had higher T_gs than those with lithium salts, the maximum room temperature conductivity of lithium and magnesium salts were not significantly different because the anions are the principal conductors. If the cations are strongly solvated by

the polymer side groups in SPEs, any cation transport would require breaking the coordination between cations and etheric oxygens. This impedes cation mobility, and the transport of cations would depend not only on polymer flexibity, but also lability of the cation-etheric oxygen interaction.[32]

2.4 Conclusions

The use of four different salts to study the effect of the cations and anions on ionic conduction in MEEP suggests that anions are the primary charge carriers. The high degree of dissociation of TFSI salts yielded MEEP electrolytes with higher ionic conductivities although the glass transition temperatures was also higher. Strong interactions between the cations and the polymer appear to limit the cation contribution to the overall ion conduction. These observations add to the information about the ion conduction mechanism in MEEP, a process that is only slowly being understood. Although this study does not support the use of magnesium salts in rechargeable battery applications, further synthetic modifications to the polyphosphazene component may enhance the mobility of Mg^{2+} ions.

Acknowledgements

We thank Drs. James Runt, Toshiki Fushimi and Daniel Welna for their input to this project.

1 D. E. Fenton, J. M. Parker, P. V. Wright, Polymer 14 (1984) 589
2 M. B. Armand, J. M. Chabagno, M. J. Ducolt, in: Abstracts of Papers, Second International Meeting on Solid Electrolytes, St. Andrews, Scotland (1978) p 65
3 F. M. Gray, Solid Polymer Electrolytes: Fundamentals and Technological Applications; VCH Publishers, Chapter 1 (1991)
4 P. M. Blonsky, D. F. Shriver, P. E. Austin, H. R. Allcock, J. Am. Chem. Soc. 106 (1984) 6854
5 H. R. Allcock, P. E. Austin, T. X. Neenan, J. T. Sisko, P. M. Blonsky, D. F. Shriver, Macromolecules 19 (1986) 1508-1512
6 P. M. Blonsky, D. F. Shriver, P. E. Austin, H. R. Allcock, Solid State Ionics 18/19 (1986) 258-264
7 J. L. Bennett, A. A. Dembek, H. R. Allcock, B. J. Heyen, D. F. Shriver, Chem. Mater. 1 (1989) 14-16
8 M. Winter, R. J. Brodd, Chem. Rev. 104 (2004) 4245 -4270.

9 F. M. Gray, C. A. Vincent, P. G. Bruce, J. Nowinski, in: Second International Symposium on Polymer Electrolytes, Editor: Scorsati, B. Elsevier Science Publishers (1990) 299-309
10 N. Yoshimoto, S. Yakushiji, M. Ishikawa, M. Morita, Solid State Ionics 152-153 (2002) 259-266
11 S. Ikeda, Y. Mori, Y. Furuhashi, H. Masuda, Solid State Ionics 121 (1999) 329-333
12 A. J. Webber, Electrochem. Soc. 138 (1991) 2586-2590
13 S. Arumugam, J. Shi, D. P. Tunstall, C. A. Vincent, J. Phys. Condens. Matter 5 (1995) 153-160
14 D. Fauteux, A. Massucco, M. McLin, M. van Buren, J. Shi, Electrochimica Acta 40 (1995) 2185-2190
15 H. Kobayashi, J. Nie, T. Sonoda, Chem. Lett. 24 (1995) 307-308
16 T. A. Luther, F. F. Stewart, J. L. Budzein, R. A. LaViolette, W. F. Bauer, M. K. Harrup, C. W. Allen, A. Elayan, J. Phys. Chem. B 107 (2003) 3168-3176
17 R. G. Pearson, Inorg. Chem. 27 (1988) 734
18 F. F. Stewart, R. E. Singler, M. K. Harrup, E. S. Peterson, R. P. Lash, Journal of Applied Polymer Science 76 (2000) 55 - 66
19 H. R. Allcock, S. Kwon, G. H. Riding, R. J. Fitzpatrick, J. L. Bennett, Biomaterials 9 (1988) 509-513
20 S. Lascaud, M. Perrier, A. Vallee, S. Besner, J. Prud'homme, M. Armand, Macromolecules 27 (1994) 7469-7477
21 W. A. Henderson, F. McKenna, M. A. Khan, N. R. Brooks, V. G. Young, R. Frech 17 Chem. Mater (2005) 2284-2289
22 M. Petrowsky, C. P. Rhodes, R. Frech, Journal of Solution Chemistry 30 (2001) 171-181
23 R. Frech, S. York, H. R. Allcock, C. Kellam, Macromolecules 37 (2004) 8699-8702
24 R. J. Klein, D. T. Welna, A. L. Weikel, H. R. Allcock, J. Runt, Macromolecules 40 (2007) 3990-3995
25 M. A. Ratner, D. F. Shriver, Chem. Rev. 8 (1988) 109-124
26 H. R. Allcock, D. L. Olmeijer, Macromolecules 31 (1998) 8036-8046
27 P. G. Bruce, C. A. Vincent, J. Chem. Soc., Faraday Trans. 89 (1993) 3187-3203
28 F. Kremer, A. Schonhals, in: Broadband Dielectric Spectroscopy, Eds: F. Kremer, A. Schonhals, Springer-Verlag, NewYork (2003) 99-130
29 H. R. Allcock, D. T. Welna, A. E. Maher, Solid State Ionics 117 (2006) 741-747
30 S. Ganapathiappan, K. Chen, D. F. Shriver J. Am. Chem. Soc. (111) 1989 4091-4095
31 F. Gray, M. Armand, in: Handbook of Battery Materials, Ed: J. O. Besenhard, Wiley-VCH: New York, (1999) Ch 8
32 F. Gray, Polymer Electrolytes, RSC:Cambridge UK (1997) Ch 4

Chapter 3 Inorganic-Organic Hybrid Polymers with Pendent Sulfonated Cyclic Phosphazene Side Groups as Potential Proton Conductive Materials for Direct Methanol Fuel Cells

3.1 Introduction

An increasing need exists for energy sources to power more durable and more portable electronic devices. Most existing portable energy technology is based on primary or secondary batteries. Batteries are a convenient technology, but they are limited by the fact that, once all their energy has been consumed, they must be discarded or recharged.

An open electrochemical device, such as a fuel cell, is a practical solution to these problems. Unlike batteries, which have only a limited amount of chemical energy stored at any time, a fuel cell can generate electricity for as long as a fuel is supplied to the system. Extra fuel can also be transported to remote areas where electricity is not available for recharging batteries [1]. Research in fuel cell technology is also important because of its potential to provide clean energy.

Several types of fuel cell technology are available [1], but the form that is considered to be the most applicable to portable electronic devices is the proton exchange membrane (PEM) fuel cell, which typically operates at a moderate temperature (below 80 ^{o}C) and still retains a high power density. This potential to operate close to room temperature is important, since it eliminates the need for thermal insulation and initial warm-up. Unlike high-power applications such as stationary or automotive power generation, where high temperature is an acceptable tradeoff for high efficiency, portable devices such as cell phones or laptop computers require a power source that functions at or even below room temperature. The fuel utilized by a PEM fuel cell is also a critical consideration. A promising type of fuel cell for portable electronic devices is

the *direct methanol fuel cell* (DMFC), which utilizes liquid methanol directly to produce electrical power. Compared to other possible fuels such as hydrogen, methanol is safer to store, handle, and transport. The bulk and mass of a methanol powered device would also be less than one that is powered by hydrogen because methanol does not require rigid containment [2].

One of the most crucial elements of a DMFC assembly is the electrolyte membrane layer across which protons are transported. Criteria for a practical PEM are chemical stability, good electrode adhesion properties and high proton conductivity [3]. In the case of a DMFC, low methanol crossover is also a crucial requirement [4], because methanol crossover results in a loss of efficiency if the fuel can be oxidized directly at the cathode without producing electrical power. Hence, there is a need to develop a membrane material that can deliver high proton conductivity combined with low methanol permeability. Because both the proton conduction and methanol permeability are often attributed to membrane microstructures [5, 6], one promising approach is to introduce new designs that differ from existing ones at a fundamental molecular chemistry level, thereby changing the microstructure and the way the materials interact with either protons or methanol [7, 8]. A number of materials have been developed for this purpose and show some degree of success, such as modified Nafion, polybenzimidazoles, and sulfonated poly(ether ketones) [9-12]. On the other hand, most of these materials are hard to fine-tune chemically for optimal performance, and progress in this field had been restricted for this reason.

Among the new materials that have been investigated for fuel cell applications, the group of nitrogen-phosphorus based polymers known as polyphosphazenes has received much attention [13-17] due to several unique advantages. These include a high level of functionality per repeating unit, control of chemical properties over a wide range of molecular reactions, and a spectrum of different architectures to allow optimization of physical characteristics. Open chain polyphosphazenes were first investigated as proton conducting membranes in hydrogen fuel cells

[17]. However, their possible utility in direct methanol fuel cells became apparent in recent years, even though the resistance to methanol crossover still needs to be improved.

Consequently, we have focused on new polymer electrolyte membranes that can combine the aforementioned advantages of phosphazenes with a higher resistance to methanol permeation and better physical properties than the alternatives. Specifically, methods have been developed for the linkage of pendent cyclic phosphazene side groups to organic polymer backbones [18, 19]. One advantage of this design is to combine the chemical reactivity and oxidation/reduction stability of phosphazenes with the physical attributes (flexibility, strength, and ease of fabrication) of an organic backbone polymer. This approach can yield a variety of functionalized polymers. An organic polymer system that is described here is based on the polynorbornene skeleton, which is accessible by ring opening metathesis polymerization (ROMP) [19, 20]. The organometallic – catalyzed ROMP is a useful synthetic approach in the sense that it gives good control over the molecular weight of the polymer while maintaining a high reaction rate, which leads ultimately to a stable performance of the resulting material and ease of scale-up for industrial manufacturing. It also allows for a wide range of modifications at the monomer stage, which gives more flexibility in designing the polymer [21, 22].

We have already investigated polynorbornenes with pendent cyclic phosphazene units for use as polymer electrolytes for secondary lithium batteries [23] and lithium sea water batteries [24]. These polymers combine the hydrophobicity of the organic polymer with the chemical tailorability of the phosphazene units. Furthermore, because each repeating unit contains a phosphazene ring with five available bonding sites, higher incorporations of functional groups per repeating unit are possible than with typical linear organic or inorganic macromolecules. Consequently, variants of these polymers should also be viable candidates for PEM applications.

Sulfonation of aryl or aryloxy groups is a common approach in the synthesis of proton conducting materials [25-30] because of the high acidity of the sulfonic acid protons coupled with the low methanol solubility of aryloxy groups. Compared to linear polyphosphazene systems, the highly stable phosphazene ring structure should reduce the possibility of side reactions during sulfonation procedures and should extend the lifetime of the membrane. In addition, the sulfonated functional groups are separated from the polymeric main chain and are clustered on the side extensions, which may lead to different interactions for the purpose of proton and methanol migration. Thus, the combination of the two concepts leads to an organic polymer with pendent cyclophosphazene units that bear sulfonic acid functional groups and hydrophobic, un-functionalized aryloxy units. This is an appealing possibility for the purpose of making a PEM material with high ionic conductivity and low methanol permeability.

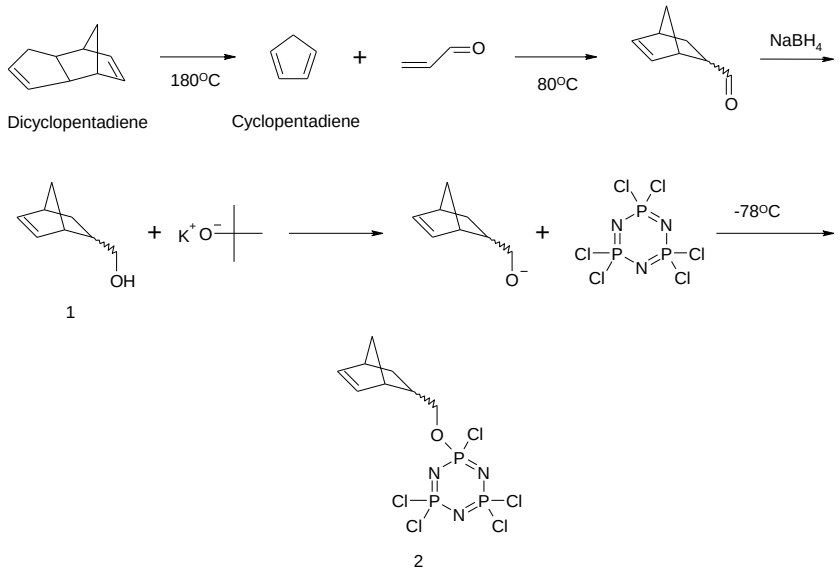

Figure 3-1 Synthetic scheme for the monomer

In this study, we first synthesized a norbornene monomer with a pendent cyclic chloro-phosphazene side group. The monomer was polymerized using a first generation Grubbs' catalyst, and the chlorine atoms in the pendent cyclic phosphazene units were replaced with *m*-

cresoxy groups. The polymer was then treated with SO_3, which preferentially reacts at the aryl rings to form sulfonic acid groups. The methyl group on the phenoxy side units was utilized to permit subsequent gamma radiation crosslinking in an attempt to further decrease methanol permeability. The objective was to synthesize a polymer that can preserve a conductive pathway for protons while suppressing excessive methanol crossover at room temperature.

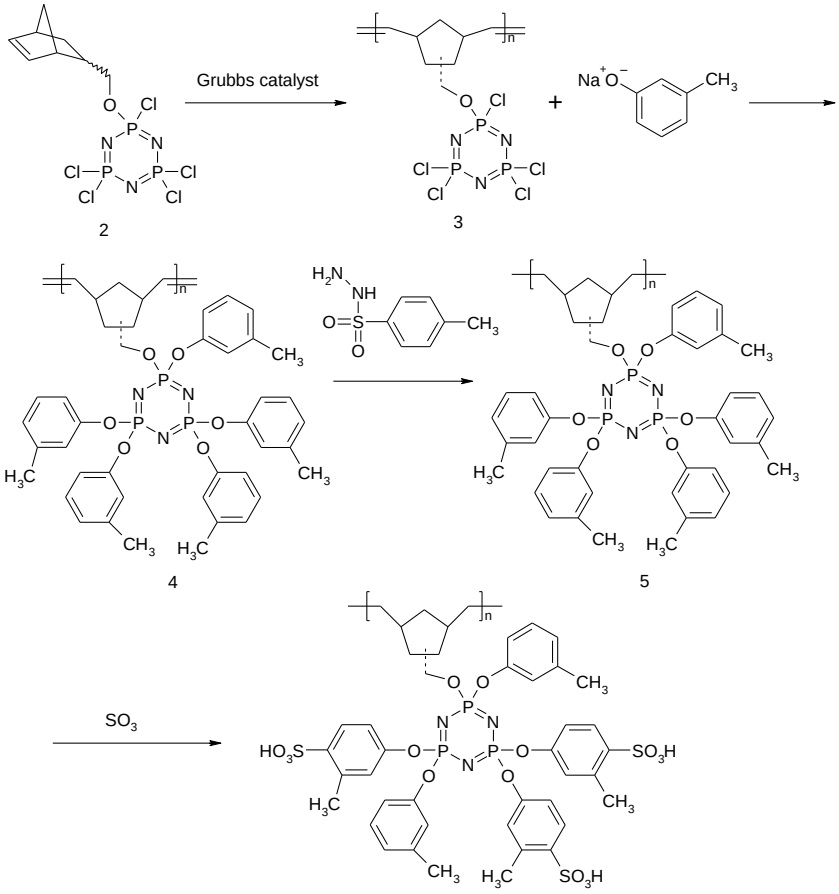

Figure 3-2 Synthetic scheme for the sulfonated polymer: Polymerization, hydrogenation and sulfonation reactions

3.2 Experimental

3.2.1 Materials:

All materials were used as received unless stated otherwise. Sodium (ACS reagent grade), ethyl vinyl ether (99%), bis(tricyclohexylphosphine)benzylidene ruthenium (IV) chloride (97%), *p*-xylene (anhydrous, 99+%), *p*-toluenesulfonhydrazide (97%), 1,2-dichloroethane (99%) and sulfur trioxide (99%) were obtained from Aldrich. Potassium *tert*-butoxide (98%) was obtained from Acros. Hexachlorocyclotriphosphazene was obtained from Fushimi Pharmaceutical Co., Ltd. and was purified by recrystallization twice from heptane followed by sublimation at 30 °C at 0.01 mmHg. 3-Methylphenol (97%, Aldrich) was distilled over calcium chloride under reduced pressure. Tetrahydrofuran (99.99%, EMD), dichloromethane (99.8%, EMD), and dioxane (99.0%, EMD) were dried by passage through Glass Contour alumina columns before use [31]**.** Pre-treated Nafion 115 (Dupont) was washed with and soaked in de-ionized water repeatedly for 48 hr before subjected to conductivity, swelling, and methanol crossover tests. De-ionized water with a resistance of 18 MΩ was obtained from a Barnstead Nanopure Diamond water purification system. All synthesis reactions were carried out under an atmosphere of dry nitrogen.

3.2.2 Instrumentation

High field ^{1}H (360 MHz), ^{13}C (90 MHz), and ^{31}P (146 MHz) NMR spectra were obtained with a Bruker AMX-360 spectrometer. ^{1}H and ^{13}C NMR peaks were referenced to external tetramethysilane. ^{31}P NMR peaks were referenced to external 85% H_3PO_4 with positive shifts recorded downfield from the reference. ^{31}P and ^{13}C spectra were proton decoupled. Molecular

weights and polydispersity indices were estimated by use of a Hewlett-Packard 1090 gel permeation chromatograph equipped with Phenomenex Phenolgel 10 μm linear columns and a HP-1047A refractive index detector. The equipment was calibrated with polystyrene standards. The samples were eluted with 0.1 wt% solution of tetra(n-butyl)ammonium nitrate in THF. Glass transition temperatures were obtained with use of a TA Instruments Q10 differential scanning calorimeter (DSC), calibrated with indium, water and cyclohexane standards. Sample dimensions were measured with Mitutoyo Digimatic calipers. Room temperature conductivity was measured using a Hewlett Packard 4192A LF impedance analyzer at a potential of 0.1 V and an alternating current frequency range of 5 Hz to 1 MHz.

3.2.3 Syntheses

*Synthesis of pentachloro-(5-norbornene-2-methoxy)-cyclotriphosphazene (**2**):* This synthesis and its subsequent polymerization were carried out following a modified published procedure [24]. 5-Norbornene-2-methanol (**1**) (87.00 g, 0.702 mol) was synthesized according to a previous literature procedure [32], and was dissolved in THF (1.5 L). Potassium tert-butoxide (74.62 g, 0.665 mol) was suspended in THF (0.5 L) and was added dropwise to the stirred solution of **1** and allowed to react overnight at room temperature. Hexachlorocyclotriphosphazene (347.00 g, 0.998 mol) was dissolved in THF (2 L). Both mixtures were cooled in a dry-ice/acetone bath and the norbornene salt was cannulated into the cyclotriphosphazene solution in a slow, dropwise fashion. When the addition was complete, the reaction vessel was allowed to warm to room temperature and was stirred overnight. The solution was concentrated by vacuum to yield a brown liquid which was dissolved in diethyl ether and washed with water (3 x 700 mL). The organic layers were combined, dried over anhydrous $MgSO_4$ and concentrated. The resultant brown oil was placed in a vacuum sublimator. Residual ether was removed in vacuum at room

temperature. Excess hexachlorocyclotriphosphazene was removed by sublimation at 40 °C at 0.01 mmHg for 5 days. Mono-substitution was confirmed by following the process by ^{31}P NMR spectra during and after the reaction. Yield = 259.79 g (68%). ^{31}P NMR ($CDCl_3$) δ (ppm): 22.75 (d, -PCl_2, 2P), 14.90 (t, -PCl(*exo*-ONb), 0.3P), 14.61 (t, -PCl(*endo*-ONb), 0.7P). ^{1}H NMR ($CDCl_3$) δ (ppm): 6.20 (q, 5-H, endo, 0.7H), 6.11 (m, 5-H, exo, 0.3H), 6.11 (m, 6-H, exo, 0.3H), 6.01 (q, 6-H, endo, 0.7H), 4.26 (m, -CH_2O-, exo, 0.3H), 4.08 (dd, -CH_2O-, exo, 0.3H), 3.97 (m, -CH_2O-, endo, 0.7H), 3.77 (dd, -CH_2O-, endo, 0.7H), 2.99 (s, 1-H, endo, 0.7H), 2.86 (s, 4-H, endo, 0.7H), 2.82 (s, 4-H, exo, 0.3H), 2.53 (m, 2-H, endo, 0.7H), 1.89 (m, 3-H, endo, 0.7H), 1.89 (m, 2-H, exo, 0.3H), 1.50 (m, 7-H, endo, 0.3H), 1.40 (m, 1-H, exo, 0.3H), 1.31 (t, 7-H, exo, 0.3H), 1.30 (t, 3-H, exo, 0.3H), 1.20 (m, 3-H, exo, 0.3H), 0.53 (m, 3-H, endo, 0.7H). ^{31}C NMR ($CDCl_3$) δ (ppm): 138.03 (5-C, endo), 137.13 (5-C, exo), 136.00 (6-C, exo), 131.92 (6-C, endo), 73.36 (-CH2O-, exo), 72.82 (-CH2O-, endo), 49.32 (7-C, exo + endo), 44.82 (1-C, exo), 43.59 (4-C, endo), 43.26 (4-C, exo), 42.23 (1-C, endo), 41.58 (2-C, exo), 38.76 (2-C, endo), 29.21 (3-C, exo), 28.56 (3-C, endo).

*Synthesis of poly[pentachloro-(5-norbornene-2-methoxy)-cyclotriphosphazene] (**3**):* The monomer to initiator ratio was ~190:1 for all reactions to ensure consistency for each batch. Monomer **2** (21.11 g, 0.0485 mol) was degassed under reduced pressure. The monomer was then dissolved in CH_2Cl_2 (200 mL). Grubbs' first generation catalyst (0.20 g, 0.243 mmol) was suspended in CH_2Cl_2 (2 mL) and added rapidly to the stirred monomer solution. The polymerization was terminated after 10 seconds by the addition of 1 mL ethyl vinyl ether. The polymer solution was diluted with 500 mL THF and was used without further purification.

*Synthesis of poly[penta(3-methylphenoxy)-(5-norbornene-2-methoxy)-cyclotriphosphazene] (**4**)*: Sodium metal (5.69 g, 0.247 mol) was suspended in THF (200 mL). *m*-Cresol (27.79 g, 0.257 mol) was added slowly and was allowed to react overnight. After the reaction was complete, as indicated by the consumption of the sodium metal, the *m*-cresol salt

solution was cannulated into the previously prepared polymer **3** solution. The reaction mixture was then refluxed for 5 days. The resultant solution was concentrated by rotary evaporation and precipitated twice into methanol and twice into hexanes. The product polymer was an adhesive, brown material which was dried in a round bottom flask in preparation for the subsequent reaction. Yield = 31.32 g (81 %) from 21.11 g of monomer 2. ^{31}P NMR ($CDCl_3$) δ ppm: 12.3 (t (endo-exo overlap), $P(OC_6H_4CH_3)$(O-CH_2-Nb), 1P), 8.8 (d, $P(OC_6H_4CH_3)_2$, 2P (86%)), 7.7 (d, $P(OC_6H_4CH_3)_2$, 2P (14%)) ^{1}H NMR ($CDCl_3$) δ ppm: 6.8 (m, Ar*H*, 20H), 5.25 ppm (s, br, C*H*=C*H*, 2H), 3.5 (d, OCH_2, 2H), 2.2 (s, ArCH_3, 15H), 1.65 (m, cyclopentane ring, 7H)

*Hydrogenation of the polymer backbone to poly[penta(3-methylphenoxy)-(5-norbornene-2-methoxy)-cyclotriphosphazene] (**5**)*: *p*-Xylene was added to the round bottom flask containing the purified polymer **4** (31.31 g, 0.0394 mol), and stirring was maintained overnight to dissolve the polymer. A large excess of *p*-toluenesulfonhydrazide (73.37 g, 0.394 mol) was added to the polymer solution and the solution was refluxed for 3 hours. The solution was then concentrated by evaporation and the product was precipitated into methanol. This polymer was redissolved in THF and precipitated into methanol twice. The polymer obtained was dried under vacuum to yield an adhesive off-white material. A molecular weight of 190 kDa and a PDI of 2.6 were estimated for the polymer. The T_g of the polymer was found to be 2 °C by DSC. Yield = 21.84 g (69%). ^{1}H NMR ($CDCl_3$) δ ppm: 6.8 (m, Ar*H*, 20H), 3.5 (d, OCH_2, 2H), 2.2 (s, ArCH_3, 15H), 1.65 (m, cyclopentane ring and -CH_2CH_2- overlap, 11H)

*Sulfonation Procedure (**6A**-**6E**)*: Polymer **5** (19.81 g, 0.0249 mol) was dissolved in dichloroethane and cooled in an ice bath. Aliquots of a 1 M SO_3 solution in dichloroethane were added to the polymer solution slowly according to desired degree of sulfonation. The reaction was allowed to proceed for 3 hours and was quenched by the addition of 50 mL saturated NaOH solution in 1:1 water and ethanol mixture. At this point, the polymer had precipitated from the solution as a dark brown solid. The solution was evaporated to dryness under reduced pressure

and the polymer was soaked for 24 hour in successive cycles in deionized water, 0.1 M aqueous NaOH, deionized water, 0.1 M aqueous HCl and deionized water. Finally, water was removed from the polymer in a vacuum oven at 0.1 mmHg and 40 °C.

*Film Casting and Radiation Crosslinking (**7A**-**7E**, **8**)*: Dried polymer **6** (5.00 g) was dissolved in 100 mL of *N*,*N*-dimethylacetamide. Six 10 x 10 cm membranes were cast from this solution on polypropylene plates. The membranes were dried under vacuum at 24 °C for 48 hours and at 80 °C for 24 hours. The membranes obtained were brown, flexible, and had an average thickness of 210 μm. The membranes were then crosslinked by exposure to 20 MRad (Sample **7A**-**7E**) or 40 MRad (Sample **8**) gamma irradiation from a ^{60}Co source at the Pennsylvania State University Breazeale Nuclear Reactor facility.

3.2.4 Characterization

Determination of IEC values: The neutral condition ionic exchange capacity (IEC) titration experiment was selected as the evaluation method for the equivalent amount of active acid groups introduced [33]. This is based on the fact that the number of protons available for actual ionic exchange is a better indication of the number of free protons that would dissociate and contribute to actual conductivity than the results from other experimental methods such as NMR. The protons from the acidic group in the polymer were exchanged with Na^+ ions by soaking a 0.10 g sample of the polymer in 50 ml of a 2 M NaCl solution for 48 hours with occasional shaking. Aliquots of the solution (10 ml) were titrated with 0.01 M NaOH to calculate the amount of protons released by the polymer. The IEC value is reported as moles of protons per gram of polymer.

Determination of Water and Methanol Swelling: The polymers were soaked in deionized water for 24 hours at 24 °C, after which time the polymers were removed from water and excess

liquid on the surface was removed by gently pressing the polymer between two halves of a filter paper. The degree of swelling is defined as the following equation:

water swelling(%) = $[(\omega_{wet} - \omega_{dry})/\omega_{dry}] \times 100$

ω_{wet} and ω_{dry} are the weights of wet and dry polymer respectively. Methanol swelling experiments were carried out in a similar manner, except that either pure methanol or a 10% v/v methanol aqueous solution was used instead of water.

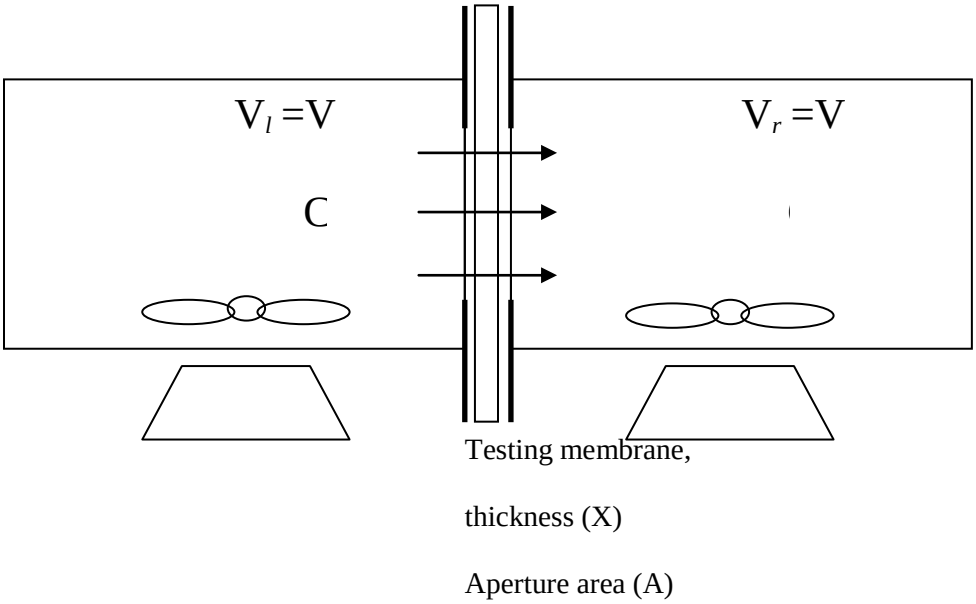

Figure 3-3 Schematic diagram for methanol permeability measurements

Determination of Methanol Permeability: Methanol permeability was measured through a modified published method [34, 35]. A film of the polymer was sandwiched between the two halves of the apparatus and was sealed tightly to prevent leaks. One chamber of the apparatus was filled with de-ionized water; the other with a 10% solution of methanol in water. After 24 hours at room temperature, the methanol content of the de-ionized water was evaluated by ^1H NMR spectroscopy by comparing the methanol CH_3 peak integration to the OH peak and by calibration via a series of standard solutions. Nafion 115 was used in this experiment as a

standard sample, and was evaluated by the same procedures to ensure that the results are comparable.

3.3 Results and Discussion

3.3.1 Polymer Synthesis

In the synthesis of monomer **2**, a 0.4 molar excess of hexachlorocyclotriphosphazene and a low reaction temperature were employed to ensure replacement of only one chlorine atom per hexachlorocyclotriphosphazene ring by the norbornene unit. This was confirmed by ^{31}P NMR spectroscopy. Although the monomer initially had a 0.3:0.7 ratio of exo:endo norbornene, the isomer ratio changed to 0.14:0.86 after polymerization as evidenced by ^{31}P NMR spectra of **4**. It is speculated that one of the isomers is more reactive than the other due to the positioning of the bulky cyclic phosphazene group. Similar observations have been made in the ring opening metathesis polymerizations of other norbornene systems [36, 37]. The different reactivity of the isomers can also be used to explain the large polydispersity index in the polymer. The backbone of the polymer was then hydrogenated to suppress crystallinity and to prevent side reactions during the subsequent sulfonation procedure. Hydrogenation was carried out using *p*-toluensulfonylhydrazide following a procedure adapted from Cohen [38]. The complete saturation of the backbone was indicated by the disappearance of the alkene peak at 5.25 ppm in the ^{1}H NMR spectra from polymer **4** to polymer **5**.

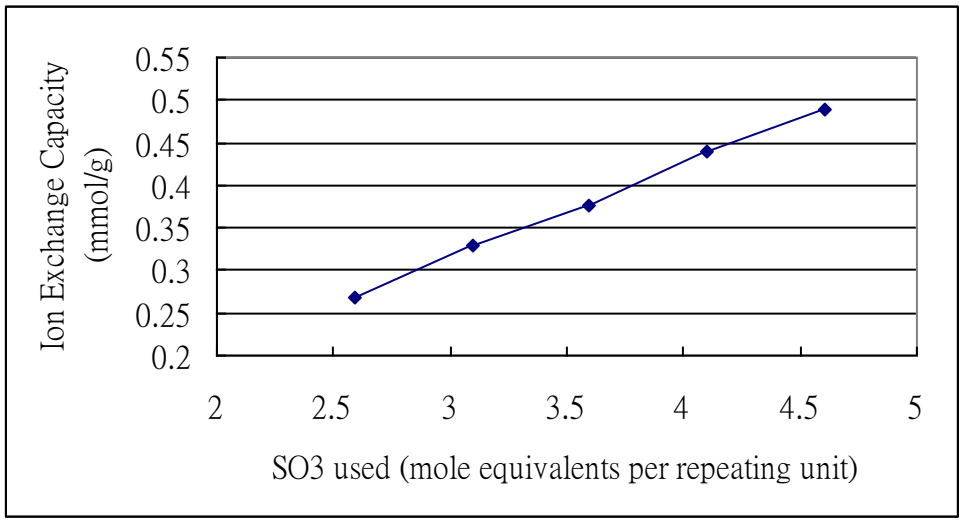

Figure 3-4 IEC values of the polymer versus the amount of SO_3 used for sulfonation.

3.3.2 Sulfonation and IEC Values

The addition of SO_3 to polymer **5** introduced sulfonic acid groups at the aryl rings. Previous studies have indicated that sulfonation occurs primarily at the *para*-position of the aryl rings [39]. From Figure 3-4, it is clear that the IEC values show a linear relationship with the amount of SO_3 added. Hence, this sulfonation procedure allows accurate control of the IEC value. From an extrapolation of the line in Fig 3-4, it appears that sulfonation began after 0.383 molar equivalents of SO_3 per repeat unit were added. This observation is consistent with the work of Montoneri [40] and Pintauro [41] who explained that SO_3 should coordinate first to the lone pair electrons of the phosphazene nitrogen atoms during sulfonation of aryloxy substituted polyphosphazenes. They reported that sulfonation of the aryl rings did not occur until < 50 % of the phosphazene nitrogen atoms were complexed with SO_3. Our results deviate from theirs because we estimate that sulfonation of the aryl rings occurs only after 13 % of the phosphazene nitrogen atoms have been complexed with SO_3 (3 nitrogen atoms per repeat unit, hence 0.383/3 * 100 = 13 %). Sulfonation of the aryl rings occurred at a lower level of added SO_3, probably

because the nitrogen atoms in the rigid cyclic phosphazene trimer ring are less accessible than those in a flexible linear polyphosphazene polymer. A comparison of the materials used during this study is summarized in Table 3-1.

Table 3-1 Properties of uncrosslinked sulfonated polymers

Sample	SO_3 used	IEC	Water Swelling
	(mole eq)	(mmol/g)	(%)
6A	2.588	0.267	35.8
6B	3.093	0.329	55.03
6C	3.598	0.377	105.18
6D	4.103	0.44	202.73
6E	4.608	0.49	309.99

3.3.2 Crosslinking and Physical Property Changes

To ensure mechanical stability, restrict water uptake, and lower the methanol crossover of the new membrane materials, ^{60}Co Gamma radiation treatment was used in our study to induce free radical crosslinking. The membranes were fabricated according to the above procedures, exposed to radiation, and compared with samples untreated by radiation. The membranes had an average thickness of 170~250 μm and showed no measurable dimensional change after radiation treatment. The Tg of the material increased as expected after both the sulfonation and crosslinking treatments. The mechanical strength of the materials improved after crosslinking, especially when in the water-swollen state. Thus, the following studies were conducted on the crosslinked films only. The results of these studies are summarized in Table 3-2.

Table 3-2 Performance data for crosslinked sulfonated polymers

Sample	IEC	Crosslink	Water Swelling	Pure MeOH Swelling	10% MeOH Swelling	MeOH Crossover	Conductivity	T_g
	(mmol/g)	(Mrad)	(%)	(%)	(%)	(10^{-9} cm^2/sec)	(10^{-5} S/cm)	(˚C)
7A	0.267	20	33.6	53.81	34.98	2.11	0.213	5.14
7B	0.329	20	49.9	57.3	47.4	2.45	0.265	16.76
7C	0.377	20	52.25	67.6	65.53	2.91	1.03	51.15
7D	0.44	20	69.92	75.67	73.01	3.3	2.89	57.93
7E	0.49	20	84.13	84.15	89.69	5.3	8.26	69.33
8	0.49	40	75.28	70.32	74.17	2.67	11.3	68.66
Nafion 115	0.88	0	15.85	61.35	27.71	498	2600	110

3.3.3 Water Swelling Behaviour

The water uptake values of each membrane were determined by comparison of the dry weight to the fully hydrated weight and are reported in Tables 3-1 and 3-2. The numbers obtained from different samples were compared as a function of the IEC value of the polymer membrane, as shown in Fig 3-5. The water swelling of the uncrosslinked materials increased exponentially as the IEC increased. This result suggests that the higher concentrations of sulfonic acid groups definitely induced the formation of aqueous clusters. Thus, increased incorporation of sulfonate groups generates higher hydrophilicity and higher IECs. The distance between the organic polymer backbone and the acidic groups may also affect the water uptake, as shown from earlier studies [42]. Although the degree of water swelling is high, this effect can be reduced by further crosslinking of the membrane because enhanced rigidity of the polymer structure should prevent the expansion of water clusters. Our results show the logical outcome of a drastic decrease of water swelling in the membrane with an increased degree of crosslinking. For example, with an IEC of 0.49 mmol g^{-1} the swelling was reduced from 310 % (**6E**) to 84 % (**7E**) after 20 Mrad of

radiation treatment, which translates to 1 : 0.27 in water uptake. However, when the highest radiation dosages were applied (**7E** to **8**) an increase in radiation dosage did not lead to decrease of water uptake. This may be caused by a saturation of the radical crosslinking reactions.

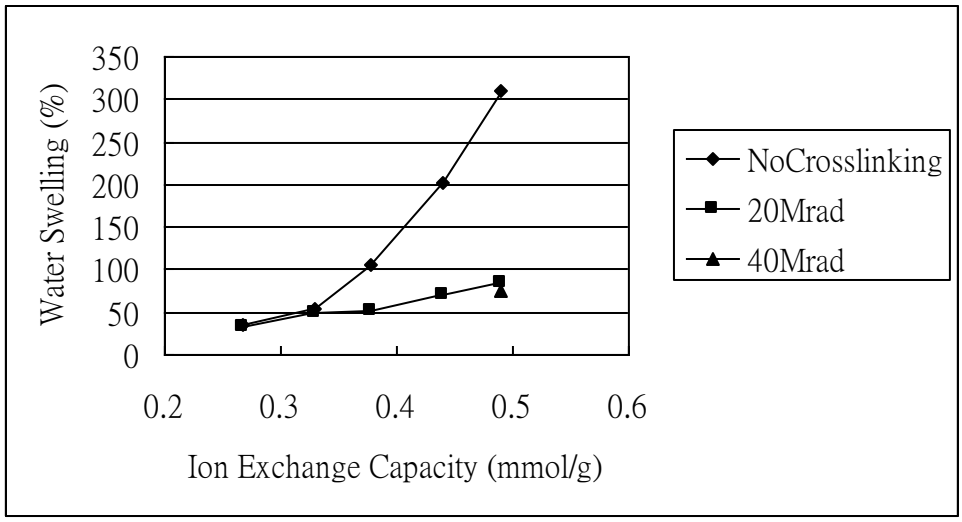

Figure 3-5 Water swelling vs the IEC value of the uncrosslinked and crosslinked polymer

3.3.4 Methanol Swelling Behavior

Methanol uptake of the samples was determined in a similar way to water uptake, with the weight of membrane fully swelled in pure methanol or in 10% methanol in water, compared with the dry mass. The results are reported in percentages as a function of IEC. As with water uptake, a decrease in methanol uptake was apparent following radiation crosslinking. An interesting point is that, although the methanol uptake by each sample was slightly higher than the water uptake, the slope for the data points is smaller than for water uptake. And all three values of uptake (water, 10% methanol, pure methanol) became nearly identical as the IEC approached 0.5. This appears to show that the affinity of the material for methanol is higher than that for water, although increases in the degree of sulfonation, and thus the increase in hydrophilicity, gradually cause a decrease in the difference of affinity.

3.3.5 Proton conductivity

The through-plane ionic conductivities of films of the sulfonated polymers were measured by electrochemical impedance spectroscopy. Through-plane conductivity is the most realistic measurement of ionic conductivity in membranes because it corresponds to the proton transmission in an actual fuel cell. The room temperature ionic conductivity data are reported in Table 3-2.

The ionic conductivities of these polymers at room temperatures were relatively low. This is understandable in terms of the low IECs. The highest measured ionic conductivity was 1.13×10^{-4} S cm^{-1} (polymer **8**), which is approximately two orders of magnitude lower than that of the commercial PEM material Nafion 115. This conductivity, although not a significant breakthrough, is acceptable for small portable devices considering that many other comparable approaches are geared toward operating temperatures much higher than that of our interest [43-45]. We expect the IEC of our materials to improve during future developments. Thus, the polymers described here remain potentially viable PEM materials, especially for powering small portable devices. For high-temperature applications, further experimental data under different temperature and humidity ranges would be required. In addition, following the trend from polymer **7A** through **7E**, the conductivity increases by nearly one order of magnitude each time the IEC increases by 0.1~0.2 units. An extrapolation of these data suggests that, if the degree of sulfonation can be increased, the conductivity could eventually reach a similar level to that of Nafion when the IEC values of the two materials are equal. It is also interesting to note that the conductivity of polymer **8** increased when the radiation dosage was increased from 20 Mrad to 40 Mrad. It is suspected that this may be due to radical-induced side reactions, which could potentially induce the formation of additional acidic groups such as POH units. Further discussion of this possibility requires future research focused on radiation effects.

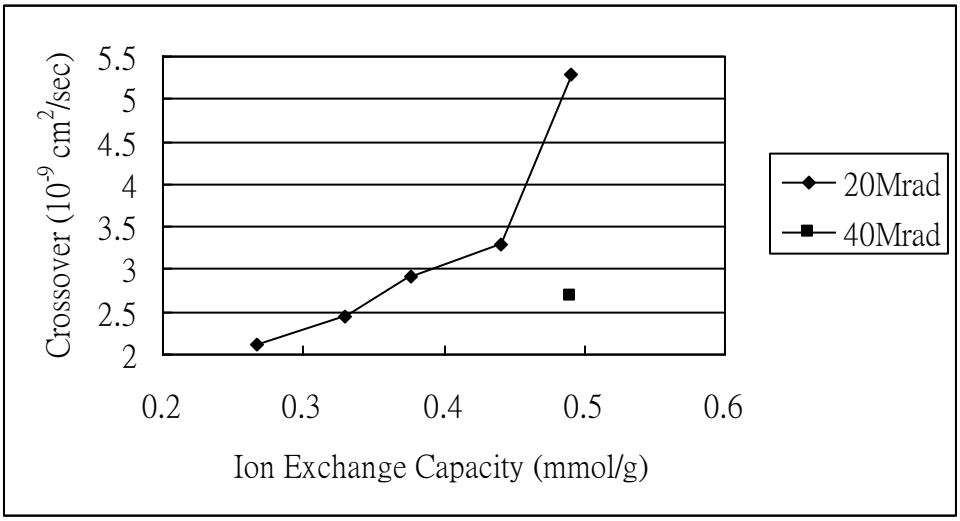

Figure 3-6 Methanol crossover of membranes relative to the IEC values of the materials

3.3.6 Methanol Permeability

The methanol permeability was measured as described above, and was calculated assuming that Fick's first law (steady state diffusion) is applicable. Fick's law can be simplified to the form shown in Eq **(1)**, where C_m is the concentration of methanol in the standard solution, C_w is the concentration of methanol in water after diffusion, and x is the thickness of the membrane.

$$J_m = -D.\frac{dC}{dX} = D.\frac{C_m - C_w}{x} \qquad \textbf{(1)}$$

Solving this equation with the initial condition of $Cw_{(0)}=0$ this yields Eq **(2)**, where D is the diffusion coefficient, V is the volume of solution, x is the thickness of the membrane, A is the cross-sectional area of the membrane, t is the time in minutes, $C_{w(t)}$ is the concentration of methanol in the water after time t, and $C_{m(0)}$ is the concentration of methanol in the standard solution at t=0.

$$C_{w(t)} = \tfrac{1}{2} C_{m(0)}.(1 - e^{\frac{-2ADt}{Vx}}) \quad \textbf{(2)}$$

Rearrangement of this equation gives us the diffusion constant D as Eq **(3)**:

$$D = -\frac{Vx}{2At} \ln\left(1 - \frac{2C_{w(t)}}{C_{m(0)}}\right) \quad \textbf{(3)}$$

In this experimental design, we used 10% methanol in water for the standard methanol solution and performed the experiments at room temperature. The reason for this arrangement is to obtain a close approximation to the actual working conditions in a possible room-temperature methanol fuel cell assembly. The methanol permeability data of polymers **7A** – **8,** as well as the value for Nafion 115 using our method, are reported in Table 3-2. The diffusion coefficients of our materials generally follow the trend of the IEC values, as shown on Figure 3-6, which is to be expected since it is assumed that the hydrophilic channels aid methanol diffusion. These data indicate that the methanol permeabilities of these materials are very low – typically two orders of magnitude lower than for Nafion. Finally, the increase in crosslink density brought about by utilizing 40 Mrad of gamma radiation reduces the methanol crossover by half, which reflects the enhanced rigidity of the polymer matrix.

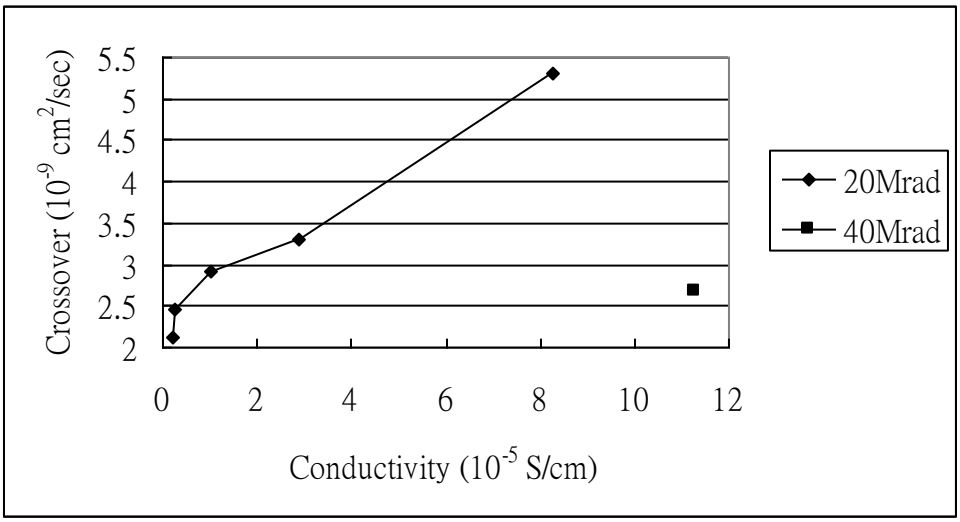

Figure 3-7 Dependence of methanol crossover on ionic conductivity of the membranes

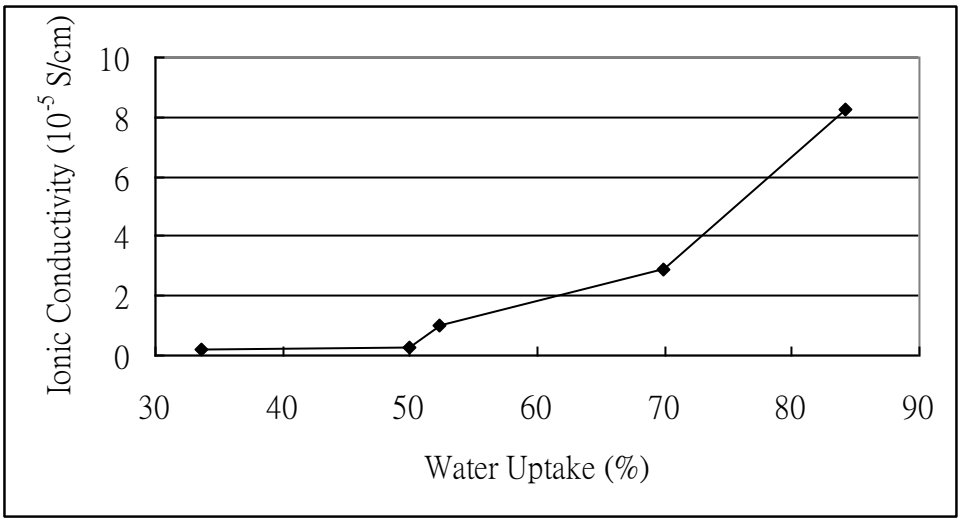

Figure 3-8 Relationship between ion conductivity and water uptake of 20Mrad crosslinked membranes

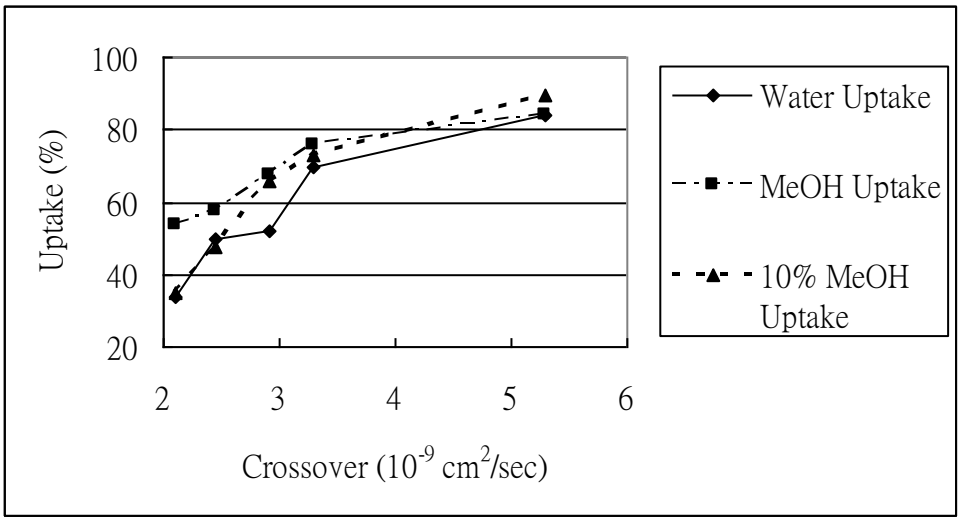

Figure 3-9 Relationship of methanol crossover to water and methanol uptake of 20Mrad crosslinked membranes

3.3.7 Relationship of IEC, Swelling, Conductivity and Permeability

At the same time, the increase in methanol diffusion with increases in conductivity seems to be minor, as shown in Fig 3-7. The linear relationship suggests that the norbornane-phosphazene membrane should still have methanol permeability ten times less than Nafion at the point where it has the same ionic conductivity.

Usually it would be expected that the low methanol crossover, when combined with low ionic conductivity, results from the presence of small amounts of hydrophilic domains that form only small or isolated clusters and thus cannot efficiently transport these water-soluble species. In such a case, there will be no continuous conductive channel in the membrane microstructure for either protons or methanol, and thus the conductivity and crossover will both remain low. However, in our case the assumption of cluster formation cannot fully explain the high water uptake compared with the ionic conductivity and IEC, because a lack of hydrophilic clusters should lower water affinity. [5] One possibility is the formation of large but isolated hydrophilic

clusters in a film structure, since our long spacer groups connecting the sulfonated side groups to the hydrophobic main chain could very well promote enough flexibility to induce large micelle – like isolated structures within the polymer matrix. Nafion, on the other hand, may be generating smaller clusters in greater numbers compared to our material and have a higher chance of forming interconnected channels. It is also possible to contemplate a different mechanism based instead on the chemical structure. Because our results indicate a high degree of hydrophilicity but low ion mobility, it is suspected that sites other than sulfonate groups may contribute to the coordination of cations [46]. These may include the nitrogen atoms on the phosphazene rings. Such immobilized protons, while still within the polymeric structure and causing the material to be more hydrophilic, would not contribute to either our IEC results or the ionic conductivity. If this assumption is correct, it might be expected that higher concentrations of cations would eventually saturate the extra coordination sites and lead to a large increase of ionic conductivity. As shown by Fig 3-8, the fact that ionic conductivity increases nonlinearly with the water swelling may be indirect evidence for this effect, although further experiments are required to confirm this assumption as well as an investigation of the actual microstructure of these membranes.

A similar model can also be used to explain the relatively low methanol crossover values compared to the water and methanol swelling, as shown in Fig. 9. Usually high methanol swelling would indicate high methanol crossover, but in our experiments the samples repeatedly show that the membranes have lower methanol crossover than Nafion under identical experimental conditions, even though Nafion has a lower methanol uptake. Again, it is possible to explain the phenomena through either microstructure or molecular interaction viewpoints: Large but isolated hydrophilic clusters are expected to absorb and hold large amounts of methanol given enough time, while diffusion throughout the material will still be restricted by barriers between clusters. On the other hand, because the high methanol uptake probably indicates strong interactions between the polymer and methanol molecules, the movement of methanol molecules within the

polymer matrix could be hindered in a way that is similar to the behavior of species within a chromatography column. Thus, the molecular interactions between the mobile and immobile species may slow the movement of mobile species. This effect is likely to be further enhanced by the radiation crosslinking, because rigidity of the polymer matrix would generate higher levels of steric restriction to methanol molecule movement. Experiments to confirm the actual mechanism will be included in future research.

3.4 Conclusions

We have synthesized polynorbornanes with pendent cyclic phosphazene groups that bear aryl sulfonic acid units as a potential proton conductive membranes material for small, portable DMFCs. The polymers were evaluated by IEC and water swelling to determine their suitability as proton conductive membrane materials in DMFCs. We also fabricated membranes of the polymer with different degrees of sulfonation and crosslinking. The differences in proton conductivity, methanol permeability, and water / methanol uptake between these membranes and that of commercially available Nafion 115 were then compared.

The IEC values of the polymers were controlled accurately through the ratio of SO_3 to repeating units in the polymer. Although the degree of water swelling of the membranes was high, it can be decreased by crosslinking the polymer by gamma radiation. The resultant polymers had lower ion exchange capacities than traditional materials such as Nafion and, as a consequence, lower conductivities. However, the methanol permeabilities of these polymers were low, and were generally of the order of 10^{-9} cm^2/sec. This is roughly two orders of magnitude lower than for the commercial polymer Nafion 115. This result can be explained by the low IECs (and hence ionic strengths) of these materials, the microstructure effect, and the affinity effect of the material on cations and methanol.

The ionic conductivities of these materials were not exceedingly high, but their low methanol permeabilities suggest that they may be viable materials for use as proton exchange membranes in direct methanol fuel cells for use in small portable devices. We plan to further improve these materials by future investigations of alternative sulfonation procedures, as well as possible utilization of double bonds in the original norbornene backbone as reaction sites or crosslink promoters.

References

[1] M. Winter, R. J. Brodd, What are batteries, fuel cells, and supercapacitors? Chem. Rev., 104 (2004) 4245-4270.
[2] N. W. Deluca, Y. A. Elabd, Polymer electrolyte membranes for the direct methanol fuel cell: A review, J. Polym. Sci., Part B: Polym. Phys., 44 (2006) 2201-2225.
[3] K. Scott, A. K. Shukla, Polymer electrolyte membrane fuel cells: Principles and advances, Rev. Enviro. Sci. BioTech., 3 (2004) 273-280.
[4] Y. A. Elabd, C. W. Walker, F. L. Beyer, Triblock copolymer ionomer membranes: Part II. Structure characterization and its effects on transport properties and direct methanol fuel cell performance, J. Membr. Sci., 231 (2004) 181-188.
[5] H. L. Yeager, A. Steck, Cation and water diffusion in Nation ion exchange membranes: Influence of polymer structure, J. Electrochem. Soc., 128 (1981) 1880-1884.
[6] K. A. Mauritz, R. B. Moore, State of understanding of Nafion, Chem. Rev., 104 (2004) 4535-4585
[7] K. D. Kreuer, On the development of proton conducting polymer membranes for hydrogen and methanol fuel cells, J. Membr. Sci., 185 (2001) 29-39.
[8] K. D. Kreuer, S. J. Paddison, E. Spohr, M. Schuster, Transport in proton conductors for fuel cell applications: Simulations, elementary reactions, and phenomenology, Chem. Rev., 104 (2004) 4637-4678
[9] J. Roziere, D. Jones, Non-fluorinated polymer materials for proton exchange membrane fuel cells, Annu. Rev. Mater. Res., 33 (2003) 503-555.
[10] T. Schultz, S. Zhou, K. Sundmacher, Current status of and recent developments in the direct methanol fuel cell, Chem. Eng. Technol., 24 (2001) 1223-1233.
[11] A. Heinzel, V. M. Barragan, A review of the state-of-the-art of the methanol crossover in direct methanol fuel cells, J. Power Sources, 84 (1999) 70-74.
[12] M. A. Hickner, H. Ghassemi, Y. S. Kim, B. R. Einsla, J. E. McGrath, Alternative polymer systems for proton exchange membranes (PEMs), Chem. Rev., 104 (2004) 4587-4612
[13] H. R. Allcock, R. M. Wood, Design and synthesis of ion-conductive polyphosphazenes for fuel cell applications: Review, J. Polym. Sci. Part B: Polym. Phys., 44 (2006) 2358-2368.
[14] R. Carter, R. Wycisk, H. Yoo, P. N. Pintauro, Blended polyphosphazene/polyacrylonitrile membranes for direct methanol fuel cells, Electrochem. Solid State Lett., 5 (2002) A195-A197.
[15] X. Zhou, J. Weston, E. Chalkova, M. A. Hofmann, C. M. Ambler, H. R. Allcock, S. N. Lvov, High temperature transport properties of polyphosphazene membranes for direct methanol fuel cells, Electrochim. Acta, 48 (2003) 2173-2180.
[16] R. Wycisk, J. K. Lee, P. N. Pintauro, Sulfonated polyphosphazene-polybenzimidazole membranes for DMFCs, J. Electrochem. Soc., 152 (2005) A892-A898.
[17] Q. Guo, P. N. Pintauro, H. Tang, S. O'Connor, Sulfonated and crosslinked polyphosphazene-based proton-exchange membranes, J. Membrane Sci., 154 (1999) 175-181.
[18] H. R. Allcock, T. J. Hartle, J. P. Taylor, N. J. Sunderland, Organic polymers with cyclophosphazene side groups: Influence of the phosphazene on physical properties and thermolysis, Macromolecules, 34 (2001) 3896-3904.

[19] H. R. Allcock, New Approaches to hybrid polymers that contain phosphazene rings, J. Inorg. Organomet. Polym., 17 (2006) 349-359.
[20] H. R. Allcock, W. R. Laredo, C. R. deDenus, J. P. Taylor, Ring-opening metathesis polymerization of phosphazene-functionalized norbornenes, Macromolecules, 32 (1999) 7719-7725.
[21] C. W. Bielawski, R. H. Grubbs, Living ring-opening metathesis polymerization, Prog. Polym. Sci., 32 (2007) 1-29.
[22] M. L. Randall, M. L. Snapper, Selective olefin metathesis – New tools for the organic chemist: A review, J. Mole. Cat. A: Chem., 133 (1998) 29-40.
[23] H. R. Allcock, W. R. Laredo, E. C. Kellam, R. V. Morford, Polynorbornenes bearing pendent cyclotriphosphazenes with oligoethyleneoxy side groups: Behavior as solid polymer electrolytes, Macromolecules, 34 (2001) 784-794.
[24] D. T. Welna, D. A. Stone, H. R. Allcock, Lithium-ion conductive polymers as prospective membranes for lithium-seawater batteries, Chem. Mater., 18 (2006) 4486-4492.
[25] J. Kim, B. Kim, B. Jung, Proton conductivities and methanol permeabilities of membranes made from partially sulfonated polystyrene-block-poly(ethylene-ran-butylene)-block-polystyrene copolymers, J. Membr. Sci., 207 (2002) 129-137.
[26] P. Xing, G. P. Robertson, M. D. Guiver, S. D. Mikhailenko, K. Wang, S. Kaliaguine, Synthesis and characterization of sulfonated poly(ether ether ketone) for proton exchange membranes, J. Membr. Sci., 229 (2004) 95-106.
[27] C. Genies, R. Mercier, B. Sillion, N. Cornet, G. Gebel, M. Pineri, Soluble sulfonated naphthalenic polyimides as materials for proton exchange membranes, Polymer, 42 (2001) 359-373.
[28] R. W. Kopitzke, C. A. Linkous, G. L. Nelson, Sulfonation of a poly(phenylquinoxaline) film, J. Polym. Sci., Part A: Polym. Chem., 36 (1998) 1197-1199.
[29] J. A. Asensio, S. Borros, P. Gomez-Romero, Proton-conducting polymers based on benzimidazoles and sulfonated benzimidazoles, J. Polym. Sci., Part A: Polym. Chem., 40 (2002) 3703-3710.
[30] H. R. Allcock, E. H. Klingenberg, M. F. Welker, Alkanesulfonation of cyclic and high polymeric phosphazenes, Macromolecules, 26 (1993) 5512-5519.
[31] A. B. Pangborn, M. A. Giardello, R. H. Grubbs, R. K. Rosen, F. J. Timmers, Safe and convenient procedure for solvent purification, Organometallics, 15 (1996) 1518-1520.
[32] J. M. Blanco, F. Fernández, García-Mera, Xerado, J. E. Rodrígues-Borges, Divergent synthesis of two precursors of 3′-homo-2′-deoxy- and 2′-homo-3′-deoxy-carbocyclic nucleosides, Tetrahedron, 58 (2002) 8843-8849
[33] G. Hoogers, Fuel Cell Technology Handbook, CRC press, New York, 2003
[34] X. Zhou, J. A. Weston, E. Chalkova, M. A. Hofmann, C. M. Ambler, H. R. Allcock, S. N. Lvov, High temperature transport properties of polyphosphazene membranes for direct methanol fuel cells, Electrochim. Acta, 48 (2003) 2173-2180
[35] M. V. Fedkin, X. Zhou, M. A. Hofmann, E. Chalkova, J. A. Weston, H. R. Allcock, S. N. Lvov, Evaluation of methanol crossover in proton-conducting polyphosphazene membranes, Mater. Lett., 52 (2002) 192-196
[36] V. Lapinte, J.-C. Brosse, L. Fontaine, Synthesis and ring-opening metathesis polymerization (ROMP) reactivity of endo-and exo-norbornenylazlactone using ruthenium catalysts, Macromol. Chem. Phys., 205 (2004) 824-833
[37] N. Seehof, S. Grutke, W. Risse, Selective reaction of exo-isomers in ring-opening olefin metathesis polymerization (ROMP) of fluoroalkyl-substituted norbornene derivatives, Macromolecules, 26 (1993) 695-700
[38] B. H. Sohn, J. A. Gratt, J. K. Lee, R. E. Cohen, Hydrogenation of ring opening metathesis polymerization polymers, J. Appl. Polym. Sci., 58 (1995) 1041-1046
[39] H. R. Allcock, R. J. Fitzpatrick, Sulfonation of (aryloxy) - and (ary1amino)phosphazenes: Small-molecule compounds, polymers, and surfaces, Chem. Mater., 3 (1991) 1120-1132
[40] E. Montoneri, M. Gleria, G. Ricca, G. C. Pappalardo, New acid-polyfunctional water-soluble phosphazenes: Synthesis and spectroscopic characterization, J. Macromol. Sci. A: Pure. Appl. Chem., 26 (1989) 645-661
[41] R. Wysick, P. N. Pintauro, Sulfonated polyphosphazene ion-exchange membranes, J. Membrane Sci., 119 (1996) 155-160

[42] Q. Li, R. He, J. O. Jensen, N. J. Bjerrum, Approaches and recent development of polymer electrolyte membranes for fuel cells operating above 100 ^{o}C, Chem. Mater., 15 (2003) 4896-4915
[43] S. R. Narayanan, S-P. Yen, L. Liu, S. G. Greenbaum, Anhydrous proton-conducting polymeric electrolytes for fuel cells, J. Phys. Chem. B, 110 (2006) 3942-3948
[44] M. Yamada, I. Honma, Anhydrous proton conducting polymer electrolytes based on poly(vinylphosphonic acid)-heterocycle composite material, Polymer, 46 (2005) 2986-2992
[45] M. Yamada, I. Honma, Alginic acid–imidazole composite material as anhydrous proton conducting membrane, Polymer, 45 (2004) 8349-8354
[46] J. Roziere, J. J. Deborah, M. Marrony, On the doping of sulfonated polybenzimidazole with strong bases, Solid State Ionics, 145 (2001) 61-68.

Chapter 4 Characterization of Water in Proton Conducting Membranes by Deuterium NMR T_1 Relaxation

4.1 Introduction

The proton conducting membrane is an integral component of polymer electrolyte fuel cells. The function of the membrane is to transport protons generated at the anode to the cathode where they are combined with oxygen to form water. At the same time, the membrane must separate the fuel from the oxidant as well as prevent internal short-circuiting of the cell. The high proton conductivity and excellent chemical stability of Nafion® make it the quintessential proton conducting membrane.[1] This high proton conductivity is due to the presence of hydrophilic, sulfonic acid-rich domains within the membrane. Water molecules that reside in these 5 nm wide hydrophilic channels conduct protons in a Grotthuss chain mechanism. However, the proton conductivity of Nafion decreases drastically at low relative humidity due to loss of water. Furthermore, the flexible structure of Nafion renders it unsuitable for high temperature operation where macroscopic deformation of the membrane and disruption of the ionic domains can occur.[2,3,4] Thus, an incentive exists to develop alternative membranes that can perform better than Nafion.

Polymers that are able to conduct protons at low humidity will enable a fuel cell to operate at higher temperatures (> 100 ˚C) which would increase the activity of the platinum catalyst and reduce poisoning of the catalyst by carbon monoxide. Moreover, higher operating temperatures allow expensive platinum catalysts to be replaced by less expensive metal oxide catalysts.[5,6] Some polymer designs that are being investigated for low humidity proton conduction incorporate heterocycles, such as imidazoles[7,8] or triazoles,[9] due to their ability to conduct protons through a Grotthuss chain mechanism. However, the proton conductivity of these systems is low because the dynamics of proton conduction is dependent on the dynamics of the larger

donor-acceptor molecules. Another approach is to synthesize poly(arylene ether) block copolymers which form distinct hydrophobic and hydrophilic phases due to a highly sulfonated hydrophilic block and a hydrophobic block.[10,11,12] The function of the hydrophobic phase is to provide mechanical stability to the sulfonated polymer, which would have poor mechanically stability when hydrated. The proton conductivity of these block copolymers are comparable to Nafion when hydrated but improvements over Nafion at low humidity is yet to be proven.[10]

Many studies on the nanophase structure of proton conducting membranes have been carried out to correlate the size and connectivity of the hydrophilic domains with proton conductivity.[1,13,14,15] However, the characterization of water that is absorbed in the membrane is equally important since water is the proton conducting medium. The nature of water in proton conducting membranes has been probed using different techniques such as dielectric spectroscopy,[16,17] differential scanning calorimetry,[18,19] infrared spectroscopy,[20] and nuclear magnetic resonance.[21,22] Computational methods are also used to model the molecular motions of water in proton conducting membranes.[23,24] It has been proposed that at least two types of water are present in fuel cell membranes, which are termed ‘free’ water and ‘bound’ water. ‘Free’ water is essentially uncoordinated water that exists within the hydrophilic pores of the membrane and displays characteristics that are similar to bulk water. ‘Bound’ water is strongly coordinated to the sulfonic acid groups of the polymer. Due to its limited mobility, bound water has characteristics that resemble solid water at room temperature and this form has been reported in various systems including inorganic solids[25,26,27] and polymer systems.[28,29] Studies have shown that the ‘bound’ water molecules cannot be removed by heating because of their strong coordination to the sulfonic acid groups.[30] Hence, it is conceivable that bound water can be used in a highly sulfonated polymer system for proton conduction at high temperatures. Proton conduction can occur through a mechanism similar to that in ice which involves Bjerrum defects and tetrahedral

jumps of the bound water molecules.[31] Therefore, understanding the state of water in relation to the chemical structure of the polymer and the morphology of the membrane will provide valuable information for planning the synthetic strategy of future proton conducting polymers.

The purpose of this study is to characterize the molecular motion of water molecules that are absorbed in proton conducting membranes. Different proton conducting polymers were chosen with varying chemical and morphological properties that should influence the molecular motion of water that is absorbed. ^{2}H NMR T_1 relaxation was used to probe the molecular motion of deuterated water ($^{2}H_2O$) that was used to hydrate the membranes. ^{2}H T_1 relaxation measurements have an advantage over other techniques because they allow *direct* observation of the molecular reorientational dynamics of the ^{2}H-O bond. Furthermore, consideration for the intermolecular dipolar interactions is not required as opposed to ^{1}H NMR experiments.[32,33] In an NMR T_1 relaxation or spin-lattice relaxation experiment, the nuclei are excited to a higher energy state by a radio-frequency (RF) pulse. The measured relaxation time is the average lifetime of the higher energy state. In other words, the time needed for the higher energy nuclei to dissipate its energy into the lattice. The ^{2}H T_1 relaxation of solid water is short because the molecular vibration frequency of solid water is comparable to the Larmor frequency of the nuclei. Therefore, the energy transfer is efficient and the nuclei relax in about 3 to 10 ms, depending on the magnetic field of the spectrometer. The field dependence of the ^{2}H T_1 relaxation is due to the different Larmor frequencies. By contrast, the ^{2}H T_1 relaxation of bulk water is 400 ms and does not show a dependence on magnetic field because the molecular motion is much faster than the Larmor frequency, and thus energy dissipation from the excited nuclei is inefficient. In work that preceded this project, Benesi was able to characterize the state of water in $^{2}H_2O$-hydrated inorganic porous solids, such as Zeolite A and kanemite, using ^{2}H T_1 relaxation measurements.[25,26,27] The ^{2}H T_1 relaxation of these hydrated inorganic solid were 3 to 10 ms at

room temperature, depending on the magnetic field of the NMR spectrometer, which indicates that ^2H_2O is in the solid state. Using the same principles, we have used NMR T_1 relaxation to characterize the state of water in proton conducting membranes.

4.2 Experimental

4.2.1 Membrane Material

Nafion® 117 was purchased from Ion Power Inc. Aquivion® E87-05 and Radel® (R-5500, M_W 63 kg/mol) were kindly donated by Solvay Solexis. Radel was sulfonated using a modified reference procedure.[34]

4.2.2 Cleaning Procedure

All membranes samples were cut into strips (approximately 3 mm x 35 mm) and were treated to an extensive cleaning procedure prior to NMR analysis. Paramagnetic impurities in commercial membranes were a particular concern because these can shorten T_1 relaxation times and hence distort the interpretation.[22] The procedure was:

i. 24 hour soak in ethanol:water (1:1) solution
ii. Rinse in distilled-deionized (*dd*) water
iii. Boil in 3% hydrogen peroxide for 1 hour
iv. Rinse in *dd* water
v. Boil in 2 M H_2SO_4 for 2 hours
vi. Rinse in *dd* water three times
vii. Drying under vacuum at 80 °C for 24 hours.
viii. Soak in D_2O

4.2.3 *In-Situ* NMR Tube Hydration

The proton conducting membranes were hydrated within an NMR tube using a similar method to the one described by Perrin.[35] Membranes were placed at the bottom of the NMR tube. A porous separator was placed above the membrane strips and a small tube (3 mm *OD* x 1.5 mm *ID* x 50 mm *L*) containing saturated salt solution of $^{2}H_2O$ was inserted to control the humidity within the NMR tube. [36] The tubes were sealed with epoxy glue and allowed to equilibrate over a minimum period of 3 weeks. To ensure full equilibration of the membrane, the NMR relaxation measurements were repeated until a consistent value was obtained. Equilibration times were shorter if the membrane started from a hydrated state as opposed to a dried state because the rate of desorption of water is an order of magnitude faster than rate of sorption of water.[37] Although, both routes ultimately gave the same ^{2}H T_1 relaxation times.

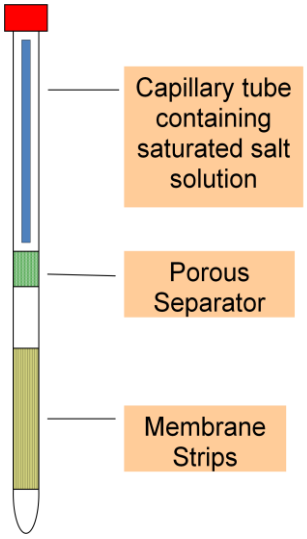

Figure 4-1 Experimental setup for *in-situ* humidification.

4.2.4 NMR T_1 Relaxation Experimental

^{2}H NMR experiments were carried out over a range of temperatures at various magnetic fields, specifically at 300, 400, 500, and 600 MHz, on four different NMR spectrometers: a homebuilt solid state Tecmag-300, a liquid state Bruker DPX-300, a solid state Chemagnetics/Varian Infinity 500 , and a liquid state Bruker AV-3-500 at a range of carefully calibrated temperatures (± 1 K).

The quadrupole echo pulse sequence, $(\pi/2)_x$-τ_1-$(\pi/2)_{\pm y}$-τ_2-Acquire$_x$ with Cyclops phase cycling was added to all pulse phases and the receiver phase, was used to obtain ^{2}H spectra on the solid state Tecmag-300 and Infinity 500 spectrometers at 45.65 and 76.77 MHz respectively ($\pi/2$ = 1.8 to 2.5 μsec, τ_1 = 30 μsec, τ_2 = 25 μsec, spectral width = 1 MHz). The T_1 value of the sharp central aqueous peak was determined at various magnetic fields as a function of temperature with the inversion recovery pulse sequence, π_x - $\tau_{variable}$ – $(\pi/2)_{\phi 1}$ - Acquire$_{\phi ref}$, with ϕ1 = x, y, -x, -y and ϕref = x, y, -x, -y, or the inversion recovery quadrupole echo experiment, π_x - $\tau_{variable}$ – $(\pi/2)_x$-τ_1-$(\pi/2)_{\pm y}$-τ_2-Acquire$_x$ (with Cyclops). At temperatures where the central peak is sufficiently sharp, $\Delta\nu_{1/2}$ < 5 kHz, the data from liquid state spectrometers were obtained using relatively "soft" pulses on a liquid state probe with $\pi/2 \approx 13$ μsec and $\pi \approx 26$ μsec. As verified by separate experiments with hard pulses ($\pi/2 \leq 2.5$ μsec) on the solid state Tecmag-300 and Infinity-500 spectrometers, this was adequate for uniform excitation of the sharp central peak at temperatures where it could be resolved. Variable temperature quadrupole echo spectra were obtained on the solid state Tecmag-300 and Infinity 500 spectrometers using a Chemagnetics variable temperature apparatus. The temperature was calibrated with a copper constantan thermocouple taped in place inside the empty sample coil of the intact probe/variable temperature apparatus operating inside the magnet. The temperatures reported on these instruments are accurate to ca. ± 1 K throughout the reported temperature range.

4.2.5 Water Uptake and Proton Conductivity

The membranes were equilibrated at 25 ˚C in an Espec SH-241 humidity chamber to measure the proton conductivity and water uptake. The proton conductivities of the membranes were measured by two-probe electrochemical impedance spectroscopy (EIS) using a Solartron 1260A frequency response analyzer coupled to a Solartron 1287 potentiostat. The isothermal water uptake of the membrane was converted to hydration number by the equation, λ = [mass of absorbed water/(dry mass of membrane × IEC × molecular mass of water)].

4.3 Results and Discussion

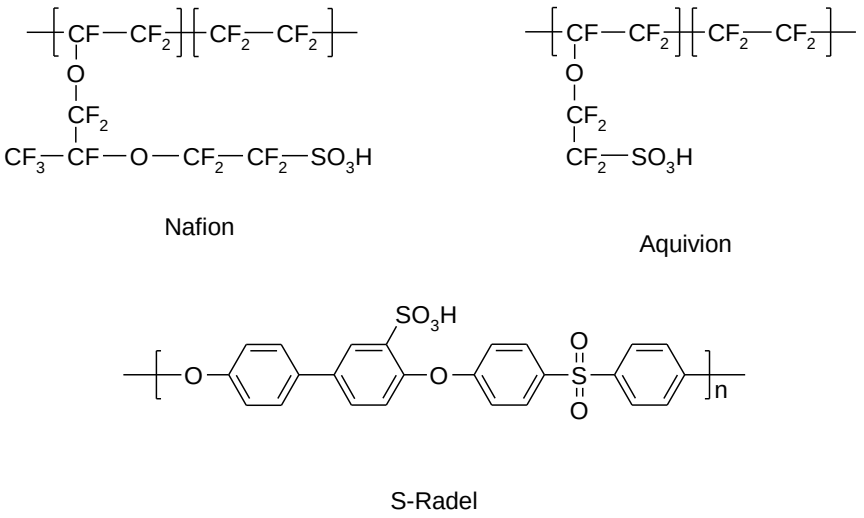

Figure 4-2 Structures of Proton Conducting Polymers

4.3.1 Overview of Membranes

Nafion and Aquivion are perfluorosulfonic acid/polytetrafluoroethlene copolymers (PFSA) which are manufactured by Dupont and Solvay Solexis respectively. Nafion has been the

mainstay in fuel cell studies for many years.[1] Recently, there has been rising interest in PFSA polymers with short side chains due to the better mechanical properties and performance in fuel cells.[38] Aquivion, also previously known as Hyflon Ion, is in many respects structurally similar to Nafion except that the sulfonic acid group is tethered to a shorter side chain (-O-C-C-, 3 atoms) instead of a longer side chain (-O-C-C-O-C-C-, 6 atoms). The Dow Chemical Company also manufactured a short side chain PFSA membrane, which has been discontinued. Although the Nafion and Aquivion membranes that were used in this study have different equivalent weights, 1100 and 870 grams/mole respectively, the average separation between sulfonic acid groups differs by one CF_2CF_2 backbone repeat unit only.

Radel is a poly(arylene ether sulfone) which is also manufactured by Solvay Solexis that can be post-sulfonated to form robust proton conducting membranes with aryl sulfonic acid groups in the main chain. The rigid aryl backbone gives Radel a high glass transition temperature (T_g) but it is less hydrophobic than a fluorinated polymer. As a hydrocarbon polymer, Radel is lower in cost and has less environmental concerns compared to fluorinated polymers, and is thus more accessible depending on the desired proton conducting membrane properties. Two sulfonated-Radel (S-Radel) membranes with two different ion exchange capacities (IEC) of 1.05 and 1.95 mmol/g are compared in this study and will be referred to as S-Radel 1.05 and S-Radel 1.95. The relevant properties of the different polymers and their membranes are summarized in Table 4-1. The different characteristics of the polymers affect how water molecules behave within the polymers.

Table 4-1 Property comparisons of different proton conducting membranes

Polymer	IEC (mmol/g)	Backbone	T_g (˚C)	Acidity (pKa)	Side Chain (atoms)	Phase Separation
Nafion 117	0.909	Perfluorinated alkyl	120	-6	6	Distinct
Aquivion E87-05	1.14	Perfluorinated alkyl	160	-6	3	Distinct
S-Radel	1.05 & 1.95	Hydrocarbon aryl	220	-1	0	Poor

a)

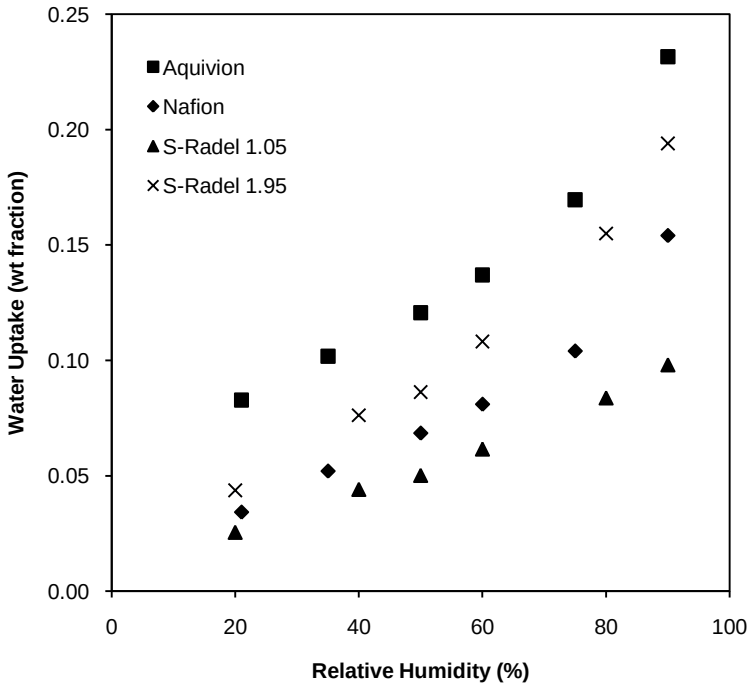

b)

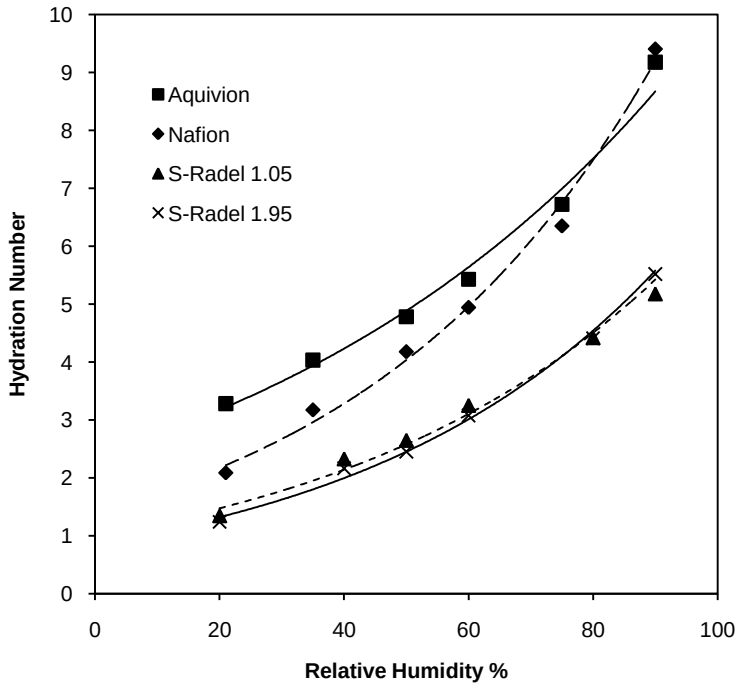

Figure 4-3 (a) Water uptake and (b) hydration number of proton conducting membranes with respect to humidity

4.3.2 Water Uptake Behavior

The proton conducting membranes were equilibrated in different relative humidities and the water uptake was measured. The hydration number, λ = (mole H_2O absorbed/mole SO_3H) in different relative humidities was also calculated. Water uptake of the proton conducting membranes showed an increasing rate of water uptake with increasing relative humidity. The hydration numbers of the both S-Radel samples at a given humidity were similar. The weight fraction of water absorbed by S-Radel 1.95 was higher than S-Radel 1.05 because the IEC of S-Radel 1.95 was higher. The same can be applied for Aquivion and Nafion membranes. In general, the PFSA membranes absorbed more water than the S-Radel membranes because the hydrophilic

channels in PFSA membranes are larger.[13] Constructing a correlation curve of hydration number versus humidity will allow the hydration number of the membranes equilibrated in the NMR tubes at given humidity to be estimated.

4.3.3 Presence of Bound Water

(a)

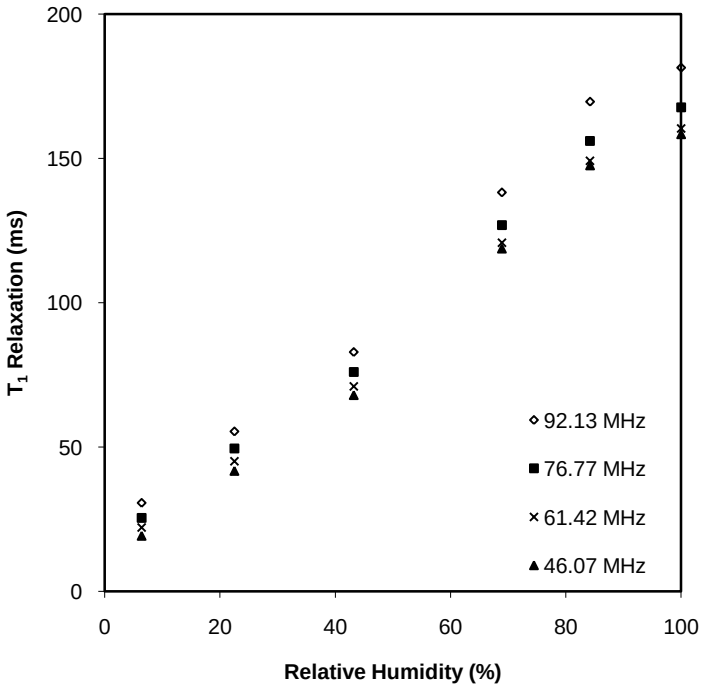

(b)

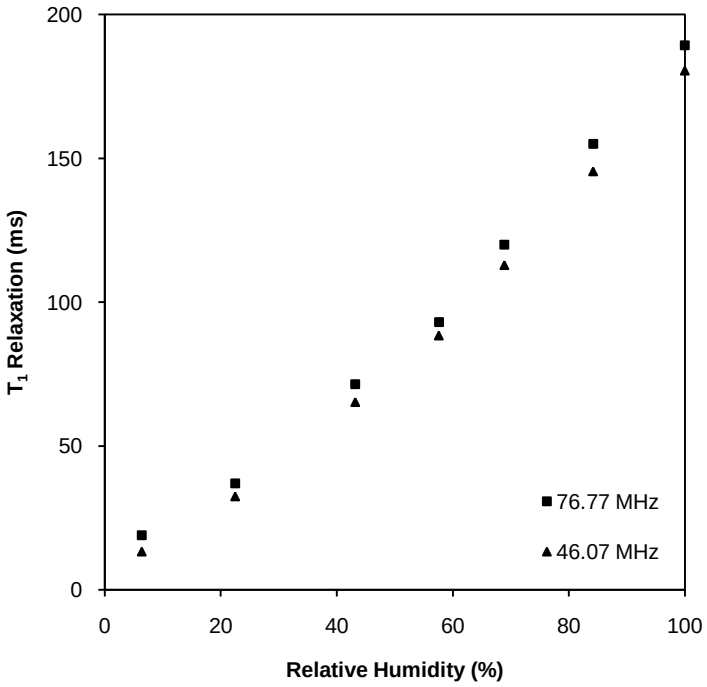
200
150
100
50
0
T_1 Relaxation (ms)
0
20
40
60
80
100
Relative Humidity (%)
76.77 MHz
46.07 MHz

(c)

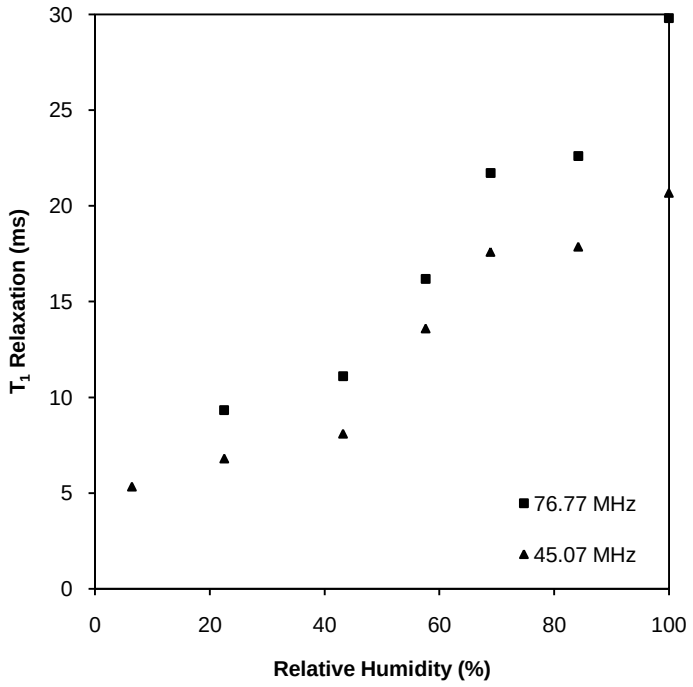

Figure 4-4 ^2H T_1 relaxation times of ^2H_2O in (a) Nafion, (b) Aquivion, and (c) S-Radel 1.95 at different magnetic fields at 25 ˚C.

The ^2H T_1 relaxation of ^2H_2O that was absorbed by the proton conducting membranes in various humidities were obtained at different magnetic fields at 25 ˚C. The ^2H Larmor frequency in the magnetic fields were 92.13, 76.77, 61.42, and 45.07 MHz. The amount of water absorbed by the proton conducting membranes was controlled by the humidity of the environment in which the sample is equilibrated.[39] T_1 relaxation in Nafion and Aquivion increases rapidly in a somewhat linear fashion relative to the humidity in the tube. Conversely, the increase in ^2H T_1 relaxation with humidity of S-Radel 1.95 is much smaller than the PFSA membranes and it shows an inflection point at around 55% RH. At low humidity, the amount of absorbed water is small and it is bound to the sulfonic acid groups as waters of hydration. These ‘bound’ water molecules

have characteristics of solid water, and therefore the ^2H T_1 relaxation is short. As the humidity level increases, 'free' water becomes present as more water is absorbed by the membrane and it is characterized by longer T_1 relaxations times. Furthermore, ^2H T_1 relaxation times of the same membrane samples measured at higher magnetic fields were also longer, indicating the presence of bound water in every membrane sample.[27] Only one resonance peak was observed in the NMR spectrum and the T_1 relaxation was a monoexponential decay because of rapid exchange between the different types of water.[40]

4.3.4 ^2H T_1 Relaxation Behavior of Different Membranes

In order to correlate the state of water to the chemical and morphological structure of the different proton conducting membranes, the ^2H T_1 relaxation at 45.05 MHz was plotted against the hydration number of the membranes that were equilibrated in different relative humidities (RH) according to the saturated salt solutions in the tube. The hydration number for each membrane was estimated by a logarithmic equation that was used to fit the λ versus RH curves of each membrane in Figure 3-3b. The hydration number is used instead of relative humidity to compare the ^2H T_1 relaxations of the different membranes because of the different water uptake behaviors of each proton conducting membrane. There are significant differences between the ^2H T_1 relaxation curves of the different membranes. The ^2H T_1 relaxation times of Nafion and Aquivion range from 19 – 148 ms and 13 – 145 ms respectively whereas the ^2H T_1 relaxation times of the S-Radel 1.05 and S-Radel 1.95 ranged from 5 – 22 ms only. Furthermore, there is an inflection point around $\lambda = 4$ for the ^2H T_1 relaxation curves for S-Radel membranes which is not detected in PFSA membranes. The relationship between the chemical and morphological structure of the proton conducting membranes to the ^2H T_1 relaxation behavior is discussed as follows

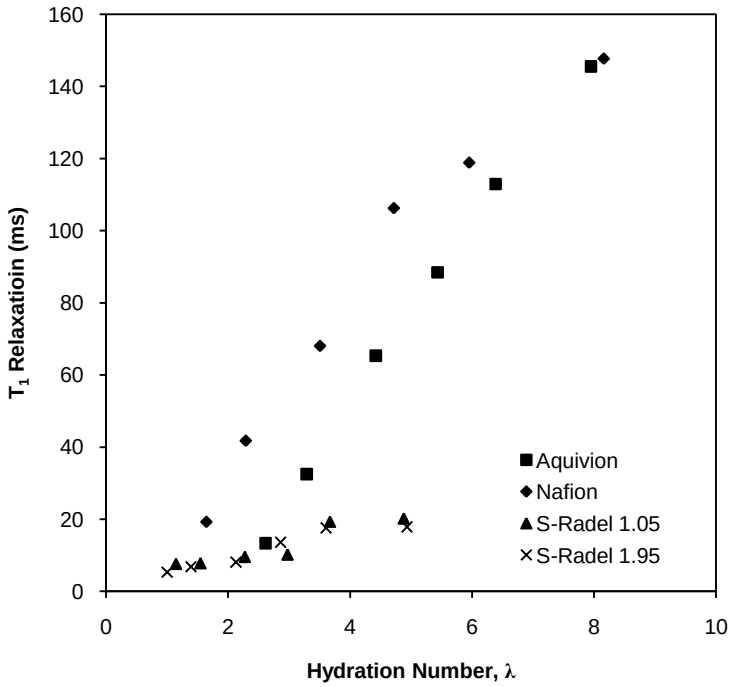

Figure 4-5 ^2H T_1 relaxation times at 45.05 MHz for different proton conducting membranes with hydration number.

The ^2H T_1 relaxations of the S-Radel membranes at low humidity are comparable to previously reported systems such as kanemite and Zeolite A.[25,26,27] We have carried out experiments on freeze dried starch and cellulose that was hydrated with ^2H_2O which also showed ^2H T_1 relaxations of 5 ms at 45.05 MHz.[41] However, the ^2H_2O in Aquivion and Nafion membranes exhibit unusually long ^2H T_1 relaxation times at low hydration, specifically at 13 ms and 19 ms respectively. The unusually long ^2H T_1 relaxation in Nafion at low hydration has been reported previously.[22,42,43] There are two possible reasons for the longer ^2H T_1 relaxations in PFSA membranes at low hydration. First, the acidity of the sulfonic groups in the PFSA membranes is higher than in S-Radel.[13] The sulfonic acid groups in Nafion and Aquivion are attached to a perfluorinated alkyl chain which has highly electronegative fluorine atoms that withdraw electron density from the sulfonate group, thus stabilizing the negative charge. The acidity of the sulfonic acid group in S-Radel is not as high as in PFSA membranes because the negative charge of the

sulfonate ion is merely delocalized on the aryl ring. Therefore, the water molecules coordinate more strongly to the aryl sulfonic acid group because it has a higher electron density than the perfluorinated sulfonic acid group.Using *p*-toluene sulfonic acid and triflic acid as analogues, computer modeling predicted that the distance between the sulfonic acid groups and the hydrating water molecules is closer for para-toluene sulfonic acid than for triflic acid, which supports our hypothesis.[44] Secondly, the flexible side chains to which the sulfonic acid groups are attached in PFSA membranes may be a contributing factor to the higher ^2H T_1 relaxations in PFSA membranes. The sulfonic acid groups in S-Radel are attached directly to a rigid polymer backbone. Therefore, the sulfonic acid groups in PFSA membranes have more mobility than in S-Radel, and could affect the molecular motion of the water that is coordinated to the sulfonic acid groups. It may also explain the slightly shorter ^2H T_1 relaxations in Aquivion, which has a shorter side chain than Nafion.

The chemical structure of the polymer influences the ^2H T_1 relaxation behavior at low hydration levels. However, influence from the morphological structure of the membrane becomes more important as the hydration level is increased. When $\lambda \approx 4$, the S-Radel membranes showed a sudden 10 ms increase in the ^2H T_1 relaxation which is attributed to the saturation of the hydration shell of the sulfonic acid groups and/or the onset of the formation of hydrophilic domains. The sudden increase in ^2H T_1 relaxation time can also be linked to the proton conductivity behavior of the S-Radel samples. When λ is less than four, the S-Radel 1.95 membrane exhibits very low proton conductivity while the S-Radel 1.05 membrane has no measureable conductivity. However, when λ reaches four, 'free' water becomes present and interconnected pores are formed. Hence, proton conductivity increases more rapidly for S-Radel 1.95 and there was measureable conductivity from S-Radel 1.05. IEC does not appear to have a major influence on ^2H T_1 relaxations of the S-Radel membranes as the difference between the two ^2H T_1 relaxation curves is minor.

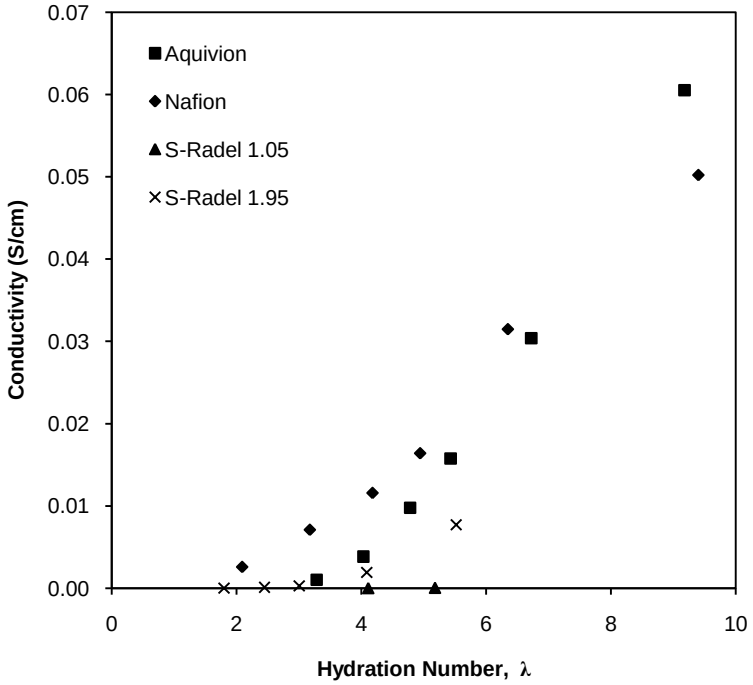

Figure 4-6 Conductivity versus hydration number of the different proton conducting membranes

The effect of morphology on the ^2H T_1 relaxation behavior is more apparent in PFSA membranes. The ^2H T_1 relaxations of PFSA membranes are long, even at relatively low levels of hydration. Moreover, there is no observable inflection point in the ^2H T_1 relaxation curve of PFSA membranes as the hydration number increases. The lack of an inflection point is because sulfonate rich domains are already present in PFSA membranes even in the dry state, which can be detected by TEM and SAXS methods,[45] and hydrophilic domains are formed with minimal hydration. Furthermore, the more flexible and hydrophobic nature of the fluorinated alkyl backbone of PFSA polymers aids in the formation of well-defined phase-separated domains with large hydrophilic pores (5 nm). Therefore, water molecules that are absorbed in PFSA membranes have more liquid character, and consequently longer ^2H T_1 relaxations. Conversely, the backbone of S-Radel is very rigid and less hydrophobic than the PFSA polymers. This leads to poor phase separation between the hydrophilic and hydrophobic phases, and formation of much

smaller hydrophilic pores. The water confined in small pores exhibit more solid character because its molecular motion is restricted.

4.4 Conclusions

The state of water within proton conducting membranes has been characterized by measuring the ^2H T_1 relaxation of ^2H_2O absorbed by these membranes. The chemical and morphological properties of the polymer that influence the molecular dynamics of water molecules absorbed by proton conducting membranes were identified. The acidity and mobility of the sulfonic acid groups have the most effect on the character of the water at low hydration levels. Phase separation and pore size of the hydrophilic domains have more influence on the state of water at higher levels of hydration. In the future, ^2H T_1 relaxations of ^2H_2O in aromatic ionomers with highly sulfonated blocks that form large hydrophilic domains, rigid poly(arylene ether)s with flexible sulfonic acid groups, and sulfonated polyphosphazenes which have a highly flexible backbone will be investigated in order to confirm our hypothesis. Understanding the character of water in proton conducting membranes will provide vital information for the design of future systems, especially ones that rely on bound water to conduct protons and perhaps, can operate at high temperatures and low humidity.

---

[1] Mauritz, K. A.; Moore, R. B. *Chem. Rev.*, **2004**, *104*, 4535-4585
[2] Lakshmanan, B.; Huang, W.; Olmeijer, D.; Weidner, J. W. *Electrochem. Solid-State Lett*. **2003**, *6*, A282–A285
[3] Rozière, J.; Jones, D. J. *Annu. Rev. Mater. Res*. **2003**, *33*, 503– 555
[4] Mathias, M. F.; Makharia, R.; Gasteiger, H. A.; Conley, J. J.; Fuller, T. J.; Gittleman, C. J.; Kocha, S. S.; Miller, D. P.; Mittelsteadt, C. K.; Xie, T.; Yan, S. G.; Yu, P. T. *Interface* **2005**, *14*, 24
[5] Gasteiger, H. A.; Kocha, S. S.; Sompalli, B.; Wagner, F. T. *Applied Catalysis B: Environmental*, **2005**, *56*, 9-35
[6] Wang, B *Journal of Power Sources* **2005**, *152*, 1-15
[7] G. Scharfenberger, W. H. Meyer, G. Wegner, M. Schuster, K.-D. Kreuer, J. Maier *Fuel Cells*, **2006**, *6*, 237-250
[8] Subbaraman, E.; Ghassemi, A.; Zawodzinski, T. A. *J. Am. Chem. Soc.*, **2007**, *129*, 2238-2239
[9] Celik, S.U.; Aslan, A.; Bozkurt, A. *Solid State Ionics*, **2008**, *179*, 683-688
[10] Bae, B.; Miyatake, K.; Watanabe, M *Macromolecules*, **2010**, *43*, 2684–2691

[11] Matsumura, S.; Hlil, A. R.; Lepiller, C.; Gaudet, J.; Guay, D.; Shi, Z.; Holdcroft, S.; Hay, A. S. Macromolecules **2008**, *41*, 281– 284
[12] Roy, A.; Yu, X.; Dunn, S.; McGrath, J. E. *J. Membr. Sci*. **2009**, *327*, 118– 124
[13] Kreuer, K. D. *J. Membr. Sci*. **2001**, *185*, 29-39
[14] Ioselevich, A. S.; Kornyshev, A. A.; Steinke, J. H. G. *J. Phys. Chem. B*, **2004**, *108*, 11953–11963
[15] Yang, Y. S.; Siu, A.; Peckham, T.J.; Holdcroft, S. In *Polymers for Fuel Cells 1*; Scherer, G. G. Ed; *Advances in Polymer Science vol. 215*; Springer: Berlin, **2008**, 55-126
[16] Lu, Z.; Polizos, G.; Macdonald, D. D.; Manias, E. *Journal of The Electrochemical Society,* **2008**, *155*, B163-B171
[17] Paddison, S.J.; Reagor, D.W.; Zawodzinski, T.A. *J. Electroanal. Chem.*, **1998**, *459*, 91–97
[18] Kim, Y. S.; Dong, L.; Hickner, M. A.; Glass, T. E.; Webb, V.; McGrath, J. E. *Macromolecules*, **2003**, *36*, 6281–6285
[19] Elomaa, M.; Hietala, S.; Paronen, M.; Walsby, N.; Jokela, K.; Serimaa, R.; Torkkeli, M.; Lehtinen, T.; Sundholmc, G.; Sundholm, F. *J. Mater. Chem.*, **2000**, *10*, 2678-2684
[20] Laporta, M.; Pegoraro, M.; Zanderighi L. *Phys. Chem. Chem. Phys.*, **1999**, *1*, 4619-4628
[21] Ye, G.; Jansen, N.; Goward, G. R. *Macromolecules* **2006**, *39*, 3283-3290
[22] MacMillan, B.; Sharp, A. R.; Armstrong, R. L. *Polymer*, **1999**, *40*, 2471–2480
[23] Kreuer, K. D.; Paddison, S. J.; Spohr, E.; Schuster, M. *Chem. Rev.*, **2004**, *104*, 4637-4678
[24] Paddison, S. J. *Annu. Rev. Mater. Res.*, **2003**, *33*, 289-319
[25] Benesi, A. J.; Grutzeck, M. W.; O'Hare, B. V.; Phair, J. W. *Langmuir*, **2005**, *21*, 527-529
[26] O'Hare, B; Grutzeck, M. W.; Kim, S. H.; Asay, D. B.; Benesi, A. J. *J. Magnetic Resonance*, **2008**, *195*, 85-102,
[27] Benesi, A. J.;O'Hare, B.; Grutzeck, M. W.; Phair, J. W. *Journal of Physical Chemistry B*, **2004**, *108*, 17783-17790
[28] Park, S.; Venditti, R. A.; Abrecht, D. G.; Jameel, H.; Pawlak, J. J.;Lee, J. M. *Journal of Applied Polymer Science*, **2006**, *103*, 3833-3839
[29] D. Radloff, C. Boeffel, W. H. Spiess *Macromolecules* **1996**, *29*, 1528-1534
[30] Bunce, N. J.; Sondheimer, S . J.; Fyfe, C. A. *Macromolecules*, **1986**, *19*, 333–339
[31] Geil, B.; Kirschgen, T. M.; Fujara, F. Physical Review B, 2005, 72, 014304-1−014304-10
[32] Schmidt-Rohr, K.; Spiess, H. W. *Multidimensional Solid-State NMR and Polymers*; Academic Press: San Diego, CA, 1994.
[33] . Hoatson, G. L.; Vold, R. L. In *Encyclopedia of Nuclear Magnetic Resonance*; Grant, D. M., Harris, R. K., Eds.; Wiley & Sons Scientific: New York, 1996; p 1582
[34] Dyck, A.; Fritsch, D.; Nunes, S. P.; *Journal of Applied Polymer Science*, **2002**, 86, 2820-2827
[35] Perrin, J. C.; Lyonnard, S.; Guillermo, A.; Levitz, P *J. Phys. Chem. B*, **2006**, *110*, 5439–5444
[36] ASTM Standard E104-02 "Standard Practice for Maintaining Constant Relative Humidity by Means of Aqueous Solutions," **2007**, ASTM International, West Conshohocken PA
[37] Majsztrik, P. W.; Satterfield, M. B.; Bocarsly, A. B.; Benziger, J. B. *Journal of Membrane Science*, **2007**, *301*, 93-106
[38] Kreuer, K. D.; Schuster, M.; Obliers, B.; Diat, O.; Traud, U.; Fuchs, A.; Klock, U.; Paddison, S. J.; Maier, J *Journal of Power Souces*, **2008**, *178*, 499-509
[39] Pushpa, K. K.; Nandan, D.; Iyer, R. M. *J. Chem. Soc., Faraday Trans. 1*, **1988**, *84*, 2047-2056
[40] Eikerling, M.;Kornyshev, A. A.;Kuznetsov, A. M.;Ulstrup, J.;Walbran, S. *J Phys Chem B* **2001**, *105*, 3646-3662
[41] Benesi, S. J.; Pokras, S. M.; Slipak, S. H. *unpublished results*
[42] Chen, R. S.; Jayakody, J. P.; Greenbaum, S. G.; Pak, Y. S.; Xu, G.; McLin, M. G.; Fontanella, J. J. *J. Electrochem. Soc.*, **1993**, *140*, 889-895
[43] Zawodzinski, T. A.; Derouin, C.; Radzinski, S.; Sherman, R. J.; Smith, V. T.; Springer, T. E.; Shimshon, G. *J. Electrochem. Soc.*, **1993**, *140*, 1041-1047
[44] Paddison, S. J. *J. New Mater. Electrochem. Systems*, **2001**, *4*, 197-207
[45] Takimoto, N.; Wu, L.; Ohira, A.; Takeoka, Y.; Rikukawa, M. *Polymer*, **2009**, *50*, 534-540

Chapter 5 Ion Conduction and Water Transport in Polyphosphazene Based Multilayers

5.1 Introduction

Many electrochemical energy conversion and storage devices such as fuel cells, batteries and dye-sensitized solar cells rely on electrolytes for ionic transport. Conventional electrolytes consist of a polar liquid capable of solvating ions. The need for a safe and lightweight solid state electrolyte has driven extensive research to replace caustic or flammable liquid electrolytes to circumvent problems associated with leakage. A known compromise in this area is the balance between high ion transport and mechanical integrity. Often high ionic conductivity values are achieved by utilizing polymers with low glass transition temperatures and low degrees of crystallization, at the expense of mechanical durability. Poly(ethylene oxide) (PEO) has been one of the most thoroughly investigated polymer electrolytes because it bears cation-solvating ether groups and a flexible backbone for facile ion mobility.[1-3] However, its crystallinity, and limited chemical stability are major limitations for realistic applications. To minimize crystallization, small molecule plasticizers have been used with PEO in lithium-ion batteries; however, these plasticizers are typically highly flammable and result in a more liquid-like electrolyte system, both of which lead to serious hazards if a device were to be breached. For applications such as fuel cell or flow cell membranes in which the electrolyte is often hydrated, the chemical stability of PEO becomes a greater issue.

To address the above issues, Allcock and coworkers have designed a hybrid organic-inorganic polymer, poly[bis(methoxyethoxyethoxy)phosphazene] (MEEP),[4,5] by functionalizing a polyphosphazene backbone with ethylene oxide chains (Figure 5-1). The phosphazene backbone has numerous advantages over that of PEO, such as higher chain flexibility and thermo-

oxidative stability. The properties of the polymer can be tuned through substitution reactions on the highly versatile parent polymer, poly(dichlorophosphazene). Furthermore, the dry (0% RH) ionic conductivity of MEEP is over two orders of magnitude higher than that of PEO in non-plasticized systems (10^{-3} vs 10^{-5} S cm^{-1}),[6] an essential property for solid polymer electrolytes to reduce electrical resistance. Due to the highly flexible nature of both its backbone and side chains, MEEP lacks mechanical integrity. Moreover, MEEP is water-soluble, which makes it impractical for use in highly hydrated environments such as fuel cells. A way to address this issue is by exposing the polymer to gamma[7] or UV[8] radiation, which results in a crosslinked MEEP network. Due to the stability of the phosphazene backbone, the crosslink occurs only on the side chain and increases the mechanical stability of MEEP. However, gamma radiation is not easily accessible and the UV radiation method involves sensitizers that need to be removed upon crosslinking process. A better strategy to stabilize MEEP films, as well as providing mechanical robustness, is much needed.

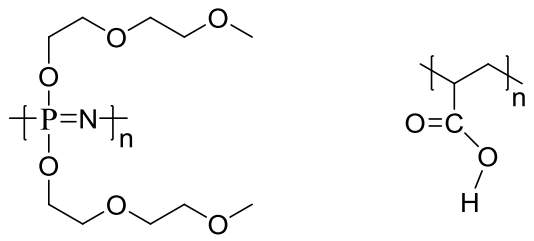

Figure 5-1 Chemical structures of poly[bis(methoxyethoxyethoxy)phosphazene] (MEEP) and poly (acrylic acid) (PAA).

Layer-by-layer (LbL) assembly is a versatile thin-film fabrication method which consists of the repeated, sequential immersion of a substrate into aqueous solutions of complementary functionalized materials.[9,10] The LbL method provides stable polymer blends and allows for composition, morphology, and property control through the adjustment of assembly parameters such as pH. The tunability, environmentally-benign aqueous processing, and nanoscale blending of materials which are otherwise impossible to construct make this system a significant

competitor to create novel solid state electrolytes for various energy applications.[11,12] In addition to commonly used electrostatic interactions for LbL film growth, secondary interactions such as hydrogen bonding have proven effective in incorporating neutral, water soluble polymers into LbL films.[13,14]

In this work, we introduce the LbL assembly method to create homogenous blends of MEEP, a hydrogen bonding acceptor, and poly (acrylic acid) (PAA), a hydrogen bonding donor, with controlled film growth, high ionic conductivity, and excellent hydrolytic stability. To the best of our knowledge, this is the first incorporation of a phosphazene based polymer into a multilayer structured thin film. These films are promising candidates as truly solid state polymer electrolytes in electrochemical devices such as fuel cells and batteries. We show the relative humidity dependence of conductivity as well as the water transport characteristics of these unique blends. The LbL assembly process allows fine tuning of the desired properties by simple adjustments to the assembly conditions. We also show the isolation of MEEP/PAA LbL assembled films from the substrate, which allows bulk characterization of free-standing films.

5.2 Experimental Section

5.2.1 Chemicals

MEEP (M_w ~ 264K determined by aqueous GPC) was synthesized according to previously published procedures.[5] Poly(acrylic acid) (PAA) (250,000 M_w, Polysciences) was used as received. Both MEEP and PAA were weighed and diluted to the desired concentration using Millipore MilliQ deionized water (18.2 MΩ cm filtered through a 0.22 □m membrane).

5.2.2 LbL Assembly Methods

Assembly of the LbL films was completed by using a programmable ZEISS DS50 slide stainer. To construct LbL films, substrates (glass, patterned ITO, polystyrene, or ZnSe) were first immersed in aqueous MEEP solution (10 mM calculated based on the repeat unit) for 20 minutes, followed by three two minute rinses in water, and then in PAA (10 mM) for 20 minutes followed by three two minute rinses in water. The pH of both polymer solutions and rinse baths were identical and adjusted prior to assembly by adding 1M HCl solution dropwise. The dipping process was repeated numerous times to produce a film of desired thickness. The free-standing films were peeled off from polystyrene substrates.

5.2.3 Ionic Conductivity

For in-plane conductivity measurements, LbL films deposited on microscope slides (VWR) were placed in a conductivity cell with platinum wires as the electrodes, and tested in a humidity and temperature controlled chamber (Electro-tech Systems, Inc.). Relative humidity was controlled down to 10% RH, and dry (0%RH) measurements were performed in a nitrogen-filled glove box with <1 ppm water content. Through-plane conductivity measurements were performed by depositing LbL films on patterned ITO substrates (Delta Technologies), and gold electrodes were thermally evaporated (~100nm) on the multilayers. The active area was 6 mm^2. Ionic conductivity values were determined by electrochemical impedance spectroscopy with a Solartron 1260 impedance analyzer by sweeping the frequency from 1 MHz down to 1 Hz.

5.2.4 Bulk Characterization

Thickness measurements were made by scoring the films with a razor blade and measuring the step change in height between the film and substrate with a Tencor P16 profilometer (1mg applied force). FTIR spectra were obtained from thin films deposited on CVD grown, IR transparent ZnSe substrates. Free standing films were analyzed with a TA Instruments Q1000 differential scanning calorimeter. Films were cut to yield samples of ~2-3 mg, and all temperature ramp rates were 10 °C/min. Samples were equilibrated at -90 °C, heated to 150 °C, and cooled back to -90 °C. At least two thermal cycles were repeated for each film. The glass transition temperature was calculated from the inflection point of the sigmoidal portion of the heating curve.

5.2.5 Water Uptake Behavior

A Masscal G1 (quartz crystal microbalance/heat conduction calorimeter) was used for analysis of water uptake and transport properties of LbL films. LbL films were deposited onto 1 inch diameter quartz crystals (5 MHz frequency) with gold electrodes from Masscal Scientific Corp. For all experiments, the temperature of the G1 sample chamber was maintained at 30 °C. Two mass flow controllers supplied nitrogen streams to the G1 sample chamber. One nitrogen stream was kept dry, while the other was humidified to 100% relative humidity (RH). Varying the ratio of these to streams through the G1 software allowed fine control of the sample chamber RH. The total gas flow rate was 50 cm^3(STP)/min for all experiments. The RH of the G1 samples chamber was monitored using a Sable Systems R300 water vapor analyzer. Films were exposed to a dry nitrogen purge to determine the amount of film formed on the crystal by comparison with the frequency of the blank crystal before coating. After the films were fully dried, a step change in RH of the sample chamber from 0 to 100% was introduced. The frequency change of the

coated crystal caused by water uptake into the films was monitored in real-time. Mass uptake is directly proportional to the frequency change, as given by the Sauerbrey equation.[15] Dried films were also exposed to incremental step changes in relative humidity (~15% per step) up to 100% RH to yield a sorption isotherm. To ensure that condensation in the sample chamber did not occur, the frequency change of a blank QCM crystal was observed to be negligible when exposed to a full range of relative humidity conditions.

5.3 Results and Discussion

5.3.1 Multilayer Assembly and Ionic Conductivity

The LbL assembly of the polymers MEEP and PAA is performed by utilizing the hydrogen bonding interaction between the COOH groups of PAA and ethylene oxide side chains of MEEP (Figure 5-1). The ionization degree of PAA is controlled during thin-film assembly by systematically varying the assembly pH from 3.50 down to 2.00 for all polymer and rinse solutions. In all cases, the MEEP/PAA films grow linearly up to as many as 75 bilayers across the entire assembly pH range. This linearity has also been observed with PEO/PAA multilayers[16] and with other hydrogen bonded systems.[14] Figure 5-2 shows the bilayer thickness of MEEP/PAA films as a function of assembly pH. The maximum bilayer thickness is greater than 200 nm/bilayer at the lowest assembly pH values, and is significantly reduced down to 50 nm/bilayer at the assembly pH =3.5. Large bilayer pair thicknesses are commonly observed in hydrogen bonded multilayer thin films due to looser network formed between weakly associative groups; furthermore, the potential for dimerization between PAA sidegroups increases the chance of greater amounts of film deposited with each cycle.

Because the MEEP/PAA system relies on hydrogen bonding to build the film, the degree of ionization in PAA greatly affects the bond attractions and like-charge repulsion between the polymer chains. At low pH, the ethylene oxide side chains of MEEP paired with the carboxylic acid groups of PAA to create enough hydrogen bond crosslinks between polymer layers to stabilize the resulting film. By changing the pH of the assembly baths, this cross-linking attraction can be varied, thus changing the stability of the film and allowing tuning of the final thickness. At higher pH values, the adsorbed PAA layer becomes increasingly thinner, as hydrogen bonding between PAA side chains (acid-acid dimerization) is decreased. The LbL film growth is suppressed at assembly pH values above pH=3.5 due to the more highly ionized PAA, which introduces large electrostatic repulsion, and limits the hydrogen bonding interaction between MEEP and PAA.

Figure 5-2 also shows the tunability of the ionic conductivity of MEEP/PAA films by varying the assembly pH. In-plane conductivity was measured at fully humidified conditions at 25 °C using platinum wires one centimeter apart on the surface of a 50 bilayer MEEP/PAA film. By increasing the assembly pH, the bulk proton conductivity increases from $1x10^{-4}$ S cm^{-1} at assembly pH =2.0 up to $7x10^{-4}$ S cm^{-1} at assembly pH = 3.5. This increase could be partially attributed to the higher ionization of PAA (more anionic sites for ion transport); however, the effect of ionization on proton conductivity is small as verified by the values obtained from pristine PAA films, and cannot account for the 7-fold increase observed for the LbL assembled films. Therefore, the observed enhancement of conductivity is due to the changes in the effective hydrogen bond network and/or composition in the films built at higher pH values, and resulting differences in ion and water transport. We hypothesize that the average number of transient hydrogen bonds per unit volume should undergo an overall decrease with these small increases in pH. The observed trend is consistent with the conductivity trend observed for the previously

assembled LbL PEO/PAA systems, with MEEP/PAA values consistently being higher than the PEO/PAA values obtained at 100% RH.[16]

To determine the impact of ambient humidity on the ionic conductivity, 25 bilayers of MEEP/PAA films are assembled on patterned ITO/Glass substrates followed by thermal gold evaporation on top of the film to yield an 8-cell ITO | MEEP/PAA | Au configuration. Through-plane conductivity measurements are then carried out by connecting the ITO and gold ends to the impedance analyzer. Figure 5-3 shows the ionic conductivity values of MEEP/PAA multilayers assembled at pH = 2.5 (circles) and pH = 3.0 (triangles) as the %RH is decreased from 60% down to 0%. In agreement with conductivity measurements taken at fully humidified conditions, LbL films assembled at high pH values yield higher values, presumably due to a more favorable, loose polymer network for ion and water transport, which would facilitate ion conduction via Grotthuss and carrier mechanisms. On the other hand, it is important to note that the difference in ionic conductivity between these two films becomes systematically less pronounced at drier conditions, namely at %RH values less than 20%, and that the ionic conductivities converge in the dry state to the value of 10^{-9} S cm^{-1}. We attribute this behavior to the crucial role of water in ion transport of hydrated ethylene oxide based systems and the impact of its relative uptake in the films on the mobility of the ionic species, a phenomenon extensively discussed in the following section. As the films approach the dry state, the differences in hydrogen bond network become irrelevant; the rate determining factor for these systems in the dry state is the inherent mobility of the ethylene oxide chain segments in the matrix. The values obtained here at 0% RH can be compared to those reported for PEO/PAA films examined under the same conditions, for which the dry state conductivity for was 3×10^{-10} S cm^{-1}.[17]

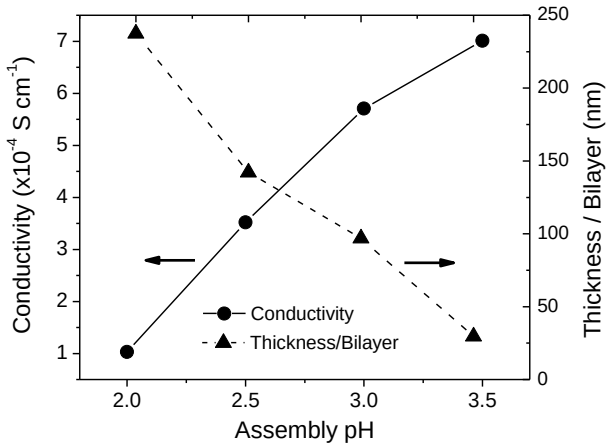

Figure 5-2 The assembly pH dependence of ionic conductivity at 100% RH (circles) and bilayer thickness (triangles).

Finally, to observe the effect of a small molecule plasticizer in a water-free environment, a drop of propylene carbonate was added onto a dry MEEP/PAA film (assembly pH =2.5) placed in a glovebox. The ionic conductivity rapidly increased by three orders of magnitude to reach 1.43 x 10^{-6} S cm^{-1} (Figure 5-3, empty circle) due to the more favorable liquid-like medium for ion transport. However, it is important to note that this value is still much lower than that of a film in fully humidified conditions indicating the crucial impact of water on proton transport through hydrated hydronium ions.[18]

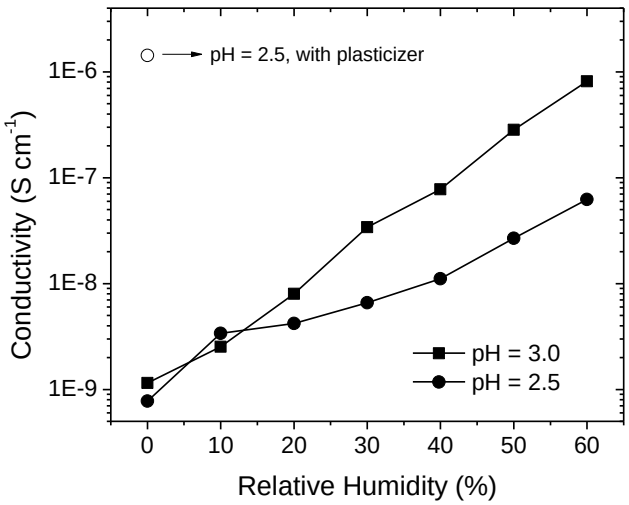

Figure 5-3 The relative humidity dependence of ionic conductivity of MEEP/PAA films assembled at pH = 2.5 and pH = 3.0. Also shown is the conductivity enhancement of a dry film upon addition of a small molecule plasticizer (propylene carbonate).

5.3.2 FTIR Analysis

In order to better understand the type and extent of hydrogen bonding versus acid ionization at different assembly pH values, we have assembled two MEEP/PAA multilayer films on IR transparent ZnSe substrates at low pH (1.80) and at high pH (3.30), as well as pristine films of MEEP and PAA. Figure 5-4 shows the carboxylic acid region of the FTIR spectra, where the hydrogen bonding characteristics of LbL films are investigated. As expected, pristine MEEP does not have any absorption in this region. Pristine PAA, on the other hand, has a strong peak centered at 1711 cm^{-1}, indicative of intra-molecular hydrogen bonding of COOH groups via acid-acid dimerization.[17,19] For the LbL films of MEEP/PAA, another peak centered at 1740 cm^{-1} is observed in addition to the peak at 1711 cm^{-1}, confirming the partial disruption of PAA's acid-dimerization and the presence of intermolecular hydrogen bonding between the acidic groups of PAA and the ether lone pair electrons of MEEP. The relative intensity of the 1711 cm^{-1} peak decreases as assembly pH increases from 1.80 to 3.30, suggesting a decrease in the extent of COOH groups participating in intra-molecular hydrogen bonding. This is primarily attributed to

the higher degree of ionization of PAA, which decreases the number of COOH neighbors available for self-dimerization, and increases hydrogen bond interactions of remaining COOH groups with MEEP. Also of interest is the COO^- region (~1550 cm^{-1}), which is indicative of changes occurring in the ionization of the carboxylic acid groups in PAA. Differences between the spectra of the PAA and MEEP/PAA films are minimal and difficult to observe in this region, due to the weakness of the ionized acid peak at low pH, and the fact that the degree of ionization varies by a fairly small fraction.

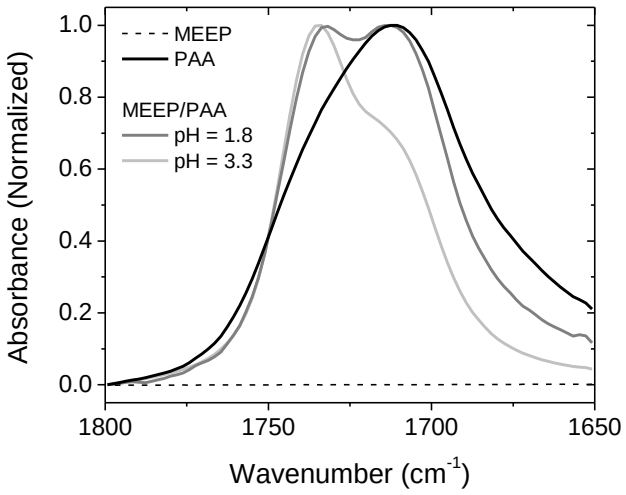

Figure 5-4 FTIR spectra of the carboxylic acid region of MEEP/PAA multilayers assembled at pH 1.8 and 3.3 on IR-transparent ZnSe substrates. The relative intensity of peak at 1710 cm^{-1} appears to decrease as assembly pH increases.

5.3.4 Bulk Characterization of Free-standing Films

To analyze the thermal and mechanical characteristics, MEEP/PAA films were deposited on low surface energy polystyrene substrates and gently peeled off with tweezers as previously described by our group.[20] The resulting films appear amber-colored and transparent, indicating a homogenous blend with minimal surface roughness. Figure 5-5 shows a DSC thermogram for a peeled-off MEEP/PAA film assembled at pH = 2.5, along with spun-cast films of neat PAA and

MEEP (inset) from water. Multiple heating/cooling cycles are performed on each sample to remove bound water from the film and ensure accurate T_g values are observed. The measured T_g values of pristine PAA and MEEP are found to be 76.0 °C and -80.5 °C, respectively.

All MEEP/PAA LbL films exhibit a single T_g between that of neat MEEP and PAA, which is indicative of a truly homogeneous blended film, and is consistent with earlier reports of DSC analysis on PEO/PAA LbL films.[17] Interestingly, the observed T_g of MEEP/PAA LbL systems show little or no variation when the pH of the assembly solutions was varied over the range of 1.8 – 3.0. All MEEP/PAA samples assembled at pH values varying from 2.0 to 3.5 exhibited a T_g of -28.0 ± 2.0 °C. For this polymer pair, a Tg of -28.0 °C corresponds to a composition of 52 wt% MEEP or 21 mol% MEEP by use of the Fox equation.[21] The lack of variation between assembly pH and T_g of the resulting LbL blend differs from a similar study on PEO/PAA LbL films, where the T_g of PEO/PAA films varied from ~60 °C when assembled below pH 2.0 to ~25 °C at assembly pH values ≥ 3.0.[17] The variation in T_g of PEO/PAA films at different assembly pH values were due to different film compositions caused by the degree of ionization of PAA and its ability to form intramolecular versus intermolecular hydrogen bonds, thus leading to decreased adsorption of PAA relative to PEO at higher pH. For the MEEP systems, the changes in intra- versus inter-molecular hydrogen bonding also seem to be responsible for changes in conductivity; however, the cause is not due to significant changes in relative MEEP content, which suggests that both the PAA and the MEEP adsorbed layers become thinner with higher pH. This difference between PEO and MEEP may be due in part to structural differences; the ethylene oxide groups attached as side chains to MEEP are very short, and would not undergo significant conformational changes to yield dense, loopy arrangements of PEO during the adsorption cycle, as anticipated with PEO when hydrogen bonding with PAA is optimized. In this case, less PAA adsorbed in the first adsorption cycle of the LbL assembly leads to lowered MEEP adsorption in the second. It is also noted that the relative increase in ionic

conductivity with pH is also more moderate than observed with PEO/PAA, indicative of the smaller differences in the composition and structure of the films with pH. The primary reason for the observed increases in conductivity are therefore likely to be due to the higher number of charged sites available in the film and the decrease in the number of hydrogen bonds acting as effective physical crosslinks in the network, yielding a "looser" network and increased ion mobility.

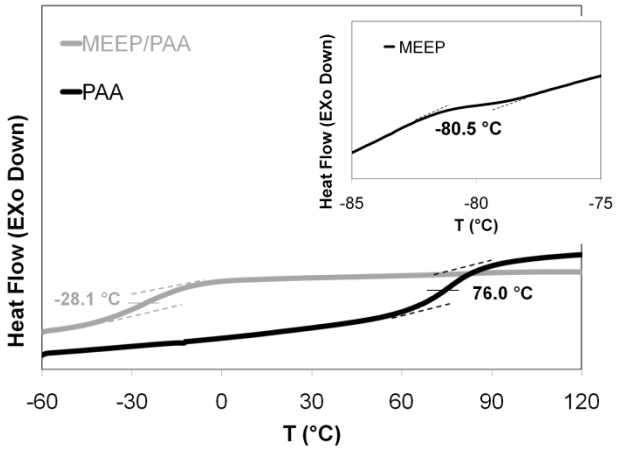

Figure 5-5 DSC thermogram for a free-standing MEEP/PAA film assembled at pH = 2.5, along with neat PAA and MEEP (inset). All MEEP/PAA LbL films displayed one T_g indicative of a homogenous blend. MEEP/PAA films assembled at different pH values showed little change in T_g.

A major concern for polymer electrolytes with low glass transition temperatures is their gum-like nature, which prohibits them from qualifying as *truly* solid-state electrolytes. To demonstrate the mechanical advantage of LbL assembled systems compared to pristine films of MEEP and PEO, we have tested the indentation response of MEEP/PAA films on glass as well as the pristine MEEP and PAA films for comparison. To minimize the substrate interference, we have assured that the thickness of the polymer film is at least ten times greater than that of the indentation distance. Preliminary results show that a typical MEEP/PAA film (~6 □m) yields an elastic modulus value of 690 ± 57 MPa at ambient conditions, over an order of magnitude higher

than a pristine MEEP film (56 ± 5 MPa). We are currently investigating to verify these values by measuring the tensile strength of free-standing LbL films.

5.3.5 Water Transport

We utilized a recently developed approach to determine the water uptake and transport of MEEP/PAA LbL films with a quartz crystal microbalance (QCM).[22,23] This QCM method has been used to determine the permeability of various gases through polymer thin films, coatings and powders. QCMs measure the change in mass per unit area of a sample by measuring the variation in frequency of a quartz resonator due to absorption and diffusion of the permeating species, in this case water, in the films. Permeability is defined as:

$$P = \frac{J \cdot l}{\Delta p} = S \cdot D \qquad (1)$$

where J, l, and Δp are the flux, film thickness, and partial pressure difference across the film, respectively. Analyzing water permeation through a film involves both an equilibrium thermodynamic property, solubility (S), and a kinetic property, the diffusion coefficient (D). Both parameters, S and D, can be obtained from mass uptake experiments using the QCM. The ability to control the relative humidity of the QCM sample chamber allows the study of the relationship between water transport in MEEP/PAA films and the dependence of humidity on ionic conductivity.

To investigate the water uptake characteristics, MEEP/PAA films (5-10 bilayers, 0.5 – 2.1 μm) were assembled on quartz crystals and equilibrated at 30 °C under a dry nitrogen atmosphere until there is no longer a loss in moisture from the film, as determined by QCM. Then, the films were exposed to a step change to 100%RH while monitoring the changes in oscillation frequency. Figure 5-6 a shows the water uptake of two MEEP/PAA films upon

exposure to a fully humidified environment followed by a step change back to dry nitrogen and the corresponding water loss. Water uptake as a function of incremental step changes in humidity is shown in Figure 5-6 b. The kinetic data from the single step experiment allows for the calculation of the diffusion coefficient through use of a simplified model of one-dimensional diffusion of water into a slab, which has been previously described.[24,25]

The linear sorption isotherm from the multi-step experiment yields the films' solubility. The permeability of the film is simply calculated from Equation 1 as the product of solubility and the diffusion coefficient. It is important to note that while deviations from the Sauerbrey Equation can exist for highly hydrated films, these deviations are minimal for thin films studied at the QCM's fundamental frequency (5 MHz).

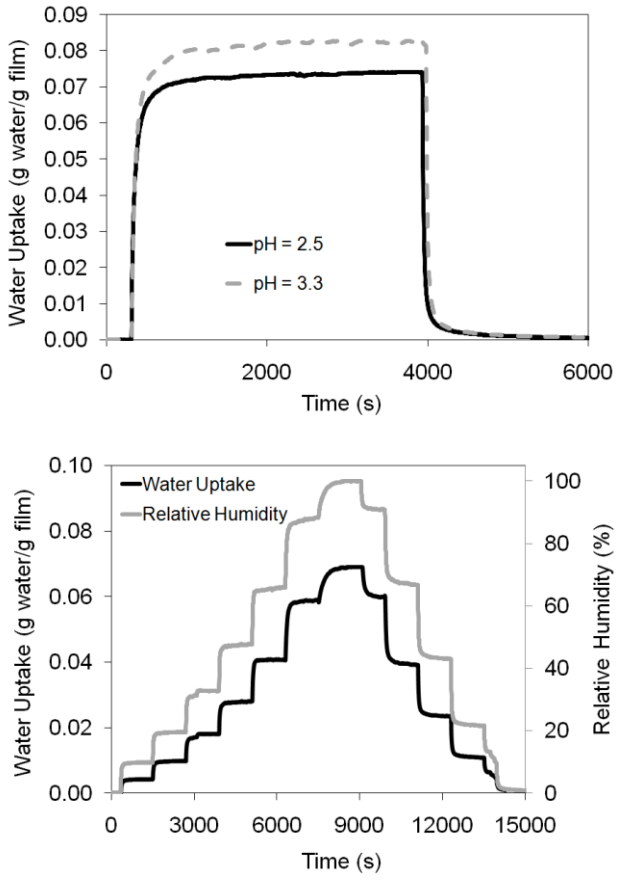

Figure 5-6 (a) Water vapor uptake and desorption as a function of time for MEEP/PAA LbL films assembled at pH=2.5 and pH=3.3 at 30°C. A step change in the sample chamber relative

humidity from 0 to 100% occurs at t=300 s, while a step change from 100 to 0% occurs at t=3900 s. (b) Water vapor sorption isotherm at 30°C for a MEEP/PAA film assembled at pH=2.5.

The solubility values, diffusion coefficients, and permeability values of water in MEEP/PAA LbL films, along with neat, spun-cast MEEP and PAA films, are given in Table 1. PAA has a water uptake value of 0.111 g H_2O/g PAA, which corresponds to 0.32 water molecules per PAA repeat unit, while MEEP uptakes 0.027 g H_2O/g MEEP or 0.38 water molecules per MEEP repeat unit. The water transport properties of PAA are in agreement with literature;[23,26] however, the water uptake of MEEP is lower than previously reported values and may be attributed to differences in film processing. The water uptake of the MEEP/PAA LbL films is between that of MEEP and PAA, which is expected because the LbL films are homogenous blends of the two polymers. MEEP/PAA films assembled at pH 3.3 absorb 22.7% more water on a gravimetric basis than pH 2.5 films, most likely due the increased charge on the incorporated PAA at pH 3.3. Overall, in the case of MEEP/PAA LbL systems, films assembled at higher pH values have larger diffusion coefficients and solubilities. For example, MEEP/PAA films assembled at pH 3.3 have diffusion coefficients approximately 30 times larger and solubility values about 25% larger than films assembled at pH 2.5; thus, films assembled at pH 3.3 have water permeability values 35 times higher than films assembled at pH 2.5. The increase in water transport properties at higher pH values is consistent with the increase in ionic conductivity values of MEEP/PAA films at higher pH values, especially under humidified conditions.[27,28] Regardless of the mechanism of ion transport through a polymer electrolyte, an increase in the water transport properties will result in higher ionic conductivities when the membrane is humidified.[29] Thus, the increase in ionic conductivity values of MEEP/PAA films assembled at higher pH values is attributed to better water transport, which is improved by a looser hydrogen bond crosslinked network and the increased presence of some ionized PAA groups.

Table 5-1 Diffusion coefficients, solubilities, and permeabilites of water in MEEP/PAA films assembled at pH=2.5 and pH=3.3, along with neat MEEP, PAA and LbL assembled PEO/PAA films (T = 30°C).

Polymer	H_2O Uptake (g H_2O/g film)	D (cm^2/s)	S (cm^3 H_2O/cm^3 film cmHg)	P (Barrer)
MEEP	0.027	1.31E-13	17.5	10.0
PAA	0.111	3.72E-13	70.6	0.03
MEEP/PAA (pH = 2.5)	0.066	1.72E-11	41.7	7.17
MEEP/PAA (pH = 3.3)	0.081	4.84E-10	52.8	255
PEO/PAA (pH = 2.5)[23]	0.090*	1.3E-11	28.1	36

Barrer = 10^{-10} cm^3 (STP) cm cm^{-2} s^{-1} $cmHg^{-1}$ *70% RH

The water transport in MEEP/PAA LbL films and previously assembled PEO/PAA LbL films both assembled at pH 2.5 compares quite closely, [23] with MEEP/PAA having a slightly higher permeability value, indicating more favorable water transport characteristics. While the functional groups of MEEP and PEO are the same, the water transport properties might also be influenced by the nature of the hydrogen bonded network formed in each case by LbL assembly. MEEP, which presents ethylene oxide groups as side chains, may form a relatively stronger LbL hydrogen bonded network as compared to the ethylene oxide groups contained in the backbone of PEO.

5.4 Summary and Perspective

In conclusion, we have demonstrated the layer-by-layer assembly of MEEP/PAA thin films by utilizing the hydrogen bonding between these two polymers. The ionic conductivity of these films is tuned by changing the assembly pH of initial polymer solutions and thereby controlling the hydrogen bonding characteristics. The growth rate of these films can be tuned

over the range of < 50 nm/bilayer up to > 200 nm/bilayer, which is quite large for an LbL assembled system. At fully humidified conditions, the ionic conductivity of MEEP/PAA is over one order of magnitude higher than previously studied hydrogen bonded LbL systems (~7 x 10^{-4} S cm^{-1} for MEEP/PAA versus 6 x 10^{-5} S cm^{-1} for PEO/PAA). This improvement in conductivity is attributed to both MEEP's superior ion transport properties and the high water transport of these blends. Using the LbL technique to tune the properties of the film is promising to obtain stable and high performance solid state electrolytes for various electrochemical energy applications. At fully dry conditions, ionic conductivity values of these films show little variation with respect to assembly conditions due to the films' similar morphology and composition, as evidenced by bulk characterization of free-standing films. Free standing films are isolated from low-energy surface substrates, which allowed for bulk characterization of thin films with DSC. Indentation experiments show that the elastic modulus of MEEP/PAA is over an order of magnitude higher that neat MEEP, which is critical for the applications of solid polymer electrolyte systems. Finally, the water transport characteristics are quantified by gradually changing the environment's relative humidity and monitoring the weight gain/loss of thin films through a QCM technique. The kinetic and thermodynamic data obtained allows for a full characterization of water solubilities, diffusion coefficients, and permeability. MEEP/PAA films assembled at higher pH values have enhanced water uptake and transport properties, which play a key role in increasing ion transport within the films at humidified conditions.

References

(1) Wright, P. V. *Electrochimica Acta* **1998**, *43*, 1137.
(2) Mendolia, M. S.; Farrington, G. C. *Advances in Chemistry Series* **1995**, *245*, 107.
(3) Murata, K.; Izuchi, S.; Yoshihisa, Y. *Electrochimica Acta* **2000**, *45*, 1501.
(4) Blonsky, P. M.; Shriver, D. F.; Austin, P.; Allcock, H. R. *Journal of the American Chemical Society* **1984**, *106*, 6854.
(5) Allcock, H. R.; Austin, P. E.; Neenan, T. X.; Sisko, J. T.; Blonsky, P. M.; Shriver, D. F. *Macromolecules* **1986**, *19*, 1508.
(6) Blonsky, P. M.; Shriver, D. F.; Austin, P.; Allcock, H. R. *Solid State Ionics* **1986**, *18-19*, 258.
(7) Bennett, J. L.; Dembek, A. A.; Allcock, H. R.; Heyen, B. J.; Shriver, D. F. *Chemistry of Materials* **1989**, *1*, 14.
(8) Nelson, C. J.; Coggio, W. D.; Allcock, H. R. *Chemistry of Materials* **1991**, *3*, 786.

(9) Decher, G.; Hong, J. D.; Schmitt, J. *Thin Solid Films* **1992**, *210*, 831.
(10) Decher, G. *Science* **1997**, *277*, 1232.
(11) Lutkenhaus, J. L.; Hammond, P. T. *Soft Matter* **2007**, *3*, 804.
(12) Argun, A. A.; Ashcraft, J. N.; Hammond, P. T. *Advanced Materials* **2008**, *20*, 1539.
(13) Sukhishvili, S. A.; Granick, S. *Journal of the American Chemical Society* **2000**, *122*, 9550.
(14) Kharlampieva, E.; Sukhishvili, S. A. *Polymer Reviews* **2006**, *46*, 377.
(15) Sauerbrey, G. *Z. Phys.* **1959**, *155*, 206.
(16) DeLongchamp, D. M.; Hammond, P. T. *Langmuir* **2004**, *20*, 5403.
(17) Lutkenhaus, J. L.; McEnnis, K.; Hammond, P. T. *Macromolecules* **2007**, *40*, 8367.
(18) Paddison, S. J. *Annual Review of Materials Research* **2003**, *33*, 289.
(19) Wang, L. Y.; Fu, Y.; Wang, Z. Q.; Fan, Y. G.; Zhang, X. *Langmuir* **1999**, *15*, 1360.
(20) Lutkenhaus, J. L.; Hrabak, K. D.; McEnnis, K.; Hammond, P. T. *Journal of the American Chemical Society* **2005**, *127*, 17228.
(21) Fox, T. G. *Bulletin of the American Physical Society* **1956**, *1*, 123.
(22) Vogt, B. D.; Soles, C. L.; Lee, H. J.; Lin, E. K.; Wu, W. *Polymer* **2005**, *46*, 1635.
(23) Smith, A. L.; Ashcraft, J. N.; Hammond, P. T. *Thermochimica Acta* **2006**, *450*, 118.
(24) Crank, J. *The Mathematics of Diffusion*; Oxford University Press: Oxford, 1979.
(25) Hernandez-Munoz, P.; Gavara, R.; Hernandez, R. J. *Journal of Membrane Science* **1999**, *154*, 195.
(26) Arce, A.; Fornasiero, F.; Rodriguez, O.; Radke, C. J.; Prausnitz, J. M. *Physical Chemistry Chemical Physics* **2004**, *6*, 103.
(27) Pourcelly, G.; Oikonomou, A.; Gavach, C.; Hurwitz, H. D. *Journal of Electroanalytical Chemistry* **1990**, *287*, 43.
(28) Zawodzinski, T. A.; Derouin, C.; Radzinski, S.; Sherman, R. J.; Smith, V. T.; Springer, T. E.; Gottesfeld, S. *Journal of the Electrochemical Society* **1993**, *140*, 1041.
(29) Pivovar, B. S. *Polymer* **2006**, *47*, 4194.

Chapter 6 Synthesis and Inclusion Behavior of Cyclotriphosphazene Molecules with Asymmetric Spiro Rings.

6.1 Introduction

Inclusion complexes are host-guest aggregates that form when the interactions between the host molecule and the guest molecule are thermodynamically stabilizing. Hydrogen bonding forces and van der Waals forces coordinate the guest molecule inside the lattice structure of the host molecule to form the complex. Inclusion complexes are significant because the host can show selective inclusion of the guest within the complex. Therefore, they can be used as storage materials or in molecular separation applications.

The cyclotriphosphazene skeleton is a convenient building block for host molecules because of the ease of preparation of various molecules with trigonal symmetry. Cyclic phosphazenes that bear spirocyclic side groups have been used as host molecules in clathrate adducts since 1964.[1] The first of these species was tris(*o*-phenylenedioxy)cyclotriphosphazene (**1**) which was formed by allowing a difunctional nucleophile, 1,2-dihydroxybenzene, to react with hexachlorocyclotriphosphazene to form a spirocyclic molecule with a paddle-wheel structure. (Figure 6-1) Since then, various other phosphazene molecules bearing spirocyclic side groups have been synthesized and found to undergo clathration behavior.[2,3] The clathration properties of these molecules have been utilized in various applications, such as selective inclusion of organic compounds,[2,4] stereocontrolled polymerization of unsaturated monomers,[5] and the construction of 1D supramolecular-wires.[6,7,8] They have also been proposed as components in organic superconductors.[9]

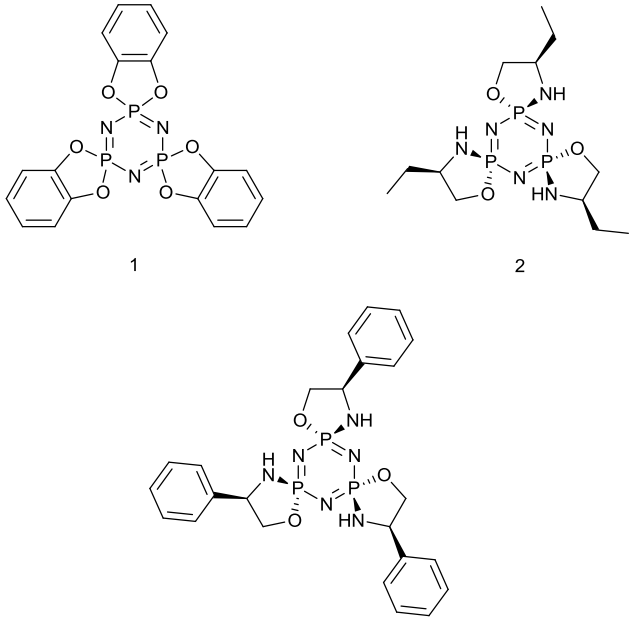

Figure 6-1 Cyclic phosphazenes with symmetric spiro rings and novel cyclic phosphazenes with asymmetric spiro rings.

Up to this time, the phosphazene molecules that show clathration behavior are spirocyclic phosphazenes with symmetric spiro rings. To extend the design and utility of phosphazene clathrates, we have attempted to synthesize spirocyclic phosphazenes with asymmetric spiro side groups. Phosphazenes **2** and **3** were synthesized with residues of chiral amino alcohols and they undergo selective formation of the *cis* isomer in which all the amino groups are on the same side of the phosphazene ring. The isomerically selective synthesis of these cyclotriphosphazenes with asymmetric spiro rings broadens the design choice for future host molecules with trigonal symmetry. In this paper, we report the synthesis, characterization, and the inclusion behavior of two novel cyclotriphosphazenes with asymmetric spiro rings, and propose a possible mechanism for the preferential formation of the *cis* isomer.

6.2 Experimental Methods

6.2.1 Reagents and Solvents

Hexachlorocyclotriphosphazene (Fushimi Pharmaceutical Co., Ltd., Japan) was purified by recrystallization from hexanes followed by sublimation. Tetrahydrofuran, triethylamine, and benzene (99.99%, EMD) were dried using Glass Contour solvent purification columns.[10] (R)-(-)-2-amino-1-butanol (98%, Aldrich), (R)-(-)-phenylglycinol (98%, Alfa Aesar), 1,2-epoxybutane (96%, Aldrich), 1,2-epoxy-2-methylbutane (97%, Aldrich), *trans*-2,3-epoxybutane (97%, alfa Aesar), *cis*-2,3-epoxybutane (98%, Alfa Aesar), 1,2-epoxyhexane (97%, Alfa Aesar), diethyl ether, hexanes, ethanol, ethyl acetate and dichloromethane (EMD) were used as received. Propylene sulfide (96%, Aldrich) was stored in a refrigerated glove box and propylene oxide (99%, Aldrich) was stored under argon. All reactions were carried out under argon using standard Schlenk-line techniques.

6.2.2 Equipment

^{31}P and ^{1}H NMR spectra were obtained using a Bruker AMX 360 WM instrument at 145 MHz and 360 MHz respectively. Single crystal x-ray diffraction data were collected on a Bruker AXS diffractometer, a molybdenum sealed-tube x-ray source equipped with a capillary collimator (MonoCap), SMART APEX 4K CCD detector and a Rigaku-MSC X-stream 2000 low temperature device. Mass spectrometric analysis data were collected using turbospray ionization technique on an Applied Biosystems API 150EX LC/MS mass spectrometer.

6.2.3 Syntheses

Synthesis of phosphazene 2: Hexachlorocyclotriphosphazene (0.014 mol, 4.87 g) in THF (150 mL) was introduced into a 500 mL three-neck round-bottom flask. Three equivalents of (R)-(-)-2-amino-1-butanol (0.042 mol, 3.74 g) and 6 equivalents triethylamine (0.084 mol, 8.50 g) were dissolved in THF (240 mL) and placed in an addition funnel. Each equivalent of the (R)-(-)-2-amino-1-butanol was allowed to react with the phosphazene in the following manner. An 80 mL aliquot of the (R)-2-amino-1-butanol (1 equivalent) and triethylamine (2 equivalents) solution was added dropwise to the chlorophosphazene solution and allowed to react for 24 hours. The same procedure was repeated for the next two 80 mL aliquots of the (R)-2-amino-1-butanol and triethylamine solution. The progress of the reaction was monitored by ^{31}P NMR spectroscopy. Excess (R)-(-)-2-amino-1-butanol (0.011 mol, 0.98 g) was added directly to the reaction solution both as a reactant and proton acceptor to complete the formation of the trispiro phosphazene. The reaction solution was filtered after 6 days of stirring at room temperature (25 ˚C). The filtrate was concentrated by rotary evaporation to produce a yellow adhesive solid. The product was purified through a silica gel column with a mobile phase of ethyl acetate:hexanes:methanol (45:45:10). The product was then recrystallized from a mixture of hexanes and benzene to give white crystals. The yield based on hexachlorocyclotriphosphazene was 36% (2.012 g). δ_P (*d*-THF): 33.2 ppm (3P, s). δ_H (*d*-THF): 4.69 (3H, br s, OC*H*H), 4.19 (3H, m, NC*H*), 3.75 (3H, m, POCH*H*), 3.47 (3H, br s, N*H*), 1.41 (6H, m,CH_2CH$_3$); 0.85 (9H, t, CH_3).

Synthesis of monospiro phosphazene 3a: Hexachlorocyclotriphosphazene (0.0144 mol, 5.00g) was dissolved in THF (150 mL) in a 500 mL three-neck round-bottom flask. R-(-)-phenylglycinol (0.0144 mol, 1.97g) and triethylamine (0.0288 mol, 2.91g) were dissolved in THF (50 mL) and were added dropwise through an additional funnel to the phosphazene solution. The reaction mixture was stirred for two days at room temperature. The mixture solution was then filtered and the filtrate was concentrated. The crude product was purified via a silica gel column using a

mobile phase of ethyl acetate:dichloromethane:hexanes (25:25:50). The resultant solid was recrystallized from ethyl acetate and hexanes to yield white crystals. The yield based on hexachlorocyclotriphosphazene was 63% (3.7397 g). δ_P ($CDCl_3$): 24.2 (2P, d, PCl_2), 22.2 (1P, t). δ_H ($CDCl_3$): 7.45-7.26 (5H, m, C_6H_5), 4.91 (1H, br s, OC*H*H), 4.60 (1H, m, NC*H*), 4.13 (1H, q, OCH*H*), 3.35 (1H, d, N*H*)

Synthesis of dispiro phosphazene 3b: Hexachlorocyclotriphosphazene (8.00 mmol, 2.78g) was dissolved in THF (150 mL) in a 500 mL three-neck round-bottom flask. Two equivalents of (R)-(-)-phenylglycinol (0.016 mol, 2.20g) and four equivalents of triethylamine (0.0321 mol, 3.25g) were dissolved in THF (100 mL) and introduced into an addition funnel. Aliquots of the phenylgylcinol and triethylamine solution (50 ml) were added dropwise as described for the synthesis of phosphazene **2**. The reaction solution was then stirred at room temperature for 5 days. The solution was filtered and concentrated. The resultant solid was recrystallized in chloroform and hexanes to give a white powder. The yield based on hexachlorocyclotriphosphazene was 38% (1.441g). δ_P (*d*-THF): 29.8 (2P, dd), 26.8 (1P, t, PCl_2). δ_H ($CDCl_3$): 7.39-7.26 (10H, m, C_6H_5), 4.92 (2H, br s, OC*H*H), 4.55 (2H, m, NC*H*), 4.11 (2H, m, OCH*H*), 3.19 (2H, m, N*H*). MS ESCI$^+$: *m/z* calcd 475; found 476 ($M+H^+$) and 498 ($M+Na^+$).

Synthesis of phosphazene 3: Hexachlorocyclotriphosphazene (0.0364 mol, 12.66 g) was dissolved in THF (150 mL) in a 500 mL three-neck round-bottom flask. Three equivalents of (R)-(-)-phenylglycinol (0.1092 mol, 14.98 g) and 6 equivalents triethylamine (0.2187 mol, 22.13 g) were dissolved in THF (300mL) and placed in an addition funnel. Aliquots of the phenylglycinol and triethylamine solution (100 mL) were added dropwise as described for the synthesis of phosphazene **2**. The reaction mixture was stirred at room temperature for 5 days and the volume of the reaction solution was reduced to 50% by rotary evaporation. (R)-(-)-phenylgylcinol (0.0364 mol, 4.99 g) was then added to the reaction solution to force the formation of the trispiro product. After nine days of reaction at room temperature, the reaction

solution was filtered and washed with THF. The filtrate was evaporated, and the resulting yellow adhesive residue was put under vacuum for two days. The product was then recrystallized from ethanol and hexanes to give white crystals. The yield based on hexachlorocyclotriphosphazene was 33% (6.5608 g). δ_P ($CDCl_3$): 33.88 ppm (3P, s). δ_H ($CDCl_3$): 7.44-7.25 (15H, m, C_6H_5); 5.16 (3H, s, N*H*), 4.77 (3H, t, OC*H*H), 4.45-4.36 (3H, m, NC*H*), 3.99-3.95 (3H, t, OCH*H*).

6.2.4 Recrystallization Methods

The crystals of phosphazene **2** and **3** were formed in three different ways, with the methods of crystallization detailed below. The crystal structure of these clathrates was determined by single crystal x-ray crystallography. ^{1}H NMR solution spectroscopy was also used as a secondary method to detect the presence of guest compounds. Crystals that formed were isolated from the mother liquor and dissolved in $CDCl_3$. The selectivity of inclusion was determined from the intensity of the unique NMR peaks of the guest compounds to determine the ratio of included compounds.

Hot Recrystallization: The host compound was dissolved in a solvent (e.g. benzene) at boiling temperature to achieve a clear, saturated solution. A non-solvent (e.g. hexanes) was added until the solution became cloudy. The solution was reheated to the boiling point and was filtered if the precipitate did not redissolve. The solution was then cooled slowly to room temperature. The resultant crystals were then washed with the non-solvent and were dried in air.

Cold Recrystallization: A saturated solution was formed by dissolving the host compound in the guest liquid (e.g. propylene oxide) at room temperature. The solution was filtered if it was cloudy. The liquid was then placed in a capped vial and cooled slowly to -30°C. If NMR spectroscopy was required, the resultant crystals were placed on a Buchner funnel filter and were

washed with a non-solvent (e.g. ether) that was chilled to -30°C. The crystals were dried briefly by passing air through the Buchner funnel.

Diffusion Recrystallization: A saturated solution was produced by dissolving the host compound in the guest liquid (propylene sulfide) at room temperature. The saturated solution was filtered into a small vial and placed inside a larger jar containing a non-solvent (e.g. ether). The jar was capped and sealed to allow diffusion of the non-solvent from the larger jar into the vial. The crystals formed this way were washed with the non-solvent (ether) and dried.

6.2.5 X-Ray Analysis

The X-ray intensity data were measured either at 298(2) K or at 113(2) K (cooled by Rigaku-MSC X-Stream 2000) on a Bruker SMART APEX CCD area detector system equipped with a graphite monochromator and a MoKα fine-focus sealed tube (λ = 0.71073Å) operated at 1600 watts power (50 kV, 32 mA). The detector was placed at a distance of 5.8 cm from the crystal. A total of 1850 frames were collected with a scan width of 0.3º in ω and exposure times of 10 - 30 seconds/frame. The frames were integrated with the Bruker SAINT software package using a narrow-frame integration algorithm. The structure was solved and refined using the Bruker SHELXTL (Version 6.1) Software Package. PLATON software was used to identify higher symmetry and to transform coordinates from $P2_1$ to $P2_12_12_1$[11]. All non-hydrogen atoms were refined anisotropically and hydrogens rode on their parent atoms. Disorder in the structure was identified with the help of difference-Fourier map.

6.3 Results and Discussion

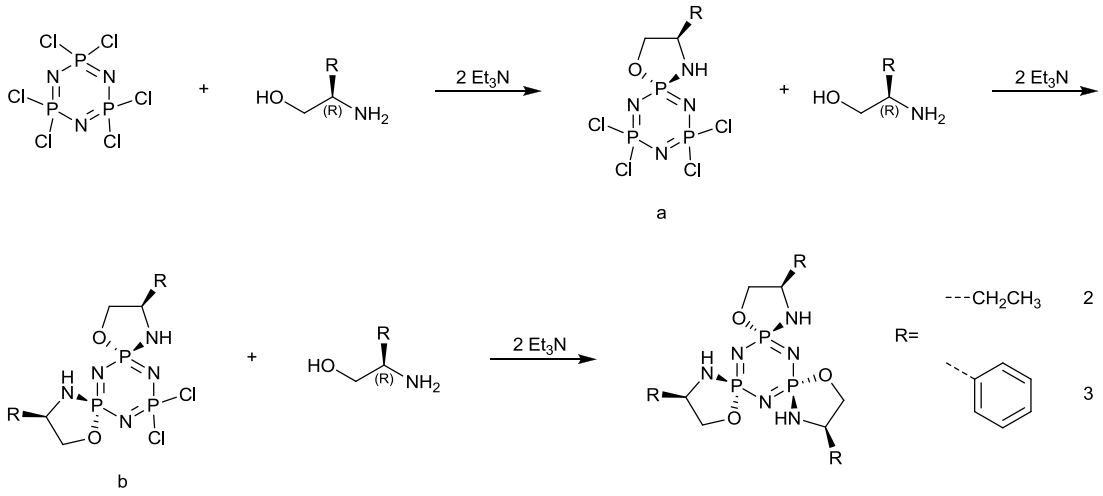

Figure 6-2 Stepwise introduction of amino alcohol residues.

6.3.1 Synthesis and Mechanism of *Cis* Isomer Formation

Phosphazenes **2** and **3** were formed by nucleophilic replacement of the six chlorine atoms of hexachlorocyclotriphosphazene by three amino alcohol residues. The reactions were carried out at room temperature in tetrahydrofuran, and triethylamine was used as the hydrogen chloride acceptor (Figure 6-2). Each charge of amino alcohol solution was added dropwise and stepwise to ensure that each equivalent of amino alcohol was consumed before the next equivalent was added. Synthesis of the phosphazenes in this manner maximized the formation of *cis* isomers. The formation of *cis* isomers was reduced if the amino alcohols were added too rapidly or if the reaction temperature was increased above room temperature. The ^{31}P NMR spectra of the reaction mixtures showed *cis:trans* isomer ratios of at least 7:3. A lack of stereoselectivity would cause the *cis:trans* ratio to be 1:3. (Figure 6-3) The isolation of the *cis* isomers was achieved by column chromatography and/or recrystallization.

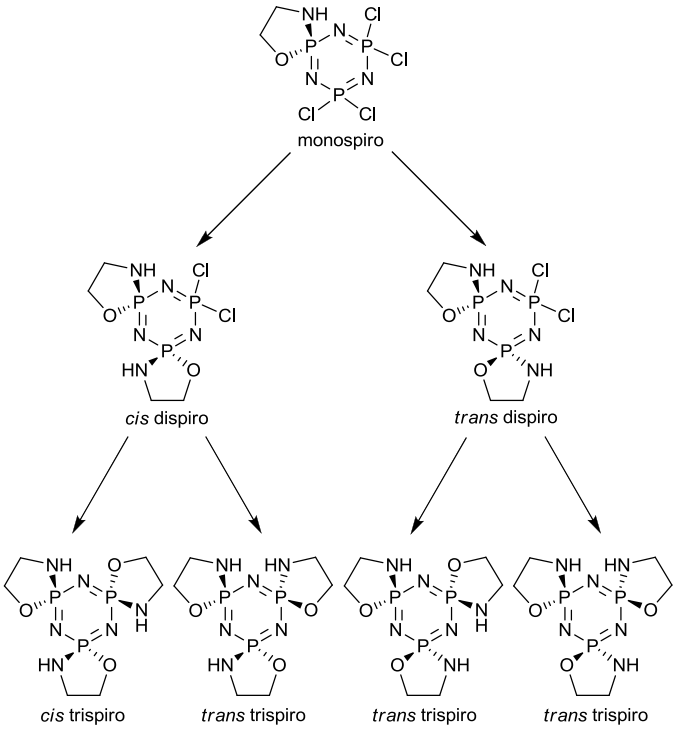

Figure 6-3 Probability of non-selective isomer formation.

A similar unusual stereoselectivity for the formation of a *cis* product has been reported previously by Chandrasekar.[12] We believe that the first asymmetric ring attached to the phosphazene has a directing effect that influences the formation of subsequent spiro rings. First, consider the initial attachment of the amino alcohol residue to the phosphazene. Our preliminary experiments, which were reactions of $N_3P_3Cl_6$ with two equivalents of $HOCH_2CH_3$ and $NH_2CH_2CH_3$ in the presence of triethylamine, showed that amine groups are more nucleophilic than hydroxyl groups. All the amines were consumed within 12 hours but only a few percent of the alcohol was consumed. Therefore, the amino group will attach first to the phosphazene, followed by a rapid intramolecular reaction between the hydroxyl group and a phosphorus-chlorine bond to form the spiro ring. After the formation of the first spiro ring, the stereoselectivity of the next amino substitution will be crucial for the formation of the *cis* product. It appears that the substituent-solvating effect (SSE) proposed by Goldschmidt plays a crucial role in the preferential formation of the *cis* isomer.[13] These earlier kinetic studies by him

indicated that *trans*-isomers of diaminocyclotriphosphazenes are generated preferentially due to formation of a six-membered ring stabilized transition state in which the departure of the chlorine atom is facilitated by solvation of a proton by the lone pair electrons on the exocyclic nitrogen atom (Figure 6-4).

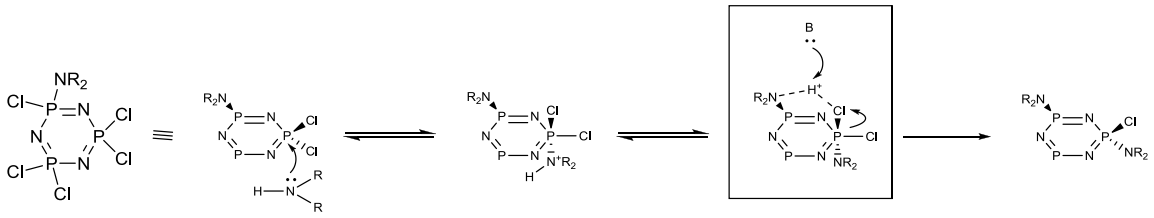

Figure 6-4 Substituent solvating effect by Goldschmidt involving a six member ring stabilized transition state.

In the case of an asymmetric spirocyclic system, it would be expected that the same behavior would lead to amino substitution *trans* to the spirocyclic amine. This is because nitrogen is more basic than oxygen, and is thus more likely to donate its lone pair for proton solvation. Furthermore, substitution from the same side of the spiro amino unit is more sterically hindered. However, in the present work, the *trans*-isomer was not the major product. Closer examination of the experimental results revealed that the nitrogen lone pair on an existing spiro ring is partially delocalized over the spirocyclic P-N bond and is not readily available for donation to protons. This is evident from three observations. First, the x-ray crystallography of the monospiro phosphazene product showed that the spirocyclic P-N bond length is 1.62 Å (Figure 6-5), which is much shorter than a conventional P-N single bond (1.77 Å).[14] Second, the spirocyclic C-N-P bond angle of 116˚ indicates that the spirocyclic nitrogen has more sp^2 trigonal-planar character than sp^3 tetrahedral characteristics. Finally, the ^{1}H NMR spectrum shows that the amine proton chemical shift is about 5 ppm, whereas a non-spirocyclic amine hydrogen is normally quoted to have a value near 2 ppm. The shortened bond length, the hybridization configuration, and the downfield proton shift all indicate delocalization of the nitrogen lone pair over the spirocyclic P-

N bond, making it less available for solvating a proton. On the other hand, the spirocyclic oxygen atom maintains its tetrahedral configuration, and the P-O bond length of 1.6 Å is close to the normally quoted bond length of 1.573 Å. Therefore, the lone pair electrons of oxygen are available for solvating protons, which facilitates the detachment of a chlorine atom from the oxygen side of the phosphazene ring. This promotes the linkage of an amine group to the opposite side of the oxygen and on the same side as the amino group.

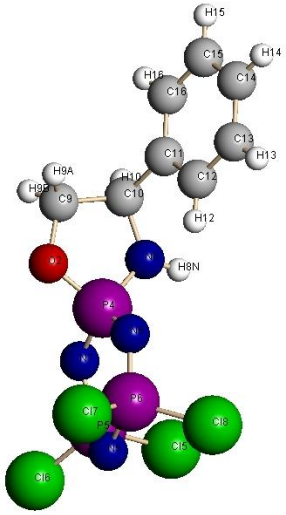

Figure 6-5 The spiro cyclic P-N bond length is 1.62 Å and the P-N-C bond angle is 116˚.

Figure 6-6 shows the two possible routes for the formation of the second spiro ring. If the amine group on the second substituent attacked *trans* to the existing amino group, there would be no stabilizing six-member ring transition state due to the delocalized lone pair electrons of the spirocyclic nitrogen. On the other hand, if the second amine group attacks *cis* to the existing nitrogen on the spiro ring, then the departure of the chlorine is more favored due to the six-member ring transition state created with the lone pairs from the oxygen. This is in agreement with work by Shaw who also showed that, when a phosphazene with an asymmetric spiro ring reacts with pyrrolidine, substitution also occurred at the side opposite to the oxygen.[15]

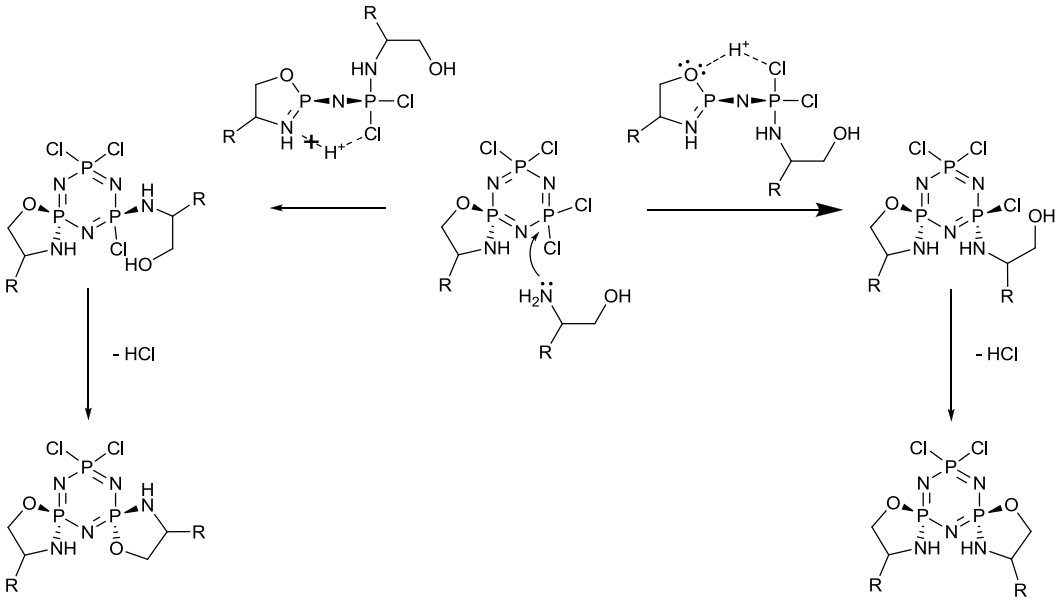

Figure 6-6 Preference for *cis*-isomer through substituent solvating effect.

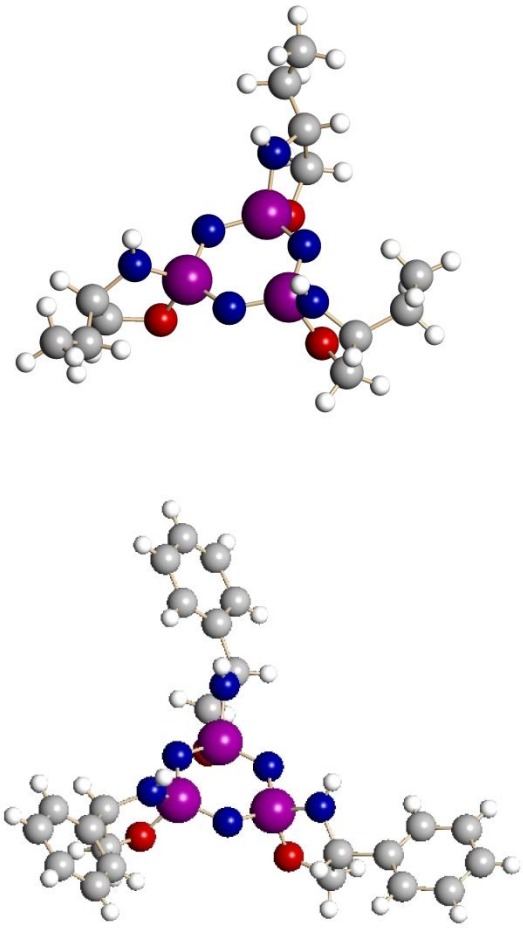

Figure 6-7 Molecular structure of phosphazenes **2** and **3** obtained from x-ray crystallography.

6.3.2 Crystallization and Inclusion Behavior

Single crystal x-ray diffraction data for phosphazenes **2** and **3** were obtained to confirm the formation of the *cis* isomer. (Figure 6-7) Although the phosphazenes were soluble in most organic solvents, only a few solvents yielded crystals that were satisfactory for x-ray diffraction. The results of the diffraction experiments are summarized in Table 5-1.

Table 6-1 Summary of crystal structures

Species	Phosphazene **2**	Phosphazene **2**	Phosphazene **3**	Phosphazene **3**
Inclusion	Benzene	Ethanol	None	Propylene sulfide
Formula	$2(C_{12}H_{24}N_6O_3P_3)\bullet C_6H_6$	$4(C_{12}H_{24}N_6O_3P_3)\bullet (C_2H_5OH)$	$C_{48}H_{54}N_{12}O_6P_6$	$2(C_{24}H_{21}N_6O_3P_3)\bullet 0.56(C_3H_2S)$
Formula Weight	1741.44	1631.19	1080.85	1136.74
Host:Guest Ratio	2:1	4:1	N/A	~4:1
Crystal Habit	Colorless cubical	Colorless block	Colorless plate	Colorless pyramid
Crystal System	Triclinic	Orthorhombic	Orthorhombic	Rhombohedral
Space group	P1	P2(1)2(1)2(1)	P2(1)2(1)2(1)	R3
a/Å	10.301(9)	10.0247(8)	9.4582(8)	30.844(4)
b/Å	13.723(12)	20.0725(16)	22.3485(18)	30.844(4)
c/Å	14.960(13)	38.752(3)	25.314(2)	16.089(4)
A	89.045(15)˚	90	90	90
B	81.827(15)˚	90	90	90
Γ	88.721(15)˚	90	90	120
Volume/ $Å^3$	2093(3)	7797.7(11)	5350.8(8)	13256(4)
Z	1	4	4	9
Reflections Measured	19196	68731	36694	26923
Independent Reflections	16021	19285	13241	9600
R_{int}(%)	3.56	4.54	2.99	11.57
R_1(%)	8.77	6.17	5.57	11.69
R_2(%)	19.64	14.17	13.98	29.73
Flack Parameter	0.11(12)	0.05(7)	-0.03(8)	0.51(8)

Phosphazene **2** was recrystallized from hot solvents and could be obtained only in the form of clathrates that included guest molecules within channels of the crystal lattice. (Figure 6-8) Two examples shown in Table 1 are with benzene and ethanol as guests. Dichloromethane also formed clathrates with phosphazene **2**. The presence of dichloromethane was detected by ^1H NMR spectroscopy and by removal of the guest by vacuum extraction. However, the crystals obtained from dichloromethane were characterized by excessive disorder, and numerous attempts failed to produce a satisfactory crystal. Phosphazene **3** was also recrystallized using the hot recrystallization techinique from various solvents such as benzene, xylene, dichloromethane, ethanol and dioxane. Crystallization from those different solvents yielded the same close-packed crystal structure with no included guest molecules (Figure 6-9). However, phosphazene **3** formed

inclusion complexes when crystallized from various epoxides and propylene sulfide. The cold recrystallization of phosphazene **3** from epoxides yielded crystals in which the presence of included epoxides was detected by ^{1}H NMR spectroscopy and by vacuum extraction. However, the crystals were too disordered to obtain a crystal structure. A satisfactory crystal structure was obtained only when phosphazene **3** that was recrystallized from propylene sulfide using diffusion recrystallization (Figure 6-10). The higher boiling point of propylene sulfide compared to propylene oxide is presumed to be the reason for the better crystals. These crystals still showed weak reflections at high resolution, and the R_{int} value of 11.57% reflects the disorder in the crystal lattice. For this reason, the structure refinement converged to a high R factor. This crystal structure serves as a good representation of how epoxides can be included in within channels of the crystal lattice of phosphazene **3**. The channel structure of the clathrates formed from phosphazenes **2** and **3** allows the removal of guest molecules by placing the clathrates under vacuum. It appears that the incorporated guest molecules stabilize the channel structure of the clathrates because removal of guest molecules by vacuum results in the collapse of the crystal.

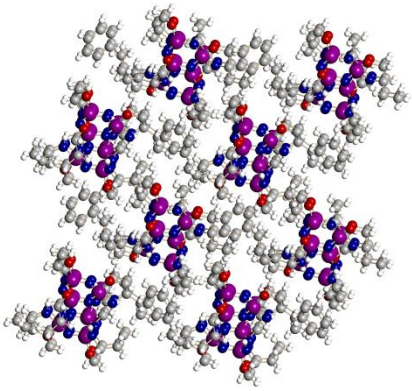

Figure 6-8 Crystal structure of Phosphazene 2 with benzene inclusion

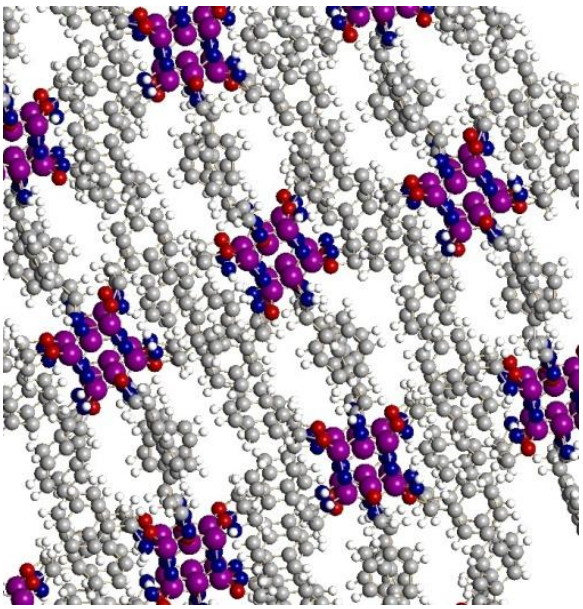

Figure 6-9 Crystal structure of Phosphazene 3 without inclusion

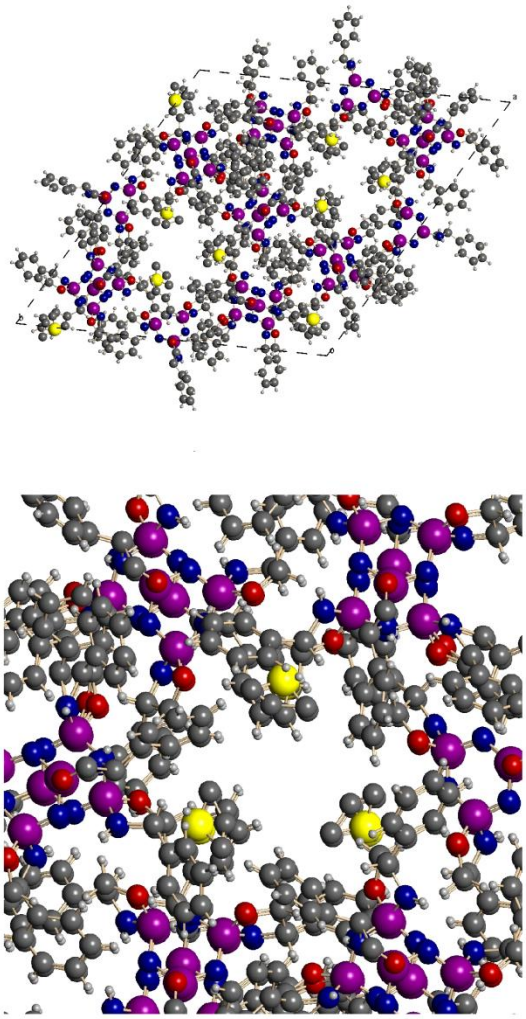

Figure 6-10 Unit cell of phosphazene 3 with propylene sulfide and detailed view of tunnel shaped clathrate.

Every crystal structure obtained from phosphazenes **2** and **3** consists of dimers in which two phosphazene molecules are face to face with each other on the nitrogen side of the ring. These interdigitated dimers are the building blocks within the overall crystal structures. The formation of the dimer is due to hydrogen bonding interactions between the spirocylic amine with the phosphazene nitrogen units, and this bonding motif has been reported previously in crystals of cyclicphosphazenes that bear amine groups.[16] The distance between these two nitrogen atoms is about 3 Å, which is within the range for hydrogen bonding. Each dimer produces six hydrogen

bonding interactions, which provides a strong driving force for interdigitation of two phosphazene molecules.

We examined the possibility that these phosphazenes with chiral side groups might be used for enantiometric separations, but crystallization of phosphazene **3** from racemic mixtures of chiral molecules, such as propylene sulfide, did not show enantiomeric selectivity. However, phosphazene **3** gave selectivity in the inclusion of epoxides as summarized in Table 2. Phosphazene **3** was first dissolved in a 50:50 molar ratio of 2 epoxides at room temperature to form a saturated solution. Crystals formed as the saturated solution was cooled slowly to -30˚C. The crystals were washed with cold ether and the selectivity of epoxide inclusion was determined by ^{1}H NMR spectroscopy.

Table 6-2 Selectivity of epoxide inclusion

	Molar ratio	
Small molecule mixture	Solution	Adduct
Propylene oxide/1,2-Epoxybutane	50:50	63:37
Propylene oxide/*trans*-2,3-Epoxybutane	50:50	69:31
Propylene oxide/ 1,2-Epoxy-2-methylpropane	50:50	72:28
Propylene oxide/1,2-Epoxyhexane	50:50	75:25
Propylene Oxide/Diethyl ether	50:50	83:17
cis-2,3-Epoxybutane/1,2-Epoxybutane	50:50	61:39
trans-2,3-Epoxybutane/1,2-Epoxybutane	50:50	56:44

The general inclusion behavior of phosphazene **3** is to incorporate the epoxide that has the smaller molar volume. This was apparent in all samples in which propylene oxide was present together with any other epoxide species. Molecules with shorter carbon chains were also preferentially included into the crystal structure in competition with molecules with longer chains and more disorder. Even though 1,2-epoxybutane and *cis/trans*-2,3-epoxybutane have the same molecular weight, both *cis* and *trans*-2,3-epoxybutane are preferentially included over 1,2-epoxybutane. Unfortunately, phosphazene **3** was not able to separate the cis-trans isomers of 2,3-

epoxybutane. Thus, when phosphazene **3** was crystallized from a 1:1 mixture of *cis* and *trans*-2,3-epoxybutane, both 2,3-epoxybutane isomers were included equally in the crystal. The preference of *cis*-2,3-epoxybutane over 1,2-epoxybutane demonstrates that the clathrates of phosphazene **3** can be used to separate molecules with similar boiling points. The boiling point of *cis*-2,3-epoxybutane is 60-61˚C, while the boiling point of 1,2-epoxybutane is 63˚C. Another example of a successful separation of compounds with similar boiling points is that of propylene oxide and diethyl ether, which have boiling points of 34˚C and 34.6˚C respectively. The use of distillation to separate these two sets of compounds would be difficult. Thus, selective inclusion is an alternative option for chemical separations.

6.4 Conclusions

Asymmetric spiro rings were formed when hexachlorocyclotriphosphazene reacted with chiral amino alcohols. A preferential formation of *cis* isomers was detected which was attributed to the delocalization of the spirocylic nitrogen lone pair electrons, and its consequent unavailability for solvating a proton. Although oxygen is less basic than nitrogen, its lone pair electrons are not delocalized. Therefore, the spirocyclic oxygen facilitates the departure of the chlorine atom from the same side of the phosphazene ring and promotes the formation of a *cis* isomer. X-ray crystallography of the crystals confirmed the formation of *cis* isomers and showed the ability of these species to include guest molecules within their crystal lattices. Phosphazene **2** was able to include solvent molecules within channels in its crystal structure, whereas phosphazene **3** was capable of selective inclusion of epoxides which have similar structures and boiling points. The design and synthesis of related host molecule that can bring about selective isomeric and enantiometric separations is an ongoing objective.

[1] H. R. Allcock, L.A. Siegel, *J. Am. Chem. Soc*., 1964, **86**, 5140-5144.

[2] H. R. Allcock, *Accts. Chem. Res*., 1978, **11**, 81-87.
[3] H. R. Allcock in , *Inclusion Compounds*, ed. J.L. Atwood, J.E.D. Davies and D.D. MacNicol, Academic Press, New York, 1984, vol. 1, ch. 8, 351-374.
[4] H. R. Allcock, R. W. Allen, E. C. Bissell, L. A. Smeltz, M. Teeter, *J. Am. Chem. Soc.*, 1976, 98, 5120-5125
[5] a) H. R. Allcock, W. T. Ferrar, M. L. Levin, *Macromolecules*, 1982, **15**, 697-703 b) H. R. Allcock, M. L. Levin, *Macromolecules*, 1985, **18**, 1324-1330. c) H. R. Allcock, E. N. Silverberg, G. K. Dudley, *Macromolecules*, 1994, **27**, 1033-1038. d) H. R. Allcock, G. K. Dudley, E. N. Silverberg, Macromolecules, 1994, **27**, 1039-1044. e) H. R. Allcock, E. N. Silverberg, G. K. Dudley, S. R. Pucher, *Macromolecules*, 1994, **27**, 7550-7555.
[6] T. Hertzsch, F. Budde, E. Weber, J. Hullinger, *Angew. Chem. Int. Ed*., 2002, **41**, 2282-2284.
[7] P. Sozzani, A. Comotti, S. Bracco, R. Simonutti, *Angew Chem Int Ed.*, 2004, **43**, 2792-2797.
[8] a) H. Kobayashi, T. Ueda, K. Miyakubo, J. Toyoda, T. Eguchi, A. Tani, *J. Mater. Chem.*, 2005, **15**, 872-879. b) H. Kobayashi, T. Ueda, K. Miyakubo, T. Eguchi, A. Tani, *Phys. Chem. Chem. Phys.*, 2008, **10**, 1263-1269.
[9] G. Gahungu, B. Zhang, J. Zhang, *J. of Phys. Chem. C*, 2007, **111**, 4838-4846.
[10] A. Pangborn, M. Giardello, R. Grubbs, R. Rosen, F. Trimmers, *Organometallics*, 1996, **15**, 1518-1520.
[11] A. L. Spek, *J. Appl. Cryst.*, 2003, 36, 7-13.
[12] V. Chandrasekhar, S. S. Krishnamurthy, H. Manohar, A. R. V. Murthy, R. A. Shaw, M, Woods, *J. Chem. Soc Dalton Trans.*, 1984, **4**, 621-625.
[13] J. M. E. Goldschmidt, R. J. Goldstein, *J. Chem. Soc., Dalton Trans.*, 1981, **6**, 1283-1288.
[14] *CRC Handbook of Chemistry and Physics*, ed. D. R. Lide, CRC Press, 89th Edition, 2009.
[15] S. Besli, S. J. Coles, D. B. Davies, M. B. Hursthouse, A. Kilic¸ R. A. Shaw, *Dalton Trans.*, 2007, **26**, 2792–2801.
[16] J. F. Bickley, R. Bonar-Law, G. T. Lawson, P. I. Richards, F. Rivals, A. Steiner, S. Zacchini, *Dalton Trans.*, 2003, **7**, 1235-1244.

Appendix Exploratory Synthesis of New Polyphosphazenes with Tethered Sulfonic Acid Groups

Introduction

Polyelectrolytes or ionomers are polymers that bear ionic groups, which can be cations or anions. They are used in many various applications such as heterogeneous catalysts, ion-exchangers or ion selective membranes,[1] biomedical applications from adhesives[2] to drug delivery,[3] and polymer electrolytes in lithium batteries and fuel cells[4]. Recently, researchers have also started to exploit the ionic nature of these polymers to form self-assembled structures[5,6] and multilayered materials.[7]

Polyphosphazenes are hybrid organic-inorganic polymers that contain an alternating P-N backbone and organic side groups.[8] With poly(dichlorophosphazene) as the starting material, various polyphosphazenes can be prepared through facile macromolecular replacement of the chlorine atoms by nucleophiles such as alkoxides and amines. The properties of the polyphosphazene can be tuned easily because they are dependent on the type of side groups that are attached to it. Further post-macromolecular substitution reactions can also be carried out to obtain the desired polymer. Previously synthesized polyelectrolyte phosphazenes were mainly investigated for the use as fuel cell membranes[9] and lithium batteries electrolytes.[10] Currently, our group is also pursuing polyphosphazenes containing quaternized ammonium groups for potential use as biomedical materials and dye-sensitized solar cell electrolytes.

Sulfonated polyphosphazenes have been made previously through various reaction routes. The most straightforward method is through the treatment of poly(diphenoxyphosphazene) with aggressive sulfonating agents such as concentrated H_2SO_4[11] or SO_3.[12] Although these methods yield sulfonated aryloxy polyphosphazenes, they also lower the molecular weight of the polymer due to electrophilic attack on of the polyphosphazene backbone. Previous studies have shown that SO_3 can coordinate with the phosphazene backbone nitrogen

atoms.[13] As an alternative process, a direct reaction of disodium alkoxy sulfonate salts to the poly(dichlorophosphazene) was reported by Shriver[14] and Adrianov.[15] However, the insolubility of the sulfonate salts in organic solvents, even with the use of phase transfer agents, did not lead to any reaction with poly(dichlorophosphazene). Therefore, an alternative method was sought for producing sulfonic acid containing polyphosphazenes.

Here we describe a synthetic route to a novel sulfonic acid-containing polyphosphazene. This polyphosphazene contains two different side groups. The majority side group component is a fluorinated alkyloxy unit to provide hydrophobicity. The minor component is an alkyl ether terminated by a sulfonic acid group. The overall goal was to examine the structure-property relationship in polyphosphazenes by systematically varying the side groups and polymer architecture in order to produce an alternative proton conducting membrane. The architecture of this proton conducting polyphosphazene is different from those synthesized in our previous efforts, all of which had sulfonic acid groups located relatively close to the polymer backbone.

In Nafion, the conventional standard for proton conducting membranes, the hydrophobic fluorinated aliphatic backbone and the tethered sulfonic acid groups cause distinct phase separation between the hydrophilic and hydrophobic domains when swelled by water.[16] Because proton conduction occurs mainly in the hydrophilic domain, it is appropriate to maximize the size of the hydrophilic domains to enhance proton conduction. Therefore, we have incorporated fluorinated groups that under other circumstances produce superhydrophobic polyphosphazenes,[17] and a tethered sulfonic acid group that increase the distance between the ionic species and the polyphosphazene backbone.

Experimental

Materials: Sodium (ACS reagent, Aldrich) and sodium hydride (60% in mineral oil, Aldrich) were stored an argon atmosphere glove box. Tetrakis(triphenylphosphine)palladium(0) (99%, Aldrich) was stored in a freezer at -4 ˚C. 2-(allyloxy)ethanol (98%, Aldrich) and 2,2,2-

trifluoroethanol (99%, Aldrich) was distilled over calcium hydride and stored under argon over molecular sieves. Phenol (99%, Aldrich) was sublimed at 40 °C at 0.01 mmHg and stored in a dessicator. Hexachlorocyclotriphosphazene (Fushimi Pharmaceutical Co. Ltd. (Japan)) was purified by recrystallization twice from heptanes followed by sublimation at 30 °C at 0.01 mmHg. Unstablized tetrahydrofuran (99.99%, EMD) was dried by passage through Glass Contour alumina columns before use. Methanol (99.8%, EMD), p-toulenesulfonic acid monohydrate (98%, Alfa Aesar) and 1,3-propane sultone (98%, Aldrich) were used as received. De-ionized water was obtained from a Barnstead Nanopure Diamond water purification system. All synthesis reactions were carried out under an atmosphere of dry argon.

Equipment: High-field ^{1}H (360.14 MHz) and ^{31}P (145.79 MHz) NMR spectra were obtained with use of a Bruker AMX-360 NMR spectrometer. ^{1}H NMR spectra were referenced to internal tetramethylsilane, while ^{31}P NMR spectra were proton-decoupled and referenced to external 85% phosphoric acid in D_2O. Polymer molecular weights and polydispersities were estimated using a Hewlett-Packard HP 1090 gel permeation chromatograph equipped with an HP-1047A refractive index detector, Phenomenex Phenogel 10 μm linear columns were calibrated against polystyrene standards. Sample elution was carried out at 40 °C with a 0.1 wt % solution of tetra-*n*-butylammonium nitrate in THF. Thermal transitions were identified with use of a TA Q10 differential scanning calorimeter. Calibration was accomplished with indium, water, and cyclohexane standards. All analyses were performed over a range of -100 to 100 °C at a heating rate of 10 °C/min.

Synthesis of Polymer (1) $[PNCl_2]_n$. The polymer was synthesized using an established procedure[8]. Hexachlorocyclotriposphazene (approximately 200 g) was sealed in an evacuated Pyrex tube and was polymerized thermally at 250 ˚C for 12 hours. Unpolymerized hexachlorocyclotriphosphazene was removed via sublimation to yield polymer 1. Typical yields were about 65 %.

Synthesis of Polymer 2 $[PN(OCH_2CF_3)_{1.7}(OCH_2CH_2OCH_2CH=CH_2)_{0.3}]_n$. Polymer 1 (10.0 g, 86.3 mmol) was dissolved in THF (700 mL) overnight. 2,2,2-Trifluoroethanol (14.7 g, 147 mmol) was allowed to react with sodium (3.28 g, 142 mmol) in THF (150 mL). 2-(Allyloxy)ethanol (4.4 g, 43 mmol) was treated with 60% sodium hydride (1.4 g, 34 mmol) in THF. The sodium alkoxides were added dropwise to the polymer solution in the following order. Half of the sodium 2,2,2-trifluoroethoxide solution was added to the polymer first, followed by all of the sodium 2-(allyloxy)ethoxide solution, and finished by the rest of the sodium 2,2,2-trifluoroethoxide solution. The reaction solution was refluxed overnight. The complete replacement of chlorine atoms was monitored by ^{31}P NMR spectroscopy. The reaction solution was concentrated and precipitated into water to form swelled fibers. The precipitation was repeated a total of 3 times from THF into water. The resultant polymer was dried over P_2O_5 in a vacuum oven at 80 ˚C for 48 hours. Yield (17.5 g, 82 %). δ_P (*d*-Acetone): -7.0 (0.3P, br s, [*P*N(OCH$_2$CF$_3$)(OCH$_2$CH$_2$OCH$_2$CH=CH$_2$)]), -8.0 (1.7P, br s, [*P*N(OCH$_2$CF$_3$)$_2$]) δ_H (*d*-Acetone): 5.87 (0.3 H, m, C*H*=CH2), 5.26 (0.3 H, d, =C*H*H), 5.14 (0.3 H, d, =CH*H*), 4.54 (3.4 H, br s, C*H*$_2$CF$_3$), 4.23 (0.6 H, br s, POC*H*$_2$), 4.00 (0.6 H, br s, OC*H*$_2$CH=CH2), 3.40 (0.6 H, br s, POCH$_2$C*H*$_2$) T_g = -23 ˚C, $M_w = 7.1 \times 10^5$, PDI = 2.5

Synthesis of Polymer 3 $[PN(OCH_2CF_3)_{1.7}(OCH_2CH_2OH)_{0.3}]_n$. Polymer 2 (14 g, 57 mmol or 17 mmol allyl) was dissolved in THF (700 mL). Tetrakis(triphenylphosphine)palladium(0) (2 g, 1.7 mmol), and p-toluenesulfonic acid (0.32 g, 1.7 mmol) were dissolved in methanol (5.4 g, 170 mmol) and were added to the polymer solution. The reaction solution was refluxed for 6 hours. The product solution was concentrated and placed in a dialysis tube and was dialyzed against methanol for 5 days. The polymer obtained was dried in a vacuum oven at 80 ˚C for 48 hours. Yield (9.9 g, 75 %) δ_P (*d*-Acetone): -7.0 (0.3P, br s, [*P*N(OCH$_2$CF$_3$)(OCH$_2$CH$_2$OH)]), -8.0 (1.7P, br s, [*P*N(OCH$_2$CF$_3$)$_2$]) δ_H (*d*-Acetone): 4.55 (3.4 H, br s, C*H*$_2$CF$_3$), 4.17 (0.6 H, br s, POC*H*$_2$), 3.78 (0.6 H, br s, C*H*$_2$OH) T_g = -48 ˚C, $M_w = 3.5 \times 10^5$, PDI = 3.1

Synthesis of Polymer 4 [$PN(OCH_2CF_3)_{1.7}(OCH_2CH_2OCH_2CH_2CH_2SO_3H)_{0.3}]_n$ Polymer 3 (3g, 13 mmol or 3.9 mmol OH) and 1,3-propane sultone (4.7 g, 39 mmol) was dissolved in THF (500 mL). 60 % Sodium hydride (0.2 g, 5 mmol) was added to the solution which was refluxed overnight. The polymer was obtained by evaporation of THF, and was boiled in aqueous H_2SO_4 (0.5 M) for 1 hour to remove unreacted reagents and to acidify the sulfonic acid groups. The acidic solution was refreshed and the solution was boiled again for another hour. The obtained polymer was soaked in deionized water which was refreshed until a pH of 6 was obtained, to ensure complete removal of sulfuric acid. Yield (2.4 g, 70 %) δ_P (*d*-DMSO): -6.0 (0.3P, br s, [*P*N(OCH_2CF_3)(OCH_2CH_2OH)]), -7.7 (1.7P, br s, [*P*N(OCH_2CF_3)$_2$]) δ_H (*d*-DMSO): 4.52 (3.4 H, br s, C*H*$_2$CF$_3$), 4.29 (0.6 H, br s, POC*H*$_2$), 3.91 (0.6 H, br s, OC*H*$_2$CH$_2$CH$_2$SO$_3$H), 3.64 (0.6 H, br s, POCH$_2$C*H*$_2$O), 2.46 (0.6 H, m, OCH$_2$CH$_2$C*H*$_2$SO$_3$H), 1.79 (0.6 H, br s, OCH$_2$C*H*$_2$CH$_2$SO$_3$H). T_g = -15 ˚C, $M_w = 2.8 \times 10^5$, PDI = 2.8

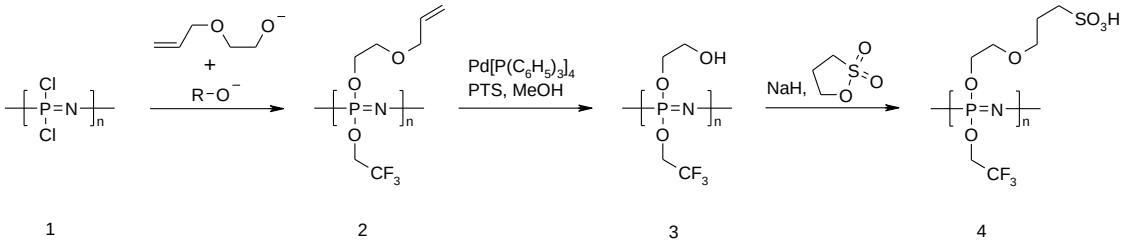

Scheme 1 Synthetic route toward the synthesis of a polyphosphazene with tethered sulfonic acid groups

Results and Discussion

The first attempt to synthesize a polyphosphazene with tethered sulfonic acid groups was to carry out a radical sulfonation reaction on allyl groups linked to a polyphosphazene. Allyl groups can react with sodium bisulfite and a radical initiator to yield a sulfonated anti-Markovnikov product.[18] A polyphosphazene with 2-(allyloxy)ethoxy side groups was synthesized but the radical sulfonation process was ineffective. This was attributed to the possible radical

scavenging ability of phosphazenes which impedes this reaction. [19] This behavior may be related to the fact that some vinyl substituted phosphazenes resist radical polymerization.[20]

The current route uses a ring opening of 1,3-propane sultone by an alkoxy nucleophile to attain the tethered sulfonic acid architecture. Previously in our program, we showed that amino-substituted phosphazenes can ring open 1,3-propane sultone to yield side chains with tethered sulfonic acid groups.[21] However, amino linkages are inappropriate for polymers that operate under strong acidic conditions as in a fuel cell. To generate the etheric linkage by the ring opening of 1,3-propane sultone, a hydroxy terminated side group is required. Thus, a mono-protected diol was linked first to the polyphosphazene and was subsequently deprotected to the hydroxyl group. This extra deprotection step is required because diols cannot be used directly in the macromolecular substitution of polyphosphazenes because they would yield highly crosslinked polymers. 2-(Allyloxy)ethoxy side group was used since the alcohol is commercially available and the allyl group can be easily removed by a Pd(0) catalyzed deprotection reaction which demonstrated in polyphosphazenes by Song[22]. The required alkyl ether tethered sulfonic acid architecture was finally achieved by treatment of the alkyl hydroxyl group containing polyphosphazene with sodium hydride and exposure to 1,3-propane sultone. This causes ring opening of 1,3-propane sultone to form the etheric linkage and a terminal sulfonic acid group.

Conclusions

We report a synthetic method to afford a novel sulfonated polyphosphazene ionomer in which the sulfonic acid groups are tethered by flexible etheric chains. This polymer was obtained to the ring opening of 1,3-propane sultone by a hydroxyl containing polyphosphazene. By distancing the hydrophilic sulfonic acid group from the hydrophobic backbone, we hope to increases proton conductivity by promoting phase separation between hydrophobic and hydrophilic domains. Future work will include comparing the morphology and performance of this new polymer with previously made sulfonated polyphosphazenes and conventional proton

conducting membranes to evaluate the structure-property relationship that is required to attain a high performance proton conducting membranes.

[1] T. Sata, T. Sata, W. Yang *Journal of Membrane Science*, **2002**, *206*, 31-60
[2] A. B. Scranton, B. Rangarajan, J. Klier In *Biolpolymers II* Eds: N. A. Peppas, R. S. Langer, in *Advances in Polymer Science*, Vol 122 Springer: Berlin, Germany, **1995**, 1-54
[3] M. Malmsten, *Soft Matter*, **2006**, *2*, 760-769
[4] F. M. Gray, *Polymer Electrolytes*, RSC:Cambridge UK **1997**
[5] A. F. Thunemann, *Prog. Polym. Sci.*, **2002**, *27*, 1473-1572
[6] M. Ballauff, *Prog. Polym. Sci*, **2007**, *32*, 1135-1151
[7] P. T. Hammond, *Adv. Mater.*, **2004**, *16*, 1271-1293
[8] H. R. Allcock, *Chemistry and Applications of Polyphosphazenes*, Wiley-Interscience: Hoboken, New Jersey, **2003**.
[9] H. R. Allcock, R. M. Wood *Journal of Polymer Science B*, **2006**, *44*, 2358-2368
[10] R. J. Klein, D. T. Welna, A. L. Weikel, H. R. Allcock, J. Runt, *Macromolecules*, **2007,** *40*, 3990-3995
[11] H. R. Allcock, R. J. Fitzpatrick *Chem. Mater.* **1991**, *3*, 1120-1132
[12] Wycisk, R.; Pintauro, P.N. *Journal of Membrane Science*, **1996**, *119*, 155-160
[13] E. Montoneri,G. Ricca, M. Gleria, M C. Gallazzit *Inorg. Chem.* **1991**, *30*, 150-152
[14] S. Ganapathiappan, K. Chen, D. F. Shriver J. Am. Chem. Soc. **1989**, *111*, 4091-4095
[15] A. K. Andrianov, A. Marin, Alexander; J. Chen, J. Sargent, N. Corbett, *Macromol.*, **2004**, *37*, 4075-4080
[16] K. A. Mauritz, R. B. Moore *Chem. Rev.*, **2004**, *104*, 4535–4586
[17] H. R. Allcock, L. Steely, A. Singh, M. D. Hindenlang, *J. Adhesion Sci. & Technol.* **2009**, *23*, 435-445
[18] S. M. Weinreb, C. E. Chase, P. Wipf, S. Venkatraman, *Organic Syntheses*, **2004**, *10*, 707
[19] Y. Hu, W. Fan, Q. Wang, T. Kawamora, N. Koseki, Y. Akutsu, M. Tamura, *Progress in Natural Science*, **1999**, *9*, 103-108
[20] H. R. Allcock *J. Inorg. Organomet. Polym. Mater.*, **2007**, *17*, 349-359
[21] H. R. Allcock; E. H. Klingenberg, M. F. Welker, M. F. *Macromolecules* **1993**, *26*, 5512-5516
[22] C. Chun, S. M. Lee, C. W. Kim, K. Hong, Sang. Kim, H. K. Yang, S. Song *Biomaterials*, **2009**, 30, 4752-4762

VITA
David Lee

David Lee, son of Kong Beng Lee and Lee Yin Fung, was born on May 22nd, 1981 in Kuala Lumpur, Malaysia. He earned his Bachelors degree in Chemistry from Franklin and Marshall College, Pennsylvania in 2004. While at F&M, he carried out undergraduate research on organic synthesis under the guidance of Professor Scott Van Arman. David pursued his graduate education at The Pennsylvania State University, where he joined the research group of Professor Harry R. Allcock. Upon graduation, he will continue his career as a postdoctoral researcher with Professor Emmanuel Giannelis at Cornell University.